Peptidoglycan recycling is critical for cell division, cell wall integrity and β-lactam resistance in *Caulobacter crescentus*

Pia Richter[1], Anna Merz[1], Jacob Biboy[2], Nicole Paczia[3], Timo Glatter[4], Waldemar Vollmer[5], Martin Thanbichler[1,6,7,*]

[1] Department of Biology, Marburg University, 35043 Marburg, Germany
[2] Centre for Bacterial Cell Biology, Institute for Cell and Molecular Biosciences, Newcastle University, Newcastle upon Tyne, United Kingdom
[3] Core facility for Metabolomics and Sgmall-Molecule Mass Spectrometry, Max Planck Institute for Terrestrial Microbiology, 35043 Marburg, Germany
[4] Core facility for Mass Spectrometry and Proteomics, Max Planck Institute for Terrestrial Microbiology, 35043 Marburg, Germany
[5] Institute for Molecular Bioscience, University of Queensland, Brisbane, QLD, Australia
[6] Max Planck Fellow Group Bacterial Cell Biology, Max Planck Institute for Terrestrial Microbiology, 35043 Marburg, Germany
[7] Center for Synthetic Microbiology (SYNMIKRO), 35043 Marburg, Germany

[*]Correspondence: thanbichler@uni-marburg.de (M.T.)

Keywords
Peptidoglycan, cell wall recycling, β-lactamase, antibiotic resistance, β-lactam, MurU pathway

Abstract

Most bacteria possess a peptidoglycan sacculus, which is continuously remodeled during cell growth and division. The peptidoglycan (PG) fragments generated in this process are typically imported into the cell and recycled for entry into the PG biosynthesis pathway. While the underlying pathways have been studied intensively in gammaproteobacteria, knowledge of their presence and physiological roles in other bacterial lineages remains limited. Here, we comprehensively investigate PG recycling in the alphaproteobacterial model organism *Caulobacter crescentus*. We show that this species contains a functional PG recycling pathway by characterizing the activities of key enzymes *in vitro* and *in vivo*. Our results reveal that PG recycling is critical for *C. crescentus* cell morphology and division, and is dynamically regulated to balance the flux of metabolic intermediates toward PG biosynthesis and central carbon metabolism. Importantly, defects in PG recycling strongly impair the intrinsic ampicillin resistance of *C. crescentus* without changing the activity of its β-lactamase BlaA, likely by limiting PG precursor biosynthesis and thereby decreasing the activity of the cell wall biosynthetic machinery in the presence of residual antibiotic. These findings underscore the central role of PG recycling in bacterial fitness and suggest that inhibiting this process could provide a promising strategy to combat β-lactam-resistant pathogens.

Introduction

15 In most bacteria, the cytoplasmic membrane is surrounded by a layer of peptidoglycan (PG), which pro-
16 tects the cell from osmotic lysis, maintains cell shape and serves as a physical barrier against environ-
17 mental assaults (Egan et al., 2020). PG is composed of a dense meshwork of glycan strands made of alter-
18 nating *N*-acetylglucosamine (Glc*N*Ac) and *N*-acetylmuramic acid (Mur*N*Ac) moieties that are connected by
19 short peptides containing unusual D-amino acids (Vollmer et al., 2008a). The integrity of the PG layer is
20 critical for bacterial fitness and survival, which makes it a major target of medically relevant antibiotics
21 (Bugg et al., 2011).

22 PG biosynthesis initiates in the cytoplasm (Barreteau et al., 2008; Höltje, 1998), starting with the trans-
23 formation of fructose-6-phosphate to UDP-Mur*N*Ac. Next, this key intermediate is modified with a tripep-
24 tide, synthesized stepwise by dedicated amino acid ligases, and then completed by the addition of a
25 preformed D-Ala–D-Ala unit, leading to UDP-Mur*N*Ac-pentapeptide (**Figure 1**). The Mur*N*Ac-pentapeptide
26 moiety is then transferred to the lipid carrier undecaprenol phosphate and linked to Glc*N*Ac. The product,
27 lipid II, is then flipped across the cytoplasmic membrane (Sham et al., 2014), where is it used by glycosyl-
28 transferase (GTases) to polymerize the glycan chains. Transpeptidases (TPases) then crosslink the peptides
29 of neighboring glycan strands, thereby establishing the mesh-like architecture of PG (Egan et al., 2020;
30 Höltje, 1998). The most abundant group of TPases are the DD-TPases, which cleave the C-terminal D-Ala–
31 D-Ala unit of a pentapeptide and then transfer the resulting tetrapeptide to an adjacent acceptor peptide
32 (Sauvage et al., 2008). This group of enzymes is also known as penicillin-binding proteins (PBPs), because
33 they recognize penicillin and other β-lactams as non-cognate substrates, based on the structural similarity
34 of their β-lactam ring to the D-Ala–D-Ala moiety of uncrosslinked peptides. These compounds form a stable
35 adduct with the active-site serine of PBPs and thus irreversibly inhibit their crosslinking activity, thereby
36 weakening the cell wall and inducing cell lysis (Cho et al., 2014; Mora-Ochomogo and Lohans, 2021). The
37 sensitivity of DD-TPases to β-lactams represents a vulnerability that is widely exploited to treat bacterial
38 infections, but resistance to this class of antibiotics is rapidly spreading among pathogens (Lima et al.,
39 2020).

40 Cells usually contain both monofunctional PBPs, which contain only a transpeptidase domain, and bifunc-
41 tional PBPs, which contain an additional glycosyltransferase domain and thus have polymerization as well
42 as crosslinking activity (Sauvage et al., 2008; Vollmer and Bertsche, 2008). To enable the tight spatio-
43 temporal control of PG biosynthesis, these enzymes are often part of dynamic multi-protein complexes
44 that include regulatory factors and cytoskeletal elements (Egan et al., 2020; Typas et al., 2012). In most

45 rod-shaped bacteria, lateral cell wall elongation is carried out by the elongasome, a complex organized by
46 the actin-like protein MreB (Jones et al., 2001). Multiple elongasomes are distributed along the longi-
47 tudinal axis of the cell and move around its circumference in helical tracks (Garner et al., 2011; van
48 Teeffelen et al., 2011), incorporating new cell wall material in a dispersed manner. Their PG biosynthetic
49 activity is mediated by the GTase RodA and the monofunctional DD-TPase PBP2 (Cho et al., 2016; Meeske
50 et al., 2016), whose functions are closely coupled (Rohs et al., 2018). Cell division, by contrast, is mediated
51 by the divisome, which is orchestrated by polymers of the tubulin homolog FtsZ (Bi and Lutkenhaus, 1991;
52 Bisson-Filho et al., 2017; Yang et al., 2017), with the glycosyltransferase FtsW and the monofunctional DD-
53 TPase PBP3 acting as the main PG biosynthetic enzymes (Taguchi et al., 2019). The division process also
54 involves bifunctional PBPs, such as PBP1B in *E. coli* (Bertsche et al., 2006; Navarro et al., 2025), although
55 this class of enzymes also appears to act outside larger complexes in the repair of cell wall (More et al.,
56 2019; Pazos and Vollmer, 2021).

57 To enable the incorporation of new cell wall material into the existing sacculus, the PG meshwork needs
58 to be opened at specific sites – a task that is achieved by a diverse set of autolysins (**Figure 1**) (van
59 Heijenoort, 2011; Vollmer et al., 2008b). DD- and LD-endopeptidases cleave the peptides and the
60 crosslinks between them, while amidases remove the entire peptide stem from the glycan chain. The
61 glycan chains are cleaved by glucosaminidases and muramidases. The latter include lytic transglycosylases
62 (LTs), which break the β-1,4-glycosidic bond between Mur*N*Ac and Glc*N*Ac, leading to the concomitant
63 formation of a 1,6-anhydro bond in the Mur*N*Ac moiety (Dik et al., 2017; Vollmer et al., 2008b). The activity
64 of autolytic enzymes generates small PG fragments, called muropeptides. Only a small fraction of these is
65 released into the environment (Goodell and Schwarz, 1985), whereas the majority is transported into the
66 cytoplasm, where they are metabolized and reused in PG synthesis. This process is known as PG recycling
67 and has so far been studied mainly in gammaproteobacteria such as *Escherichia coli* or *Pseudomonas*
68 *aeruginosa* (Dik et al., 2018; Gilmore and Cava, 2025; Park and Uehara, 2008).

69 During one division cycle, more than 50% of the PG sacculus are broken down in *E. coli*. Most of the
70 turnover products in this and other Gram-negative species are 1,6-anhydro-muropeptides (Vollmer et al.,
71 2008b). They are transported into the cytoplasm by the proton-driven Major Facilitator Superfamily (MFS)
72 permease AmpG (Cheng and Park, 2002; Jacobs et al., 1994), where the sugars and the peptide are
73 separated from each by the combined action of the LD-carboxypeptidase (LD-CPase) LdcA (Templin et al.,
74 1999), the amidase AmpD (Höltje et al., 1994) and the β-hexosaminidase NagZ (Cheng et al., 2000). The
75 Glc*N*Ac moiety is then recycled by conversion to Glc*N*Ac-6-P and then GlcN-6-P, which can either be trans-
76 formed into the PG precursor UDP-Mur*N*Ac or directed into central carbon metabolism by deamination to

77 fructose-6-P (Gilmore and Cava, 2025; Vollmer et al., 2008b). The fate of the anhMur*N*Ac moiety, on the
78 other hand, varies between species. In *E. coli*, it is converted to Glc*N*Ac-6-P (Uehara et al., 2005), whereas
79 *P. aeruginosa* employs the MurU pathway to convert anhMur*N*Ac into UDP-Mur*N*Ac, thereby channeling
80 it directly back into PG biosynthesis (Borisova et al., 2017; Fumeaux and Bernhardt, 2017; Gisin et al., 2013)
81 (**Figure 1**). As the last component, the peptide is typically broken down to single amino acids that are
82 subsequently reused to synthesize new peptide stems (Gilmore and Cava, 2025). An alternative route has
83 been reported for *E. coli*, which trims the released peptide by removal of the terminal D-ala residues and
84 then attaches the resulting tripeptide to UDP-Mur*N*Ac using the peptide ligase Mpl (Mengin-Lecreulx et
85 al., 1996).

86 The recycling of PG degradation products is an efficient way to save energy and resources, which may be
87 particularly relevant during growth in nutrient-limiting conditions (Gilmore and Cava, 2025). For human
88 commensals or pathogens, it also represents an important strategy for evading detection by the innate
89 immune system, which senses released muropeptides through the NOD1 and NOD2 receptors (Trindade
90 and Chen, 2020). Apart from that, some gammaproteobacteria such as *Citrobacter freundii* and *P. aeru-*
91 *ginosa* use PG recycling as a sensory mechanism to detect the presence of β-lactam antibiotics and initiate
92 a resistance response (Dik et al., 2018). These species possess the inducible β-lactamase AmpC, whose
93 gene is controlled by the the LysR-type transcriptional regulator AmpR. The activity of AmpR is modulated
94 through its interaction with muropeptides (Jacobs et al., 1994; Lindquist et al., 1989). In the absence of β-
95 lactams, it is associated with UDP-Mur*N*Ac-pentapeptide, acting as a repressor that prevents *ampC*
96 expression (Jacobs et al., 1997). When cells are exposed to β-lactam antibiotics, the disruption of PG
97 metabolism leads to an increased accumulation of anhydro-muropeptides, thus raising the levels of PG
98 recycling intermediates in the cytoplasm. Some of these intermediates, especially anhMur*N*Ac-pentapep-
99 tide (Dietz et al., 1997; Vadlamani et al., 2015), can interact with AmpR and competitively displace its co-
100 repressor UDP-Mur*N*Ac-pentapeptide. As a result, AmpR transforms into a transcriptional activator that
101 stimulates *ampC* expression, thereby establishing β-lactam resistance (Dietz et al., 1997; Dik et al., 2018;
102 Jacobs et al., 1997). While PG recycling and its impact on cell physiology as well as β-lactam resistance
103 have been extensively investigated in gammaproteobacteria, these processes are still poorly investigated
104 in other bacterial lineages.

105 Here, we studied PG recycling in the alphaproteobacterium *Caulobacter crescentus*, a species intrinsically
106 resistant to β-lactam antibiotics due to production of the β-lactamase BlaA, extending recent work on this
107 topic by Modi et al. (Modi et al., 2025). We found that *C. crescentus* encodes a functional PG recycling
108 pathway and characterized the activities of key enzymes, using a combination of biochemical, cell biologic-

al, metabolomics and proteomics analyses. Our results demonstrate that PG recycling is required to sustain proper cell morphology and division in this species, especially upon transition to stationary phase. They further show that *C. crescentus* cells regulate their PG recycling pathway to control the flux of internal and external Glc*N*Ac into PG biosynthesis and central carbon metabolism, while employing the MurU pathway to directly convert anhMur*N*Ac back into the PG precursors. Importantly, PG recycling-deficient cells show severe defects in β-lactam resistance, despite normal BlaA production and activity. For the model β-lactam ampicillin, this phenotype can be explained by increased sensitivity of the septal TPase PBP3 to ampicillin-mediated inhibition, likely resulting from a reduced supply of PG building blocks in the absence of PG recycling. Together, our findings indicate that β-lactam efficacy is modulated by the availability of PBP substrates, uncovering a new aspect of the complex interplay between this major class of antibiotics and their cellular targets.

Results

120 **The genome of *C. crescentus* encodes a full PG recycling pathway**

121 To initiate the analysis of PG recycling in *C. crescentus*, we first mined the genome of this species for hom-
122 ologs of proteins that are central to the well-studied PG recycling pathway of *E. coli*. Reciprocal BLAST
123 analysis revealed clear counterparts for the muropeptide permease AmpG as well as for most enzymes
124 involved in the processing of the imported anhydro-muropeptides and the transformation of their sugar
125 and peptide moieties into new PG building blocks (**Table 1** and **Figure 1**). Notably, no homologs were found
126 for the LD-CPase LdcA and the peptide ligase Mpl, which trim tetrapeptides to tripeptides and attach these
127 to UDP-Mur*N*Ac, respectively. Another key enzyme missing in *C. crescentus* is the etherase MurQ, a critical
128 player in the recycling of anhMur*N*Ac that converts Mur*N*Ac-6-P into Glc*N*Ac-6-P and thus enables its re-
129 utilization through the Glc*N*Ac recycling/degradation pathway (Jaeger et al., 2005; Uehara et al., 2006).
130 Instead, we identified a three-step pathway initially found in *P. aeruginosa* (Borisova et al., 2017; Fumeaux
131 and Bernhardt, 2017; Gisin et al., 2013) that leaves the Mur*N*Ac moiety intact and uses it directly to
132 regenerate UDP-Mur*N*Ac. These findings suggest that the two sugar moieties of anhydro-muropeptides
133 are recycled independently in *C. crescentus*. The protein homologs identified are generally well-conserved
134 at the sequence level (**Table 1**) and show the same domain architectures as their *E. coli* and *P. aeruginosa*
135 counterparts. The only exception is the homolog of AmpD, in which the amidase_2 domain is fused to a C-
136 terminal PG_binding 1 domain that is not present in the *E. coli* protein. Due to this difference, this protein
137 will be referred to as 'AmiR' (*Ami*dase for PG *R*ecycling) throughout the present study.

138 **Predicted key players in the PG recycling pathway are functionally active**

139 To test the prediction that *C. crescentus* can recycle PG degradation products, we aimed to verify the acti-
140 vity of the two first enzymes in the recycling pathway, AmiR and NagZ, which mediate the release of the
141 sugar and peptide moieties, thereby providing the basis for their refunneling into PG biosynthesis (see
142 **Figure 1**). To this end, pentapeptide-rich PG sacculi isolated from a DD-carboxypeptidase-deficient *E. coli*
143 strain were treated with the LT Slt from *E. coli* (Betzner and Keck, 1989) to release anhydro-muropeptides
144 (**Figure 2A**). These were then first incubated with AmiR or a catalytically inactive variant of the protein
145 (AmiR*) in which three conserved amino acid residues coordinating the essential Zn^{2+} cofactor of AmpD-
146 like amidases (Généreux et al., 2004; Liepinsh et al., 2003; Uehara and Park, 2007) were replaced by
147 alanine (**Figure 2–Figure supplement 1A**). HPLC analysis of the reaction products revealed that AmiR was
148 able to remove the peptide stems from all detectable anhydro-muropeptides, regardless of the length of
149 the peptide or the number of crosslinked peptides (**Figure 2B**). By contrast, no amidase activity was

150 detected in the control reactions containing the mutant AmiR* protein, confirming the critical role of the
151 metal cofactor in the amidase reaction. To determine whether, despite its broad substrate specificity,
152 AmiR had a preference for certain anhydro-muropeptides, we repeated the enzyme assay with limiting
153 enzyme concentrations. The results showed that AmiR efficiently hydrolyzed tetrapeptide-containing frag-
154 ments, whereas anhydro-muropeptides with tripeptide or pentapeptide stems were cleaved with lower
155 efficiency (**Figure 2–Figure supplement 1B**). Notably, unlike *E. coli* AmpD (Höltje et al., 1994), it also
156 showed activity towards muropeptides that were produced with the muramidase cellosyl and thus
157 contained reducing Mur*N*Ac instead of anhMur*N*Ac moieties, although the efficiencies were slightly lower
158 under these conditions (**Figure 2–Figure supplement 1C**). By contrast, no activity was detectable with
159 undigested peptidogylcan sacculi, consistent with a role of the protein in the recycling of PG fragments
160 (**Figure 2–Figure supplement 2**). Together, these results confirmed that AmiR was a genuine amidase with
161 a role in PG recycling. Next, we used the same approach to study the biochemical activity of *C. crescentus*
162 NagZ. For this purpose, anhydro-muropeptides or reducing muropeptides were incubated with wild-type
163 NagZ or a catalytically inactive variant (NagZ*) in which an essential aspartic acid residue at the catalytic
164 site (Bacik et al., 2012) was replaced with an alanine (**Figure 2–Figure supplement 3A**). NagZ removed the
165 Glc*N*Ac moiety from both types of muropeptides and, in each case, hydrolyzed all detectable muropeptide
166 variants, irrespective of the length of the peptide or the degree of crosslinkage (**Figure 2C and Figure 2–**
167 **Figure supplement 3B**). By contrast, NagZ* did not show any activity. Thus, similar to its *E. coli* homolog
168 (Cheng et al., 2000), NagZ acts as an *N*-acetyl-β-D-glucosaminidase with broad substrate specificity.
169 Together, these findings demonstrate that *C. crescentus* possesses the enzymes mediating the two initial
170 key steps of PG recycling.

171 In *E. coli*, PG turnover products are imported by various transporters with different binding specificities
172 (Gilmore and Cava, 2025), but only AmpG recognizes muropeptides containing a Glc*N*Ac–anhMur*N*Ac unit,
173 as typically produced by LTs (Chang et al., 2025; Cheng and Park, 2002; Jacobs et al., 1994). To clarify
174 whether the AmpG homolog of *C. crescentus* has a similar role, we used a metabolomics approach to
175 detect imported anhydro-muropeptides, using the NagZ cleavage products anhMur*N*Ac-pentapep-
176 tide, -tetrapeptide and -tripeptide as a proxy (**Figure 3A**). In the wild-type strain, the levels of these PG
177 fragments were close to the detection limit, suggesting that they are rapidly processed into smaller units.
178 Consistent with this notion, and in line with previous results (Jacobs et al., 1994; Simpson et al., 2023), a
179 strong accumulation of these species was observed in a Δ*amiR* mutant, which lacks the amidase to remove
180 the peptide stem (**Figure 3B**). Upon the deletion of *ampG* in the Δ*amiR* background, the three anhydro-

181 muropeptides were again barely detectable, confirming that AmpG functions as the primary importer of
182 LT-generated PG degradation products in *C. crescentus*.

183 The analysis of cytoplasmic PG degradation intermediates also provided a means to obtain further insight
184 into the nature and relevance of the reactions catalyzed by AmiR and NagZ. Consistent with the results of
185 the *in vitro* activity assays (compare **Figure 2C**), the accumulation of anhMur*N*Ac-peptide species in the
186 absence of AmiR (**Figure 3B**) shows that NagZ can hydrolyze the glycosidic bond in the Glc*N*Ac–anhMur*N*Ac
187 unit while the peptide stem is still attached. Moreover, it indicates that the reaction catalyzed by AmiR is
188 a bottleneck in the PG recycling pathway, because the removal of the peptide appears to be critical for
189 downstream reactions to occur. To clarify whether cleavage of the Glc*N*Ac–anhMur*N*Ac bond was required
190 to further process the disaccharide unit after peptide removal, we assessed the levels of the free disac-
191 charide in different mutant background. Metabolomics analysis revealed that Glc*N*Ac–anhMur*N*Ac was
192 barely detectable in the wild-type strain, suggesting that AmiR catalyzes the rate-limiting step in the initial
193 decomposition of anhydro-muropeptides. The disaccharide was also not enriched in Δ*ampG* and Δ*amiR*
194 cells, but highly accumulated in the Δ*nagZ* mutant (**Figure 3C**). Thus, the two sugars need to be separated
195 before further processing steps can initiate.

196 Together, our analyses verify that *C. crescentus* possesses the machinery required to import anhydro-
197 muropeptides and break them down into their sugar and peptide components. Moreover, they indicate
198 that AmiR and NagZ have a broad binding specificity, so that the initial steps of the recycling process do
199 not occur in a strictly linear fashion.

200 **PG recycling is necessary for proper cell division and β-lactam resistance in *C. crescentus***

201 Although a considerable fraction of the PG sacculus is turned over and recycled during each cell division
202 cycle, the model species *E. coli* and *P. aeruginosa* typically do not display any obvious morphological
203 phenotype upon disruption of the PG recycling pathway (Gilmore and Cava, 2025). The only exception are
204 *E. coli* cells with a defect in the DD-carboxypeptidase LdcA, which promotes the erroneous ligation of UDP-
205 Mur*N*Ac with unprocessed tetrapeptides, blocking the addition of the terminal D-Ala–D-Ala unit and
206 inducing cell lysis in the stationary growth phase (Templin et al., 1999). To determine the relevance of PG
207 recycling in *C. crescentus*, we examined the morphology of Δ*ampG*, Δ*amiR* and Δ*nagZ* cells growing in rich
208 (PYE) medium by light microscopy. In each case, the mutation caused significant cell filamentation and
209 widening, with the defects becoming more pronounced upon transition of the cells from the exponential
210 to the stationary growth phase (**Figure 4A,B**). Notably, strains in which *amiR* and *nagZ* genes were replaced
211 with alleles encoding the catalytically inactive AmiR* or NagZ* showed phenotypes similar to those of the

212 respective deletion mutants, verifying that the defects observed were due to the absence of the enzymatic
213 activities (**Figure 4–Figure supplement 1**). These results indicate that PG recycling is critical for proper cell
214 division and, to some extent, also lateral growth in *C. crescentus*, particularly under nutrient limitation.
215 Notably, the lack of AmpG or AmiR, which prevents the recycling of the peptide stem (**Figure 3B**), caused
216 a more severe phenotype than the lack of NagZ, which blocks the processing of the free Glc*N*Ac–
217 anhMur*N*Ac disaccharide (**Figure 3C**). Therefore, the supply of amino acids rather than sugars appears to
218 be the major limiting factor in PG precursor biosynthesis. To further investigate the effect of nutrients on
219 the phenotypes of the different mutant strains, we also analyzed cells grown to stationary phase in
220 minimal (M2G) medium. Interestingly, none of the mutant strains showed obvious morphological defects
221 under these conditions (**Figure 4–Figure supplement 2**), suggesting that PG recycling is less important at
222 lower growth rates or that the high glucose content of M2G medium compensates for the lack of PG
223 recycling by promoting *de novo* PG synthesis.

224 Apart from promoting growth, PG recycling was found to critically contribute to the regulation of β-lactam
225 resistance in *C. freundii* and *P. aeruginosa*, because these species use the level of anhMur*N*Ac-pentapep-
226 tide as a readout to sense the presence of β-lactams and control the production of the β-lactamase AmpC
227 (Dietz et al., 1997; Dik et al., 2018; Jacobs et al., 1997). Previous work has also suggested a link between
228 PG recycling and β-lactam resistance in *C. crescentus* (Modi et al., 2025), which produces a metallo-β-
229 lactamase (BlaA) conferring intrinsic high-level resistance to ampicillin and related β-lactam antibiotics
230 (Docquier et al., 2002; West et al., 2002). To further clarify the underlying mechanism, we analyzed the
231 ability of the *C. crescentus* Δ*ampG*, Δ*amiR* and Δ*nagZ* mutants to grow on nutrient-agar (PYE) plates at
232 different ampicillin concentrations (**Figure 4C**). Wild-type cells tolerated high levels (50 µg/mL) of the anti-
233 biotic without any apparent fitness defects. In comparison, all three mutant strains showed a significant
234 reduction in ampicillin resistance. The strongest effect was observed for Δ*amiR* cells, whose sensitivity
235 approached that of Δ*blaA* cells (**Figure 4C**). Surprisingly, the Δ*ampG* mutant showed the least pronounced
236 resistance phenotype, although it exhibited the largest fraction of filamentous cells (compare **Figure 4A,B**),
237 indicating that the defects in β-lactam resistance and cell morphology are not strictly connected. Together,
238 these findings show that PG recycling is important for proper growth and β-lactam resistance in *C. cres-*
239 *centus*.

240 Notably, previous work has shown that inactivation of the divisome-associated soluble LT SdpA also leads
241 to a severe decrease in ampicillin resistance in otherwise wild-type cells (Zielinska et al., 2017). This
242 observation suggested that SdpA could represent the main LT in *C. crescentus*, producing the largest share
243 of the anhydro-muropeptides that are fed into the PG recycling pathway. Consistent with this notion, cells

244 lacking SdpA were highly sensitive to even low concentrations of ampicillin (**Figure 4–Figure supplement**
245 **3A**). Surprisingly, however, their resistance defect was more pronounced that of any of the PG recycling-
246 deficient mutants investigated (compare **Figure 4C**). Moreover, in accordance with previous work, Δ*sdpA*
247 cells did not show any signs of cell filamentation, indicating that their reduced ampicillin resistance may
248 not be primarily due to a decrease in the supply of anhydro-muropeptides available for PG recycling (**Figure**
249 **3–Figure supplement 3B,C**). Metabolomics analysis indeed showed that the absence of SdpA barely
250 affected the levels of cytoplasmic anhMur*N*Ac-peptide species accumulating in the Δ*amiR* background
251 (**Figure 3–Figure supplement 3D**). This finding supports the idea that SdpA is not the main producer of
252 anhydro-muropeptides and likely affects β-lactam resistance through a different pathway, e.g., by contri-
253 buting to proper cell wall biosynthesis and/or maintenance.

254 **The recycling of Glc*N*Ac involves two partially redundant enzymatic systems**

255 After removal of the peptide and cleavage of the Glc*N*Ac–anhMur*N*Ac moiety, the two sugars are recycled
256 in different ways. In *E. coli*, Glc*N*Ac is transformed to Glc*N*Ac-6-P by NagK, which is then reintroduced into
257 *de novo* PG biosynthesis by conversion into GlcN-6-P, catalyzed by the deacetylase NagA (**Figure 1**). Bioin-
258 formatic analysis revealed that this branch of the PG recycling pathway is conserved in *C. crescentus*. Inter-
259 estingly, however, this species contains two NagA homologs (75% identity), which we have named NagA1
260 and NagA2 (**Table 1**). To determine the physiological relevance of Glc*N*Ac recycling, we generated *C. cres-*
261 *centus* Δ*nagK*, Δ*nagA1* and Δ*nagA2* mutants and analyzed their cell morphologies and resistance to
262 ampicillin. None of the strains showed a significant morphological (**Figure 5A,B**) or resistance (**Figure 5C**)
263 phenotype, again suggesting that the supply of sugars is not a major constraining factor in PG biosynthesis.
264 Since it was conceivable that NagA1 and NagA2 had redundant functions, we also aimed to generate a
265 double mutant lacking both *nagA* homologs to fully interrupt the second reaction of the Glc*N*Ac recycling
266 branch. Surprisingly, this was not possible, even though blocking the first step by deletion of *nagK* did not
267 cause any obvious fitness defect, suggesting that the accumulation of Glc*N*Ac-6-P in the complete absence
268 of NagA activity (Plumbridge, 2009) may be toxic to the cells, possibly by allosterically activating the GlcN-
269 6-P deaminase NagB (Álvarez-Añorve et al., 2016) and thus preventing *de novo* PG biosynthesis.

270 In *E. coli*, the expression of *nagA* is controlled by Glc*N*Ac-6-P, which interacts with the transcription factor
271 NagC, thereby converting it from a repressor to an activator (Plumbridge, 1991). The system can also be
272 activated by periplasmic Glc*N*Ac, because *E. coli* possesses a phosphotransferase system (PTS) permease
273 (NagE) that takes up and concomitantly phosphorylates this sugar, releasing it in the cytoplasm as Glc*N*Ac-
274 6-P (Mukhija and Erni, 1996; Plumbridge, 2009). Since *C. crescentus* possesses two *nagE* homologs (**Table**
275 **1**), we decided to analyze its response to externally added Glc*N*Ac to better understand the regulation of

276 NagA1 and NagA2 in this species. Comparing the total proteomes of wild-type cells grown in minimal
277 (M2G) medium with or without Glc*N*Ac, we found that the presence of sugar strongly stimulated the ex-
278 pression of two distinct but similar gene clusters, containing *nagA1* and *nagA2* respectively (**Figure 5D,E**).
279 One of these clusters (CCNA_00452-CCNA_00458) has previously been implicated in the uptake and meta-
280 bolism of Glc*N*Ac in *C. crescentus*, based on the fact that it includes a gene for an outer-membrane TonB-
281 dependent receptor that transports Glc*N*Ac and is essential for its utilization (Eisenbeis et al., 2008). The
282 other genes in the cluster encode a NagE-like PTS permease, its cognate PTS phosphotransferase, NagA2
283 and a NagB homolog (**Figure 5E**), thus providing the complete set of proteins required to import Glc*N*Ac
284 from the periplasm and then funnel it either into PG biosynthesis or central caron metabolism (see **Figure**
285 **1**). Finally, the cluster contains genes for a β-*N*-acetylhexoaminidase, catalyzing the release of Glc*N*Ac from
286 chitin oligomers, and a transcriptional regulator of unknown function, which does not have an obvious
287 homolog in *E. coli*. The second cluster (CCNA_00566-CCNA_00574) includes homologs of all the above-
288 mentioned genes and additionally features genes for a predicted mannosidase and a predicted mannonate
289 dehydratase, suggesting that it could be additionally involved in the metabolism of mannose derivatives.
290 Collectively, the results of the mutational and proteomics analyses suggest that NagA1 and NagA2 are
291 functionally redundant enzymes whose synthesis is activated by their substrate Glc*N*Ac-6-P.

292 **anhMur*N*Ac is recycled through the MurU pathway**

293 Bioinformatic analysis suggested that *C. crescentus* contains all enzymes of the *P. aeruginosa* MurU path-
294 way, which recycles anhMur*N*Ac independently of the Glc*N*Ac recycling branch, converting it directly back
295 to UDP-Mur*N*Ac (Borisova et al., 2017; Fumeaux and Bernhardt, 2017; Gisin et al., 2013) (**Figure 1** and
296 **Table 1**). To verify the functionality of this predicted pathway and clarify its impact on cell physiology, we
297 introduced deletions in the *anmK* or *amgK* gene, thereby blocking essential steps in the reaction sequence.
298 Microscopic analysis revealed that resulting single mutants did not have any significant morphological
299 defects (**Figure 6A,B**). Importantly, however, both strains showed a moderate increase in their
300 susceptibility to ampicillin (**Figure 6C**). This finding indicates that the MurU pathway is active and relevant
301 for β-lactam resistance in *C. crescentus*, thus playing a more important role than the Glc*N*Ac recycling
302 branch (compare **Figure 5A-C**). To determine whether this pathway was the only means for *C. crescentus*
303 to metabolize anhMur*N*Ac, we tested whether its disruption would lead to an accumulation of recycling
304 intermediates. Metabolomics analysis indeed revealed a considerable increase in the cytoplasmic level of
305 Mur*N*Ac in cells lacking the Mur*N*Ac kinase AmgK, suggesting the absence of alternative recycling
306 pathways for the anhMurNAc moiety (**Figure 6D**). Notably, previous work has shown that the formation
307 of UDP-Mur*N*Ac from recycled anhMur*N*Ac by the MurU pathway reduces the sensitivity of *P. aeruginosa*

308 to the antibiotic fosfomycin, which inhibits MurA and thus hinders the *de novo* synthesis of this central PG
309 precursor (Borisova et al., 2014). We reasoned that this effect should also be observable in *C. crescentus*
310 if the MurU pathway was active in this species. Antibiotic resistance assays revealed that the Δ*amgK*
311 mutant indeed showed higher sensitivity to fosfomycin than the wild-type strain or the Δ*nagK* mutant,
312 which is defective in Glc*N*Ac recycling (**Figure 6E**). Taken together, these findings strongly suggest that
313 anhMur*N*Ac is recycled via the MurU pathway in *C. crescentus*, thereby enhancing the supply of precursors
314 for peptidoglycan biosynthesis. This process may be more significant than Glc*N*Ac recycling (compare
315 **Figure 5A-C**) because a reduced production of GlcN-6-P may be compensated by an increased production
316 of this intermediate from fructose-6-phosphate, supplied by central carbon metabolism.

317 As the recycling of Glc*N*Ac and anhMur*N*Ac is mediated by two distinct metabolic routes, cells blocked in
318 one of these routes can still recycle half of the sugars generated by anhydro-muropeptide processing,
319 potentially explaining the relatively mild phenotypes observed for the different single mutants. To clarify
320 the effect caused by inhibiting both sugar recycling pathways, we generated a Δ*nagK* Δ*amgK* double
321 mutant and analyzed its cell morphology and ampicillin resistance. Cells of this strain showed a slightly
322 higher tendency to form filaments than the wild-type strain (**Figure 7A,B**). Interestingly, however, its
323 susceptibility to ampicillin was not reduced beyond the level seen for the Δ*amgK* single mutant (**Figure C**).
324 This observation may be attributed to the presence of Glc*N*Ac in the rich medium used to grow the cells,
325 which can be taken up and concomitantly phosphorylated by the NagE1 and NagE2 permease systems,
326 thereby compensating for the loss of the Glc*N*Ac kinase activity normally provided by NagK (see **Figure 1**).

327 **Defects in PG recycling do not change the levels or activity of the β-lactamase BlaA**

328 In gammaproteobacteria such as *P. aeruginosa* and *C. freundii*, β-lactam resistance is established by in-
329 creased synthesis of the β-lactamase AmpC in the presence of excess anhydro-muropentapeptide, mediat-
330 ed by the transcriptional regulator AmpR (Dietz et al., 1997; Dik et al., 2018; Jacobs et al., 1997). Previous
331 work has suggested that the *C. crescentus* β-lactamase BlaA is constitutively active (Docquier et al., 2002;
332 Modi et al., 2025), raising the question of how its protective effect could be dependent on PG recycling.
333 To address this conundrum, we aimed to reinvestigate the regulaton of BlaA activity at the transcriptional,
334 protein accumulation and activity level.

335 Inspecting the genomic contexts of PG recycling genes (**Table 1**), we found that *amiR* is located in a three-
336 gene operon that also includes genes for a predicted drug/metabolite transporter (named TraX) and a
337 PaiB-family transcriptional regulator (named RegX), suggesting that these proteins could be involved in PG
338 recycling and/or the regulation of β-lactam resistance (**Figure 8–figure supplement 1A**). However, in line

339 with the dominant role of the permease AmpG in anhydro-muropeptide import (see **Figure 3**), the absence
340 of TraX did not markedly affect the accumulation of anhMur*N*Ac-peptides observed in the Δ*amiR* back-
341 ground. Similarly, whole-cell proteome analysis showed that the regulon of RegX did not include *blaA* or
342 any genes related to PG recycling. Apart from this, neither Δ*traX* nor Δ*regX* showed any obvious defects in
343 cell division or ampicillin resistance, indicating that these two genes are not involved in PG-related pro-
344 cesses (**Figure 8–figure supplement 1B-F**).

345 Interestingly, the *blaA* gene is located in a five-gene operon, which additionally encodes a predicted trans-
346 criptional regulator and three proteins involved in methionine biosynthesis (**Figure 8A**). To test whether
347 the expression of this operon changes in response to β-lactam stress or disruption of the PG recycling
348 pathway, we fused its upstream region (400 bp) to a β-galactosidase reporter gene (*lacZ*) and analyzed it
349 for promoter activity in the Δ*ampG*, Δ*amiR* and Δ*nagZ* backgrounds both in the absence or in the presence
350 of ampicillin. The results showed that *lacZ* expression was constant in all conditions tested (**Figure 8B**),
351 indicating that the operon as a whole was not subject to transcriptional regulation. However, it was possi-
352 ble that the transcriptional regulator controlled *blaA* expression by acting on an internal promoter. To test
353 this hypothesis, we compared the whole-cell proteomes of the wild-type strain and a mutant lacking the
354 regulatory gene (CCNA_02225). Surprisingly, in the mutant strain, the methionine biosynthetic proteins
355 encoded by the genes flanking *blaA* were significantly upregulated, whereas the levels of BlaA remained
356 essentially unchanged (**Figure 8–figure supplement 2**). This finding may suggest that *blaA* is expressed
357 from a strong and constitutive internal promoter, so that moderate changes in the transcription of the
358 whole operon do not markedly affect the overall levels of the *blaA* transcripts (Plumbridge, 1996). Finally,
359 we tested whether the activity of BlaA could be regulated post-transcriptionally at the level of enzyme
360 activity. To this end, we incubated cells with the chromogenic β-lactam nitrocefin (O'Callaghan et al., 1972)
361 and used its property of developing red color upon cleavage to measure β-lactamase activity *in vivo*. We
362 found the Δ*ampG*, Δ*amiR* and Δ*nagZ* mutants showed behaviors similar to that of the wild-type strain,
363 while the Δ*blaA* mutant lacked activity, validating the assay (**Figure 8C**). Consistent with this finding, whole-
364 cell proteomic analyses showed that cells impaired in PG recycling accumulated BlaA at levels comparable
365 to those in the wild-type strain (**Figure 8D**). Collectively, these results demonstrate that the severe reduc-
366 tion in β-lactam resistance observed in PG recycling-deficient strains is not due to changes in BlaA accu-
367 mulation or activity. This conclusion is supported by the results of growth assays showing that defects in
368 the PG recycling pathway also reduce the resistance of cells to aztreonam, a β-lactam antibiotic that is not
369 cleaved by metallo-β-lactamases such as BlaA (Bush et al., 1982) (**Figure 8E**). Thus, the ampicillin sensitivity

370 phenotypes observed are likely due to changes in the susceptibility and/or activity of target proteins rather
371 than impaired degradation of this antibiotic in the absence of PG recycling.

372 **PG recycling defects sensitize the PG biosynthetic machinery to the inhibitory effect of ampicillin**

373 To shed more light on the connection between PG recycling and β-lactam resistance, we aimed to investi-
374 gate the growth defects induced by the exposure of cells to ampicillin in more detail. To this end, we
375 cultivated wild-type and Δ*amiR* cells in liquid medium containing different concentrations of the antibiotic
376 and analyzed their morphology by light microscopy. Wild-type cells tolerated substantial concentrations
377 of ampicillin without noticeable changes in cell shape (**Figure 9A,B**). However, at 500 µg/mL, they devel-
378 oped a pronounced filamentous phenotype, while exposure to 5,000 µg/mL led to growth arrest and cell
379 lysis. For the Δ*amiR* mutant, similar phenotypes were observed, but cell filamentation and lysis already
380 occurred at the lowest ampicillin concentration tested and were consistently more pronounced than for
381 the wild type across all conditions (**Figure 9A,B**). To better characterize the development of the observed
382 morphological defects, we monitored the growth behavior of the two strains following a shift from plain
383 rich medium to medium supplemented with a low concentration of ampicillin (20 µg/ml). Whereas the
384 wild-type strain grew normally in both conditions (**Figure 9C** and **Figure 9–video 1**), Δ*amiR* cells started to
385 become filamentous and swollen shortly after exposure to the antibiotic and were unable to divide (**Figure**
386 **9C** and **Figure 9–video 2**). Together, these results indicate that, in *C. crescentus*, ampicillin preferentially
387 targets cell division, although it also affects lateral growth when applied at elevated concentrations. More-
388 over, they suggest that PG recycling defects enhance the efficacy of ampicillin by rendering the PG biosyn-
389 thetic machinery more sensitive to its inhibitory effect.

390 To shed more light on the inhibitory activity of ampicillin, we aimed to identify its target proteins. For this
391 purpose, we adapted an assay enabling the visualization of PBPs in SDS-gels after labeling with the fluor-
392 escent β-lactam bocillin-FL (Zhao et al., 1999). Using Δ*blaA* cells to prevent β-lactam degradation, this
393 approach detected all known functional transpeptidases of *C. crescentus* except for PBP2 (Strobel et al.,
394 2014; Yakhnina and Gitai, 2013) as well as the predicted carboxypeptidase CrbA (**Figure 9D**). However,
395 when these proteins were incubated with ampicillin prior to the addition of bocillin-FL, all but one of them
396 (PbpX) remained unlabeled, indicating that ampicillin had blocked their active-site serine, thereby prevent-
397 ing the subsequent reaction with bocillin-FL. Among the ampicillin targets identified were the essential,
398 cell division-specific monofunctional transpeptidase PBP3 as well as the bifunctional PBPs Pbp1A, PbpY
399 and PbpC. The labeling of PBP3 and some bifunctional PBPs was also abolished by preincubation with
400 cephalexin, a β-lactam that specifically targets PBP3 in *E. coli* (Kocaoglu and Carlson, 2015), whereas the
401 PBP2-specific β-lactam mecillinam had only minor effects on the labeling pattern (**Figure 9D**). Given that

402 Pbp1A, PbpY and PbpC have been shown to be dispensible for cell division in *C. crescentus* (Strobel et al.,
403 2014; Yakhnina and Gitai, 2013), these results indicate that the cell filamentation phenotype induced by
404 ampicillin is primarily due to inhibition of PBP3 activity.

405 **PG recycling defects may increase ampicillin sensitivity by limiting the supply of PG precursors**

406 The results obtained suggest that impaired PG recycling does not affect BlaA activity and may rather en-
407 hance the inhibitory effect of ampicillin on PG biosynthesis. It was conceivable that the accumulation of
408 unrecycled PG degradation products in the periplasm could impair the activity of certain PG biosynthetic
409 enzymes, thereby disrupting PG homeostasis. However, sacculi isolated from wild-type and Δ*amiR* cells
410 did not show any significant differences in their muropeptide composition (**Figure 9–figure supplement**
411 **1**), suggesting that a defect in PG recycling does not perturb the global balance of PG biosynthetic and
412 autolytic processes. Notably, mutants blocked in the PG recycling pathway also exhibit a conditional cell
413 division defect, even when not exposed to ampicillin. It was therefore possible that their higher β-lactam
414 sensitivity was linked to a decrease in the overall efficiency of PG biosynthesis, caused by impaired replen-
415 ishment of PG precursors from recycling products. Metabolomics analysis revealed that the Δ*ampG*, Δ*amiR*
416 and Δ*nagZ* mutants indeed showed significantly lower levels of UDP-sugars than the wild-type strain (**Fig-**
417 **ure 9E**). The absence of AmpG and NagZ led to a more than 50% decrease in the UDP-Glc*N*Ac pool, confirm-
418 ing that *de novo* synthesis alone is not sufficient to satisfy the cellular demand for this central metabolite.
419 By contrast, UDP-Glc*N*Ac levels remained unchanged in Δ*amiR* cells, consistent with the observation that
420 Glc*N*Ac can still be released from imported anhydro-muropeptides in the absence of amidase activity (see
421 **Figures 2C** and **3C**). Even stronger effects were observed on the UDP-Mur*N*Ac pool, which was drastically
422 reduced in all three mutant strains (**Figure 9E**). Its depletion in the absence of PG recycling suggests that
423 the formation of UDP-Mur*N*Ac constitutes a bottleneck in the *de novo* PG biosynthetic pathway, with cells
424 relying heavily on anhMur*N*Ac recycling via the MurU pathway to maintain an adequate supply. Collec-
425 tively, these results demonstrate that PG recycling is critical to provide sufficient activated sugars for PG
426 precursor biosynthesis. However, although the Δ*ampG*, Δ*amiR* and Δ*nagZ* mutants show a very similar
427 decrease in cytoplasmic UDP-Mur*N*Ac levels, their morphological and resistance defects differ significant-
428 ly, indicating that the reduced availability of UDP-sugars may not be the only reason for the phenotypes
429 observed. Consistent with this notion, an increase in cytoplasmic Glc*N*Ac-P levels through supplementa-
430 tion of the growth medium with Glc*N*Ac (see **Figure 5**) was not sufficient to improve ampicillin tolerance
431 in the three mutant strains (**Figure 9–figure supplement 2**).

432 It was conceivable that the limited supply of PG precursors in the absence of proper PG recycling causes
433 cell filamentation and lysis by reducing the level of association between PBPs and their substrates, thereby

434 slowing their catalytic activity. To test this idea, we investigated whether the cell division defect of the
435 Δ*amiR* mutant could be ameliorated by artificially increasing the activity of the septal PG biosynthetic
436 machinery. To this end, employed a hyperactive (A246T) variant of the glycosyltransferase FtsW (FtsW*)
437 that leads to increased activity of the septal FtsW-PBP3 PG biosynthetic complex (Lariviere et al., 2019;
438 Modell et al., 2014), resulting in elevated cell constriction rates and shorter cell lengths, especially in
439 stationary phase (**Figure 10A,B**). Interestingly, introduction of the *ftsW** allele almost completely rescued
440 the cell filamentation phenotype of the Δ*amiR* mutant in stationary phase, although it had only little effect
441 in exponentially growing cells, possibly because PG precursors are more limiting under conditions of rapid
442 growth. Thus, hyperactivation of the FtsW-PBP3 complex can, at least in part, reverse the cell division
443 defect induced by defective PG recycling, suggesting that the cell filamentation phenotype observed in the
444 mutant backgrounds could indeed be due to a reduced activity of this complex. Notably, however, the
445 presence of the *ftsW** allele did not relieve the ampicillin sensitivity of Δ*amiR* cells (**Figure 10C**), indicating
446 that an increased activity of the septal PG biosynthetic complex does not reduce its ampicillin-mediated
447 inactivation.

Discussion

448 Bacterial PG biosynthesis has been studied intensively over the past decades. Importantly, apart from the
449 proper spatiotemporal control of peptidoglycan incorporation and cleavage during cell growth and cell
450 division, the recycling of PG degradation products has emerged to play a major role in cellular fitness and
451 survival. This process not only conserves valuable resources (Gilmore and Cava, 2025) but also plays an
452 important role in infection by enabling bacteria to evade the human innate immune system (Trindade and
453 Chen, 2020). Moreover, it was found to critically contribute to AmpR-mediated regulation of β-lactam
454 resistance in *P. aeruginosa* and various enterobacterial pathogens (Dik et al., 2018). Although substantial
455 advances have been made in elucidating the mechanisms and physiological roles of PG recycling within
456 Gammaproteobacteria, these aspects remain incompletely characterized across other bacterial lineages
457 (Gilmore and Cava, 2025). In this study, we demonstrate that the alphaproteobacterial model organism
458 *C. crescentus* possesses a functional PG recycling pathway that includes components from both the *E. coli*
459 and *P. aeruginosa* systems, extending the results of a recent study on this topic (Modi et al., 2025). We
460 find that its function is required for maintaining an adequate supply of peptidoglycan precursors, com-
461 plementing *de novo* synthesis. *C. crescentus* cells impaired in PG recycling show marked defects in cell
462 division and cell wall integrity, in particular upon transition to the stationary growth phase. Moreover,
463 they exhibit a pronounced decrease in intrinsic β-lactam resistance, although the levels and activity of
464 their major β-lactamase BlaA remain unchanged. Blocking critical steps in the recycling pathway therefore
465 emerges as a promising new strategy to combat β-lactam resistant pathogens and thus mitigate the global
466 antibiotic crisis.

467 Our analyses revealed that *C. crescentus* possesses almost all core PG recycling enzymes identified in gam-
468 maproteobacteria. Notable exceptions are the LD-CPase LdcA (Templin et al., 1999), which trims sugar-
469 linked and free tetrapeptides to tripeptides, as well as the murein peptide ligase Mpl, which re-attaches
470 free peptide stems to UDP-Mur*N*Ac, thereby obviating the need for their *de novo* synthesis (Mengin-
471 Lecreulx et al., 1996). In *E. coli*, the activity of LdcA is critical for cell envelope integrity, because its inactiv-
472 ation leads to the accumulation of free tetrapeptides, which are then erroneously ligated with UDP-
473 Mur*N*Ac, giving rise to non-crosslinkable tetrapeptide-containing PG precursors, whose incorporation into
474 peptidoglycan severely destabilizes the cell wall structure (Templin et al., 1999). In some gammaproteo-
475 bacteria, the function of LdcA is taken over by other, unrelated peptidases (Dai et al., 2021; Hernández et
476 al., 2020; Simpson et al., 2021), opening the possibility that *C. crescentus* possesses a thus-far unknown
477 peptide-processing LD-CPase. However, metabolomic analysis showed that Δ*amiR* cells accumulated high
478 concentrations of anhMur*N*Ac-tetrapeptide in their cytoplasm (**Figure 3B**), making the existence of such

479 an enzyme unlikely. In line with the absence of Mpl, *C. crescentus* may thus not recycle tripeptides but
480 rather degrade peptide stems released by AmiR into individual amino acids, which are subsequently re-
481 used for *de novo* PG biosynthesis. A similar situation may be seen for many other Gram-negative and Gram-
482 positive species that lack both an LdcA and an Mpl homolog (Gilmore and Cava, 2025).

483 Apart from the removal of the peptide stem by AmiR, the cleavage of the Glc*N*Ac–anhMur*N*Ac moiety by
484 NagZ is a critical step in the initial processing of imported anhydro-muropeptide species. The results of our
485 enzyme assays (**Figures 2**) and metabolomic analyses (**Figure 3**) show that these two reactions do not
486 follow a defined order but occur independently of each other. Once released, the two amino sugars follow
487 distinct metabolic routes. Glc*N*Ac is phosphorylated to Glc*N*Ac-6-P and then deacetylated by NagA, yield-
488 ing GlcN-6-P, which is then either used as the starting point of *de novo* PG biosynthesis or, alternatively,
489 fed into central carbon metabolism through deamination to frucose-6-P by NagB (**Figure 1**). This branch
490 point is critical since Glc*N*Ac is not only produced during peptidoglycan degradation but also acquired from
491 the environment as a readily available carbon source, primarily derived from the breakdown of chitin
492 (Beier and Bertilsson, 2013). In the presence of external GlcNAc, two related gene clusters are highly
493 upregulated, each of them including genes for an outer-membrane TonB-dependent receptor, a PTS
494 permease together with its cognate phosphorylation system as well as a homolog of the deacetylase NagA
495 and the deaminase NagB (**Figure 5D,E**). Their regulation is likely mediated by GntR-type transcriptional
496 regulators encoded in the same clusters, which may sense the accumulation of Glc*N*Ac-6-P as the first
497 common cytoplasmic intermediate of the PG recycling and Glc*N*Ac uptake pathways, thereby adapting the
498 flux through the Glc*N*Ac recycling/utilization pathway to substrate availability. While one of the TonB-
499 dependent receptors (CCNA_00455) was shown to be specific for Glc*N*Ac (Eisenbeis et al., 2008), the
500 substrate range of the other transport systems still remains to be determined. Overall, the Glc*N*Ac
501 recycling/utilization system of *C. crescentus* shows parallels to that of *E. coli*, which also involves two
502 different PTS permeases, NagE and ManXYZ, for Glc*N*Ac transport (Plumbridge and Vimr, 1999). However,
503 *E. coli* lacks a Glc*N*Ac-specific TonB-dependent receptor, shows a different organization and regulation of
504 the genes involved and only possesses a single set of NagA and NagB proteins. Even more pronounced
505 differences are observed for the recycling of anhMur*N*Ac, which in both species initiates with the
506 formation of anhMur*N*Ac-6-P. In *E. coli*, this intermediate is converted to Glc*N*Ac-6-P by the etherase MurQ
507 and thus funneled into the Glc*N*Ac recycling pathway (Jaeger et al., 2005; Uehara et al., 2006). *C. cresentus*,
508 by contrast, lacks this enzyme and instead uses the alternative MurU pathway, a short-cut that transforms
509 Mur*N*Ac-6-P to UDP-Mur*N*Ac and thus feeds it back directly into PG biosynthesis (**Figures 6 and 7**). This
510 pathway has so-far only been observed in a few other species such as the gammaproteobacteria *P. aeru-*

511 *ginosa* (Borisova et al., 2017; Fumeaux and Bernhardt, 2017; Gisin et al., 2013) and *Legionella pneumophila*
512 (Ratna et al., 2025) as well as *Tannerella forsythia* (Hottmann et al., 2021), a member of the Bacteroidia.
513 Our results, combined with those of a previous study (Modi et al., 2025), show that it is more widespread
514 than previously anticipated and also conserved in the alphaproteobacterial lineage.

515 In previously studied model species, PG recycling was found to be dispensable under laboratory conditions
516 and defects in this process did not lead to any obvious morphological defects (Gilmore and Cava, 2025),
517 except for the lack of LdcA, which causes cell rounding and lysis in stationary phase in *E. coli* (Templin et
518 al., 1999). In *C. crescentus*, it was also possible to introduce single deletions in all PG recycling-related
519 genes, although it was not possible to create a strain lacking both *nagA* homologs simultaneously, suggest-
520 ing that the accumulation of Glc*N*Ac-6-P may be toxic to the cells. Notably, however, and contrary to a
521 previous report (Modi et al., 2025), most mutants displayed cell division defects and cell filamentation,
522 especially when transitioning to stationary phase. These phenotypes were particularly pronounced for
523 Δ*ampG* and Δ*amiR* cells, which are impaired in anhydro-muropeptide uptake or peptide stem cleavage. By
524 contrast, single disruptions in the sugar recycling pathways generally did not result in cell elongation,
525 suggesting that the observed filamentation phenotype is linked to impaired peptide recycling. Interesting-
526 ly, while completely abolishing sugar recycling through inactivation of NagZ did not cause any obvious
527 morphological defects, blocking both the Glc*N*Ac and anhMur*N*Ac recycling branches led to cell filamen-
528 tation. This conundrum may be explained by the accumulation of metabolic intermediates in the double
529 mutant that may cause misregulation of PG biosynthesis by affecting gene expression or enzyme activities.
530 The precise link between PG recycling and cell division remains to be clarified. However, we observed that
531 blocking the initial steps of PG recycling leads to a severe reduction in the levels of PG precursors such as
532 UDP-Glc*N*Ac and UDP-Mur*N*Ac (**Figure 9E**). This effect may be even more pronounced for the peptide-
533 containing downstream products of the PG biosynthetic pathway, which were not detectable with our
534 methods, in particular in mutant backgrounds preventing the recycling of the peptide stem. Importantly,
535 the cell division defects caused by impaired PG recycling were alleviated by hyperactivation of the FtsW-
536 PBP3 complex (**Figure 10**). Together, these findings suggest that reduced PG precursor levels impair the
537 association of divisome-associated GTases and PBPs with their substrates, leading to lower catalytic rates
538 and a slow-down of cell constriction. This effect may be further aggravated in the presence of ampicillin,
539 because β-lactam-mediated inhibition of transpeptidase activity can hyperactivate the GTase domain of
540 bifunctional PBPs. As a consequence, they produce an abundance of non-crosslinked glycan strands that
541 are rapidly degraded after synthesis, leading to further depletion of the lipid II pool (Banzhaf et al., 2012;
542 Cho et al., 2014; Kohlrausch and Höltje, 1991). Moreover, apart from decreasing PG synthase activity,

543 defects in PG recycling may also cause an accumulation of anhydro-muropeptides in the periplasm, which
544 could potentially interfere with normal PG biosynthesis by occupying binding sites or promoting non-
545 productive side-reactions. Interestingly, elongation appears to continue normally under these conditions,
546 likely because it requires significantly less PG incorporation than cell constriction and the formation of the
547 new cell poles. Notably, the limitation of PG precursors can be compensated by enhancing the overall
548 catalytic activity of the FtsW-PBP3 complex and thereby increasing its reaction rate under conditions of
549 reduced binding site occupancy.

550 Strikingly, defects in PG recycling not only caused cell filamentation but also strongly reduced the intrinsic
551 resistance of *C. crescentus* to ampicillin. This phenomenon was most pronounced for mutants with defects
552 in the first PG recycling steps that completely abolished peptide and/or sugar recycling (**Figure 4**). A milder
553 effect was observed for mutants blocked in the MurU pathway, whereas disrupting Glc*N*Ac recycling did
554 not produce any obvious ampicillin sensitivity phenotype. Our results suggest that the formation of UDP-
555 Mur*N*Ac as the first committed step in PG biosynthesis represents a metabolic bottleneck (**Figure 9E**),
556 making anhMur*N*Ac recycling through the MurU shunt essential for maintaining adequate PG precursor
557 levels. UDP-Glc*N*Ac, by contrast, which is used in the biosynthesis in various cell envelope polysaccharides,
558 can be more readily replenished because its biosynthesis is supported not only by *de novo* synthesis and
559 peptidoglycan (PG) recycling but also by the uptake of external Glc*N*Ac from the growth medium (Eisenbeis
560 et al., 2008) (**Figure 5D,E**). Notably, even high concentrations of external Glc*N*Ac were not sufficient to
561 restore ampicillin resistance in any of the PG recycling-deficient mutants tested (**Figure 9–figure supple-**
562 **ment 2**). Contrary to a previous report (Modi et al., 2025), this finding supports the notion that their β-
563 lactam sensitivity is not attributable to an inadequate supply of Glc*N*Ac for PG precursor biosynthesis.

564 A role of PG recycling in β-lactam resistance has been previously reported for gammaproteobacteria such
565 as *P. aeruginosa* and *C. freundii*. In these species, β-lactam exposure leads to an increase in the cytoplasmic
566 level of anhMur*N*Ac-pentapeptide, thereby stimulating its interaction with the transcriptional regulator
567 AmpR and inducing expression of the *ampC* β-lactamase gene (Dik et al., 2018). However, recent work has
568 indicated that different mechanisms may be at work in Alphaproteobacteria (Gilmore and Cava, 2022;
569 Modi et al., 2025). Our data show that, in *C. crescentus*, the accumulation and activity of the main β-
570 lactamase BlaA remain unchanged in the presence of ampicillin and upon inhibition of PG recycling. The
571 lower ampicillin resistance level of PG recycling-deficient mutants may therefore not be due to less
572 efficient inactivation of ampicillin but rather an increased susceptibility of PBPs to this antibiotic. This
573 effect could potentially be explained by competition of ampicillin and PG precursors for the substrate-
574 binding sites of target PBPs (**Figure 11**). In wild-type cells, the abundant supply of precursor ensures the

575 saturation of PBPs with their cognate substrate. As a consequence, most ampicillin molecules will be
576 cleaved by BlaA before they manage to covalently modify their target proteins, leaving the vast majority
577 of PBPs in a functional state. However, if defects in PG recycling limit the availability of PG precursors, the
578 substrate binding sites of PBPs remain unoccupied for extended periods of time. As a consequence, they
579 become more susceptible to interaction with residual ampicillin molecules, leading to an increase in the
580 fraction of inactive enzymes. The resulting defect in cell division and cell wall integrity may be further
581 aggravated by the reduced activity of the remaining PBPs due to inadequate substrate levels and the
582 interference of periplasmic anhydro-muropeptides with proper PG biosynthesis. In different PG recycling-
583 deficient mutants, these factors may be manifested to varying degrees, which could account for differ-
584 ences in the severity between the cell filamentation and ampicillin sensitivity phenotypes in many of the
585 mutant strains.

586 Collectively, our results demonstrate that PG recycling is critical for proper growth, cell division and β-
587 lactam resistance in *C. crescentus*, thus playing a more significant role in bacterial fitness and survival than
588 previously appreciated. Moreover, they support the idea that bacterial β-lactam resistance is a complex
589 trait, determined not only by specific resistance proteins but also by the supply of PG building blocks and
590 the dynamics of PG biosynthesis. Given the widespread occurrence of PG recycling among bacteria, it will
591 be important to determine the impact of this process on cell viability and antibiotic resistance in other
592 species and to evaluate its inhibition as a potential new strategy to potentiate the efficacy of β-lactam
593 antibiotics in antibacterial therapies.

Methods

Experimental models

594 The bacterial strains used in this study are derivatives of *Caulobacter crescentus* NA1000 (CB15N)
595 (Poindexter, 1964), *Escherichia coli* TOP10 (Thermo Fisher Scientific, Germany) or *Escherichia coli*
596 Rosetta(DE3)pLysS (Merck, Germany). The sequences of all genes and proteins investigated are based on
597 the genome sequence of *C. crescentus* NA1000 (Nierman et al., 2001).

598 **Cultivation of bacterial strains**

599 *C. crescentus* NA1000 (CB15N) and its derivatives were grown at 28 °C in peptone-yeast-extract (PYE) medi-
600 um (Poindexter, 1964), double-concentrated PYE (2xPYE) medium or M2 salts-glucose (M2G) minimal
601 medium (Hottes et al., 2004) under aerobic conditions, shaking at 210 rpm. To prepare PYE plates, liquid
602 medium was solidified by the addition of 1.5% agar. To ensure the maintenance of integrative plasmids,
603 media were supplemented with kanamycin (5 µg/mL for liquid cultures, 25 µg/mL for plates). To counter-
604 select against cells carrying the *sacB* marker, solid PYE medium was supplemented with 3% D-sucrose.
605 *E. coli* TOP10 (Invitrogen, Germany) was used for cloning purposes, whereas *E. coli* Rosetta(DE3)pLysS
606 (Novagen, Germany) was used for protein overproduction. Cells were grown aerobically at 37 °C in LB
607 Broth or on LB Agar (Carl Roth, Germany), supplemented when appropriate with antibiotics at the follow-
608 ing concentrations (µg/mL; liquid/solid): kanamycin (30/50), ampicillin (200/200), chloramphenicol
609 (20/30).

610 **Plasmid and strain construction**

611 The bacterial strains, plasmids and oligonucleotides used in this study are listed in **Tables S1-S3**. *E. coli*
612 TOP10 (Invitrogen) was used as host for cloning purposes. *C. crescentus* was transformed by electropora-
613 tion (Ely, 1991). Gene replacement was achieved by double homologous recombination using the counter-
614 selectable *sacB* marker (Thanbichler and Shapiro, 2006). Proper chromosomal integration or gene replace-
615 ment was verified by colony PCR.

616 **Antibiotic susceptibility assay**

617 Overnight cultures were serially diluted (10^{-2} to 10^{-7}) in PYE medium and spotted on PYE plates containing
618 ampicillin (10-50 µg/mL) or aztreonam (95-105 µg/mL) at the indicated concentrations. When appropriate,
619 the media were additionally supplemented with 0.3% Glc*N*Ac. The plates were incubated for three days at
620 room temperature (25 °C) and imaged using a ChemiDocTM XRS+ Imager (Biorad, Germany) and Image

621 Lab™ software (version 5.0) (Biorad, Germany). To account for the high instability of ampicillin in aqueous
622 solution, ampicillin stocks were prepared freshly before every experiment.

623 The resistance against fosfomycin was assessed using Fosfomycin MIC Test Strips (Liofilchem, Italy). Over-
624 night cultures were diluted with PYE medium to an OD_{600} of 0.1. Subsequently, 100 µL of the suspensions
625 were added to 20 mL of sterile liquid PYE agar that had been cooled to slightly above the gelation temper-
626 ature (~45 °C). After mixing, the suspension was immediately poured into cultivation dishes. After solidifi-
627 cation of the medium, the plates were briefly dried and the test strips were applied on their top. Subse-
628 quently, they were incubated for three days at 28 °C and imaged using a ChemiDocTM XRS+ Imager and
629 Image Lab™ 5.0 software (Bio-Rad Laboratories, Germany).

630 **Widefield fluorescence microscopy**

631 Unless indicated otherwise, cells were grown in PYE medium, transferred to 1% agarose pads and imaged
632 with a Zeiss Axio Imager.Z1 microscope equipped with a Plan Apochromat 100×/1.45 Oil DIC and a
633 100×/1.40 Oil Ph3 M27 phase contrast objective. Images were recorded with a pco.edge 4.2 sCMOS
634 camera (PCO). An X-Cite 120PC metal halide light source (EXFO, Canada) and an ET-DAPI filter cube
635 (Chroma, USA) were used for the detection of fluorescence signals. Images were recorded with VisiView
636 4.0.0.14 (Visitron Systems, Germany) and processed with Fiji 1.53 (Schindelin et al., 2012). Cell length
637 measurements were performed with Oufti (Paintdakhi et al., 2016), using phase-contrast images as an
638 input.

639 **Microfluidics-based ampicillin sensitivity assay**

640 Microfluidic-based imaging was performed using a CellASIC ONIX B04A plate for bacterial cells (Merck,
641 Germany) that was connected to a CellASIC® ONIX2 microfluidic system (Merck, Germany) and imaged
642 with an Zeiss Axio Observer.Z1 (see above) in a heatable enclosure adjusted to 28 °C. Exponentially grow-
643 ing *C. crescentus* wild-type and Δ*amiR* cells were diluted to an OD_{600} of 0.2 and flushed into different cham-
644 bers of the microfluidic plate. They were then first incubated for 3 h with a constant flow of PYE medium
645 and then for 5 h with a constant flow of PYE medium containing 20 µg/mL ampicillin at a pressure of 5 kPa.
646 DIC images were taken at 5-min intervals to follow cell growth and division.

647 **β-lactamase activity assay**

648 ß-lactamase activity was assessed using the chromogenic cephalosporin derivative nitrocefin (Merck,
649 Germany) as a substrate (O'Callaghan et al., 1972). Cells were grown to exponential phase in 3 mL PYE
650 medium, harvested by centrifugation for 5 min at 7,000 ×*g* and room temperature, and resuspended in
651 1 mL PBS. After transfer of the suspensions into a 24-well polystyrene microplate (Carl Roth, Germany),

652 the reactions were started by the addition of 100 µL nitrocefin (1 mg/mL). The hydrolysis of nitrocefin was
653 then monitored by measuring the increase in absorbance at 482 nm every 2 min over a period of 180
654 minutes at 30 °C using an Epoch™ 2 microplate reader (BioTek, California, United States).

655 **Identification of ampicillin target proteins**

656 *C. crescentus* CS606 (Δ*blaA*) cells were grown to exponential phase in 100 mL PYE medium, harvested,
657 washed with PBS and lysed by three passages through a French press at 10,000 psi. Insoluble material,
658 including the membrane fraction, was collected by centrifugation for 15 min at 21,000 ×g (4 °C). After
659 resuspension of the pellet in 2 mL of PBS, 100-µL aliquots were incubated with 0, 1, 10 or 100 µg/mL
660 ampicillin, 5 µg/mL cefalexin or 100 µg/mL mecillinam for 2 h at room temperature. The membranes were
661 collected again by centrifugation (1 min, 13,000 ×g, room temperature), washed twice with PBS and resus-
662 pended in a final volume of 100 µL PBS containing 5 µg/mL Bocillin-FL (Thermo Fisher Scientific, Germany).
663 After 10 min of incubation, the membranes were collected by centrifugation (1 min, 13,000 ×g, room
664 temperature), washed with PBS, dissolved in 30 µL of 2x SDS sample buffer (0.125 M Tris Base, 20 % [v/v]
665 glycerol, 4 % [w/v] SDS, 200 mM DTT, 0.01 % [w/v] bromophenol blue, pH 6.8), heated for 10 min at 90 °C
666 and loaded onto an 8% SDS-polyacrylamide gel. After separation by electrophoresis, proteins labelled with
667 Bocillin-FL were detected with a ChemiDoc™ MP imager (Bio-Rad Laboratories, Germany) using a 526 nm
668 short-pass filter.

669 **β-galactosidase assay**

670 Cultures were grown to exponential phase in PYE medium. After determining the cell densities (OD_{600}), the
671 cells were harvested by centrifugation for 7 min at 12,000 ×*g* and 4 °C and resuspended in 1 mL of Z-buffer
672 (60 mM Na_2PO_4, 40 mM NaH_2PO_4, 10 mM KCl, 1 mM $MgSO_4$, 50 mM β-mercaptoethanol, pH 7.0). Following
673 the addition of 100 µL chloroform and 0.1 % SDS, the suspensions were briefly agitated and then incubated
674 for 7 min at room temperature to permeabilize the cells. 500-µL samples of the suspensions were mixed
675 with 500 µL of Z-buffer. The reactions were then started by the addition of 200 µL *o*-nitrophenyl-β-D-
676 galactopyranoside (4 mg/mL), incubated at room temperature until the mixtures turned yellow, and
677 stopped by the addition of 500 µL 1 M Na_2CO_3. Cell remnants were pelleted by centrifugation and the
678 extinction of the supernatant was measured photometrically at 550 nm and 420 nm. β-galactosidase
679 activities were then calculated as follows: Activity (in Miller units)=$1000*(OD_{420}–1.75*OD_{550})/(t*V*OD_{600})$,
680 where *t* is the time of incubation (min) and *V* the culture volume used for the reaction (mL).

681 **Protein purification**

682 To purify **AmiR and AmiR*** (H26A/H133A/D143A), *E. coli* Rosetta(DE3)pLysS was transformed with plas-
683 mids encoding His_6-SUMO-tagged derivatives (Marblestone et al., 2006) of the proteins (pPR029 or
684 pPR041) and grown in LB medium to an OD_{600} o 0.4. After reduction of the growth temperature to 18 °C,
685 the cultures were supplemented with isopropyl-β-D-thiogalactopyranoside (IPTG) to a final concentration
686 of 1 mM, and incubated further overnight. The cells were harvested by centrifugation (12 min, 5000 ×g,
687 4 °C), washed in buffer A (50 mM Tris-HCl, 500 mM NaCl, 10 mM imidazole, 10% glycerol, pH 7.0) and
688 stored at -80 °C until needed. After thawing, the cells were resuspended in buffer A containing 100 µg/mL
689 phenylmethylsulfonyl fluoride (PMSF) and 10 µg/mL DNaseI and lysed by three passages through a French
690 press at a pressure of 10,000 psi. The lysate was cleared by centrifugation (30 min, 25,000 ×g, 4 °C) and
691 loaded onto a His-Trap HP 5 mL Ni-NTA affinity column (Cytiva, Germany) equilibrated with buffer A. After
692 washing of the column with buffer A, protein was eluted at a flow rate of 2 mL/min with a linear gradient
693 of imidazole generated by mixing buffer A and buffer B (50 mM Tris-HCl, 500 mM NaCl, 250 mM imidazole,
694 10% glycerol, pH 7.0). The peak fractions were pooled, supplemented with SUMO protease (His_6-Ulp)
695 (Marblestone et al., 2006) at a molar ratio of 1:1,000 relative to the purified protein, and dialyzed overnight
696 at 4 °C against buffer C (50 mM Tris-HCl, 500 mM NaCl, 10% glycerol, 1 mM dithiothreitol, pH 7.0). The
697 solution was then loaded again onto a His-Trap HP 5 mL column to remove His_6-SUMO and His_6-Ulp. Flow-
698 through fractions containing the protein of interest were collected, concentrated using Amicon® Ultra cen-
699 trifugation filters (10kDa MWCO; Merck, Germany), and loaded onto a Superdex 75 GL10/300 size-
700 exclusion column (Cytiva, Germany) equilibrated with buffer D (50 mM HEPES-NaOH, 500 mM NaCl, pH
701 7.0) and eluted at a flow rate of 10 mL/min. Fractions containing the protein of interest at high concen-
702 tration and purity were combined, concentrated, snap-frozen in liquid nitrogen and stored at -80 °C until
703 further use.

704 To purify **NagZ and NagZ*** (D259A), His_6-SUMO-tagged derivatives of the proteins were overproduced in
705 *E. coli* Rosetta(DE3)pLysS carrying suitable plasmids (pPR102 or pPR107) as described above. The fusion
706 proteins were then purified on a His-Trap HP 5 mL column, cleaved with SUMO protease, and separated
707 from His_6-SUMO and His_6-Ulp by a second affinity purification step essentially as described for AmiR, with
708 the exceptions that buffers A and B contained 300 mM instead of 500 mM NaCl and buffer C contained
709 150 mM instead of 500 mM NaCl. Flow-through fractions from the His-Trap HP column that contained the
710 protein of interest at high concentration and purity were concentrated, snap-frozen in liquid nitrogen and
711 stored at -80 °C.

712 **Muropeptide analysis**

713 The *C. crescentus* wild type and the Δ*amiR* mutant were grown to stationary phase ($OD_{600} \approx 1.2$) in 400 mL
714 PYE medium and harvested by centrifugation at 16,000 ×*g* and 4 °C for 30 min. The pelleted cells were
715 resuspended in 6 mL of ice-cold double-ionized water ($_{dd}H_2O$) and added dropwise to 6 mL of a boiling
716 solution of 8% sodium dodecylsulfate (SDS), which was vigorously stirred. The suspension was boiled for
717 an additional 30 min, and double-deionized water was added regularly to maintain a constant volume.
718 Subsequently, the lysate was cooled to room temperature and stored at 4 °C until further use. Peptido-
719 glycan was isolated following previously described procedures (Glauner, 1988; Takacs et al., 2010) and
720 digested with the muramidase cellosyl (kindly provided by Hoechst, Frankfurt, Germany). The resulting
721 muropeptides were reduced with sodium borohydride and separated by HPLC as described previously
722 (Takacs et al., 2010). The identity of eluted fragments was assigned based on the retention times of known
723 muropeptides (Takacs et al., 2010).

724 **AmiR and NagZ activity assays**

725 To test the activity of AmiR towards anhydro-muropeptides, peptidoglycan from *E. coli* D456 (Edwards and
726 Donachie, 1993), which lacks three major DD-carboxypeptidases and thus has elevated levels of penta-
727 peptides, was treated with the soluble lytic transglycosylase Slt70 from *E. coli* (Banzhaf et al., 2020; Betzner
728 and Keck, 1989). The products were incubated with wild-type AmiR or a catalytically inactive AmiR deriva-
729 tive (AmiR*) in a total volume of 50 µl in buffer H (20 mM HEPES-NaOH, 50 mM NaCl, 1 mM $MgCl_2$, pH 7.5)
730 at 37 °C for 16 h in a thermal shaker set to 900 rpm. The reactions were stopped by incubation at 100 °C
731 for 10 min in a dry-bed heater. After clearance of the mixtures by centrifugation at 17,000 ×*g* for 10 min,
732 the supernatants were acidified to pH 4.0 – pH 4.5 with 20% phosphoric acid. Subsequently, the reaction
733 products were separated by HPLC as described previously (Izquierdo-Martinez et al., 2023). The activity of
734 AmiR towards muropeptides with reducing ends was tested in a similar manner. However, peptidoglycan
735 from *E. coli* D456 was treated with the muramidase cellosyl from *Streptomyces coelicolor* (Bräu et al.,
736 1991). After incubation with the enzyme, heat inactivation and centrifugation, the supernatants were
737 mixed with an equal volume of 0.5 M sodium borate (pH 9.0), followed by reduction of the muropeptides
738 with ~1 mg of sodium borohydride. The samples were then acidified to pH 4.0 – pH 4.5 with 20% phos-
739 phoric acid and analyzed by HPLC as described previously (Glauner, 1988).

740 The enzymatic activity of NagZ towards anhydro-muropeptides or reducing muropeptides was analyzed as
741 described for AmiR, but with the following modifications. Peptidoglycan from *E. coli* CS703-1 (Meberg et
742 al., 2001), which lacks all major DD-carboxypeptidases, was treated with the lytic transglycosylase MltA
743 from *E. coli* (Lommatzsch et al., 1997) to produce anhydro-muropeptides or with cellosyl to produce muro-

744 peptides with reducing ends. The lytic products were incubated with NagZ or a catalytically inactive NagZ
745 variant (NagZ*) (10 µM) and processed as described above.

746 To test the activity of AmiR towards undigested peptidoglycan, sacculi isolated from *E. coli* D456 (Glauner,
747 1988; Takacs et al., 2010) were incubated with AmiR or AmiR* (10 µM) in buffer H at 37 °C for 16 h in a
748 thermal shaker set to 900 rpm. The reactions were stopped by heating at 100 °C for 10 min in a dry-bed
749 heater. Subsequently, the sacculi were digested with cellosyl overnight. After heat inactivation of cellosyl
750 at 100 °C for 10 min and clearance of the mixtures by centrifugation, the reaction products were reduced
751 with borohydride. The samples were then acidified to pH 4.0 – pH 4.5 with 20% phosphoric acid and anal-
752 yzed by HPLC as described previously (Glauner, 1988).

753 Disaccharide-containing muropeptides and anhydro-muropeptides were identified based on their known
754 retention times and peak patterns (Glauner, 1988). The identities of the Glc*N*Ac–anhMur*N*Ac disaccharide
755 generated by AmiR and the anhMur*N*Ac-peptides generated by NagZ were determined by HPLC separation
756 of the reaction products and mass spectrometric analysis of the different peak fractions (**Figure 2–figure**
757 **supplement 4**).

758 **Metabolomics analysis**

759 Anhydro-muropeptides were quantified essentially as described previously (Jacobs et al., 1994; Simpson
760 et al., 2023). In brief, cultures were grown overnight in 10 mL PYE medium (OD_{600} = 1.2) and harvested by
761 centrifugation for 10 min at 21,000 ×*g* and 4 °C. The pelleted cells were washed three times with 0.9%
762 NaCl, resuspended to a final volume of 100 µL in 0.9% NaCl and heated for 7 min at 98 °C. The suspension
763 was cleared by centrifugtation for 15 min at 21,000 ×*g.* The supernatant was isolated, centrifuged again
764 to remove residual cell debris, and then subjected to liquid chromatography-mass spectrometric (LC-MS)
765 analysis for semi-quantitative determination of PG recycling or biosynthesis intermediates. The chromato-
766 graphic separation was performed on an Agilent Infinity II 1290 HPLC system using a ZicHILIC SeQuant
767 column (150 × 2.1 mm, 3.5 µm particle size, 100 Å pore size) connected to a ZicHILIC guard column (20 ×
768 2.1 mm, 5 µm particle size) (Merck KgAA) at 25° C and at a constant flow rate of 0.3 mL/min, with mobile
769 phase A being 0.1% formic acid in 99:1 water:acetonitrile (Honeywell, Morristown, NJ, USA) and phase B
770 being 0.1% formic acid in 99:1 acetonitrile:water (Honeywell, Morristown, NJ, USA). The injection volume
771 was 5 µl. The mobile phase profile comprised the following steps and linear gradients: 0 – 1 min constant
772 at 80% B; 1 – 10 min from 80 to 10% B; 10 – 12 min constant at 10% B; 12 – 12.1 min from 10 to 80% B; 12
773 to 14 min constant at 80% B. An Agilent 6546A QTOF mass spectrometer was used in high-resolution,
774 positive mode with a mass range of 70 – 1700 m/z and a scan rate of 1.5 spectra/second. An electrospray

775 ionization source was used at the following conditions: ESI spray voltage 4000 V, nozzle voltage 500 V,
776 sheath gas 250° C at 12 l/min, nebulizer pressure 60 psig and drying gas 100 °C at 11 l/min. Compounds
777 were identified based on their accurate mass and retention time, applying an extraction tolerance of 5
778 ppm. Chromatograms were integrated using MassHunter software (Agilent, CA, USA). Relative abundance
779 was determined based on the peak area.

780 To determine the cytoplasmic amounts of the PG precursors UDP-Glc*N*Ac and UDP-Mur*N*Ac, the strains to
781 be analyzed were cultivated overnight in PYE medium, followed by determination of their optical densities
782 (OD_{600}). Subsequently, 1-mL samples of the cultures were mixed with 1 mL of 70% LC-MS-Grade MeOH
783 (Merck, Germany) and subjected to centrifugation at 13,000 ×*g* and -9 °C for 10 min. To extract the endo-
784 metabolome, the pelleted cells were mixed with 100 µL per OD_{600} unit of extraction fluid (50% LC-MS-
785 Grade MeOH, 5 mM Tris, 0.5 mM EDTA) and the same amount of chloroform, followed by incubation at
786 4 °C for 2 h. After separation of the phases by centrifugation (max. speed, -9 °C, 10 min), the upper phase
787 was isolated, filtered using PTFE membrane filters (0.2 µm pore size) (Sartorius, Germany) and subjected
788 to LC-MS analysis. The chromatographic separation was performed on an Agilent Infinity II 1290 HPLC
789 system using a SeQuant ZIC-pHILIC column (150 × 2.1 mm, 5 µm particle size, peek coated, Merck) con-
790 nected to a guard column of similar specificity (20 × 2.1 mm, 5 µm particle size, Phenomoenex) at 40° C
791 and at a constant flow rate of 0.1 mL/min, with mobile phase A composed of 10 mM ammonium acetate
792 in water (pH 9) supplemented with medronic acid to a final concentration of 5 µM and mobile phase B
793 composed of 10 mM ammonium acetate in 90:10 acetonitrile:water (pH 9). The injection volume was 5 µl.
794 The mobile phase profile comprised the following steps and linear gradients: 0 – 1 min constant at 75 % B;
795 1 – 6 min from 75 to 40% B; 6 to 9 min constant at 40% B; 9 – 9.1 min from 40 to 75% B; 9.1 to 20 min
796 constant at 75% B. An Agilent 6546A QTOF mass spectrometer was used in high-resolution, negative mode
797 with a mass range of 50 – 1700 m/z and a scan rate of 1.5 spectra/second. An electrospray ionization
798 source was used at the following conditions: ESI spray voltage 4000 V, nozzle voltage 500 V, sheath gas
799 300° C at 12 L/min, nebulizer pressure 20 psig and drying gas 150° C at 11 L/min. Compounds were
800 identified based on their accurate mass and retention time applying an extraction tolerance of 5 ppm.
801 Chromatograms were integrated using MassHunter software (Agilent, Santa Clara, CA, USA). Relative
802 abundance was determined based on the peak area.

803 **Whole-cell proteomics**

804 Cells were grown to exponential phase in 10 mL PYE medium, harvested by centrifugation (15,000 ×g, 10
805 min, 4 °C), washed three times with ice-cold PBS and resuspended in 300 µL of lysis buffer (2% sodium
806 lauroyl sarcosinate [SLS], 100 mM ammonium bicarbonate). The samples were then heated for 10 min at

807 90 °C, followed by sonication with a VialTweeter Sonicator (Hielscher Ultrasonics, Germany). Proteins were
808 reduced with 5 mM Tris(2-carboxyethyl)phosphine (Thermo Fischer Scientific, Germany) at 90 °C for 15
809 min and alkylated using 10 mM iodoacetamid (Sigma Aldrich, Germany) at 20 °C for 30 min in the dark.
810 Subsequently, they were precipitated by the addition of a sixfold excess of ice-cold acetone and incubation
811 for 2 h at -20 °C, followed by two washing steps with methanol. After drying, the proteins were reconsti-
812 tuted in 0.2% SLS and their amount was determined using a bicinchoninic acid (BCA) protein assay (Thermo
813 Scientific, Germany). Subsequently, 50 µg protein were subjected to tryptic digestion by incubation with 1
814 µg of trypsin (Serva) in 0.5% SLS at 30 °C overnight. After digestion, SLS was precipitated by adding a final
815 concentration of 1.5% trifluoroacetic acid (TFA, Thermo Fisher Scientific, Germany). The peptides were
816 desalted using CHROMAFIX C18 solid phase extraction cartridges (Macherey-Nagel, Germany), which were
817 prepared by the addition of acetonitrile and subsequent equilibration with 0.1% TFA. They were then
818 loaded on the equilibrated cartridges, washed with a mixture of 5% acetonitrile and 0.1% TFA, and finally
819 eluted with a mixture of 50% ACN and 0.1% TFA. After drying, the peptides were reconstituted in 0.1% TFA
820 and then analyzed using liquid-chromatography-mass spectrometry on an Exploris 480 instrument con-
821 nected to an UltiMate 3000 RSLCnano HPLC system and a Nanospray Flex ion source (all Thermo Scientific,
822 Germany). The following gradient was used for separation: 94% solvent A (0.15% formic acid) and 6%
823 solvent B (99.85% acetonitrile, 0.15% formic acid) to 25% solvent B over 40 min, followed by an increase
824 to 35% solvent B over 20 min at a flow rate of 300 nl/min. Peptides were ionized at a spray voltage of 2.3
825 kV, with the ion transfer tube temperature set at 275 °C. 445.12003 m/z was used as internal calibrant.

826 MS raw data were acquired on an Orbitrap Exploris 480 instrument (Thermo Scientific, Germany) in data-
827 independent acquisition (DIA) mode. The funnel RF level was set to 40. For DIA experiments, full MS resolu-
828 tion was set to 120.000 at m/z 200. The AGC target value for fragment spectra was set at 3000%. 45 win-
829 dows of 14 Da were used with an overlap of 1 Da between m/z 320-950. Resolution was set to 15,000 and
830 IT to 22 ms. A stepped HCD collision energy of 25, 27.5, 30 % was used. MS1 data were acquired in profile,
831 MS2 DIA data in centroid mode.

832 The analysis of DIA data was performed with DIA-NN version 1.8 (Demichev et al., 2020), based on a
833 protein database for *Caulobacter crescentus* NA1000 retrieved from UniProt (UniProt Consortium, 2025)
834 to generate a dataset-specific spectral library. The DIA-NN suite was used to perform noise interference
835 correction (mass correction, RT prediction and precursor/fragment co-elution correlation) and peptide
836 precursor signal extraction on the DIA-NN raw data. The following parameters were used: Full tryptic
837 digest was allowed with two missed cleavage sites, oxidized methionines and carbamidomethylated
838 cysteins. “Match between runs” and “Remove likely interferences” were enabled. The precursor FDR was

839 set to 1%. The neural network classifier was set to the single-pass mode, and protein inference was based
840 on genes. The quantification strategy was set to any LC (high accuracy). Cross-run normalization was set
841 to RT-dependent. Library generation was set to smart profiling. DIA-NN outputs were further evaluated
842 using the SafeQuant script (Ahrné et al., 2013; Glatter et al., 2012), modified to process DIA-NN outputs.
843 A detailed summary of the proteomics data obtained is provided in **Supplementary File 1**.

844 **Bioinformatic analysis**

845 Protein similarity searches were performed with BLAST (Altschul et al., 1990), using the BLAST server of
846 the National Institutes of Health (https://blast.ncbi.nlm.nih.gov/Blast.cgi). Protein structures were
847 predicted with Alphafold 3 (Abramson et al., 2024) and visualized using PyMOL v2.6.0a0 (Schrödinger LLC).
848 Proteomics data were visualized with VolcaNoseR (Goedhart and Luijsterburg, 2020).

849 **Quantification and statistical analysis**

850 Details on the number of replicates and the sample sizes are given in the figure legends. Datasets were
851 displayed using the SuperPlotsOfData web application (Goedhart, 2021), and an unpaired two-sided
852 Welch's *t*-test implemented in the application was used to assess the statistical significance of differences
853 between strains or conditions. Standard deviations were calculated in Microsoft Excel 2019.

854 **Availability of biological material**

855 The plasmids and strains used in this study are available from the corresponding author upon request.

Data availability

856 The proteomics data generated in this study have been deposited to the ProteomeXchange Consortium
857 via the PRIDE partner repository (Perez-Riverol et al., 2025) under the dataset identifier PXD069004. All
858 other data supporting the findings of this study are included in the main text or the supplementary
859 material.

References

860 Abramson, J, Adler, J, Dunger, J, Evans, R, Green, T, Pritzel, A, Ronneberger, O, Willmore, L, Ballard, AJ,
861 Bambrick, J*, et al.* (2024). Accurate structure prediction of biomolecular interactions with AlphaFold 3.
862 *Nature* **630**:493-500.

863 Ahrné, E, Molzahn, L, Glatter, T, Schmidt, A (2013). Critical assessment of proteome-wide label-free
864 absolute abundance estimation strategies. *Proteomics* **13**:2567-2578.

865 Altschul, SF, Gish, W, Miller, W, Myers, EW, Lipman, DJ (1990). Basic local alignment search tool. *J Mol Biol*
866 **215**:403-410.

867 Álvarez-Añorve, LI, Gaugué, I, Link, H, Marcos-Viquez, J, Diaz-Jiménez, DM, Zonszein, S, Bustos-Jaimes, I,
868 Schmitz-Afonso, I, Calcagno, ML, Plumbridge, J (2016). Allosteric activation of *Escherichia coli* glucos-
869 amine-6-phosphate deaminase (NagB) *in vivo* justified by intracellular amino sugar metabolite concen-
870 trations. *J Bacteriol* **198**:1610-1620.

871 Bacik, JP, Whitworth, GE, Stubbs, KA, Vocadlo, DJ, Mark, BL (2012). Active site plasticity within the glyco-
872 side hydrolase NagZ underlies a dynamic mechanism of substrate distortion. *Chem Biol* **19**:1471-1482.

873 Banzhaf, M, van den Berg van Saparoea, B, Terrak, M, Fraipont, C, Egan, A, Philippe, J, Zapun, A, Breukink,
874 E, Nguyen-Disteche, M, den Blaauwen, T*, et al.* (2012). Cooperativity of peptidoglycan synthases active
875 in bacterial cell elongation. *Mol Microbiol* **85**:179-194.

876 Banzhaf, M, Yau, HC, Verheul, J, Lodge, A, Kritikos, G, Mateus, A, Cordier, B, Hov, AK, Stein, F, Wartel, M*,*
877 *et al.* (2020). Outer membrane lipoprotein NlpI scaffolds peptidoglycan hydrolases within multi-enzyme
878 complexes in *Escherichia coli*. *EMBO J* **39**:e102246.

879 Barreteau, H, Kovac, A, Boniface, A, Sova, M, Gobec, S, Blanot, D (2008). Cytoplasmic steps of peptidogly-
880 can biosynthesis. *FEMS Microbiol Rev* **32**:168-207.

881 Beier, S, Bertilsson, S (2013). Bacterial chitin degradation–mechanisms and ecophysiological strategies.
882 *Front Microbiol* **4**:149.

883 Bendezu, FO, Hale, CA, Bernhardt, TG, de Boer, PA (2009). RodZ (YfgA) is required for proper assembly of
884 the MreB actin cytoskeleton and cell shape in *E. coli*. *EMBO J* **28**:193-204.

885 Bertsche, U, Kast, T, Wolf, B, Fraipont, C, Aarsman, ME, Kannenberg, K, von Rechenberg, M, Nguyen-
886 Disteche, M, den Blaauwen, T, Holtje, JV*, et al.* (2006). Interaction between two murein (peptidoglycan)
887 synthases, PBP3 and PBP1B, in *Escherichia coli*. *Mol Microbiol* **61**:675-690.

888 Betzner, AS, Keck, W (1989). Molecular cloning, overexpression and mapping of the *slt* gene encoding the
889 soluble lytic transglycosylase of *Escherichia coli*. *Mol Gen Genet* **219**:489-491.

890 Bi, EF, Lutkenhaus, J (1991). FtsZ ring structure associated with division in *Escherichia coli*. *Nature* **354**:161-
891 164.

892 Bisson-Filho, AW, Hsu, YP, Squyres, GR, Kuru, E, Wu, F, Jukes, C, Sun, Y, Dekker, C, Holden, S,
893 VanNieuwenhze, MS*, et al.* (2017). Treadmilling by FtsZ filaments drives peptidoglycan synthesis and
894 bacterial cell division. *Science* **355**:739-743.

895 Borisova, M, Gisin, J, Mayer, C (2014). Blocking peptidoglycan recycling in *Pseudomonas aeruginosa*
896 attenuates intrinsic resistance to fosfomycin. *Microb Drug Resist* **20**:231-237.

897 Borisova, M, Gisin, J, Mayer, C (2017). The *N*-acetylmuramic acid 6-phosphate phosphatase MupP
898 completes the *Pseudomonas* peptidoglycan recycling pathway leading to intrinsic fosfomycin resis-
899 tance. *mBio* **8**:e00092-00017.

900 Bräu, B, Hilgenfeld, R, Schlingmann, M, Marquardt, R, Birr, E, Wohlleben, W, Aufderheide, K, Puhler, A
901 (1991). Increased yield of a lysozyme after self-cloning of the gene in *Streptomyces coelicolor* "Müller".
902 *Appl Microbiol Biotechnol* **34**:481-487.

903 Bugg, TD, Braddick, D, Dowson, CG, Roper, DI (2011). Bacterial cell wall assembly: still an attractive
904 antibacterial target. *Trends Biotechnol* **29**:167-173.

905 Bush, K, Freudenberger, JS, Sykes, RB (1982). Interaction of azthreonam and related monobactams with β-
906 lactamases from Gram-negative bacteria. *Antimicrob Agents Chemother* **22**:414-420.

907 Chang, N, Kim, H, Kim, U, Cho, Y, Yoo, Y, Lee, H, Kim, JW, Kim, MS, Lee, J, Cho, YL*, et al.* (2025). Structural
908 and functional insights of AmpG in muropeptide transport and multiple β-lactam antibiotics resistance.
909 *Nat Commun* **16**:5744.

910 Cheng, Q, Li, H, Merdek, K, Park, JT (2000). Molecular characterization of the beta-*N*-acetylglucosamini-
911 dase of *Escherichia coli* and its role in cell wall recycling. *J Bacteriol* **182**:4836-4840.

912 Cheng, Q, Park, JT (2002). Substrate specificity of the AmpG permease required for recycling of cell wall
913 anhydro-muropeptides. *J Bacteriol* **184**:6434-6436.

914 Cho, H, Uehara, T, Bernhardt, TG (2014). Beta-lactam antibiotics induce a lethal malfunctioning of the
915 bacterial cell wall synthesis machinery. *Cell* **159**:1300-1311.

916 Cho, H, Wivagg, CN, Kapoor, M, Barry, Z, Rohs, PDA, Suh, H, Marto, JA, Garner, EC, Bernhardt, TG (2016).
917 Bacterial cell wall biogenesis is mediated by SEDS and PBP polymerase families functioning semi-
918 autonomously. *Nat Microbiol* **1**:16172.

919 Dai, Y, Pinedo, V, Tang, AY, Cava, F, Geisinger, E (2021). A new class of cell wall-recycling l,d-carboxy-
920 peptidase determines β-lactam susceptibility and morphogenesis in *Acinetobacter baumannii*. *mBio*
921 **12**:e0278621.

922 Demichev, V, Messner, CB, Vernardis, SI, Lilley, KS, Ralser, M (2020). DIA-NN: neural networks and
923 interference correction enable deep proteome coverage in high throughput. *Nat Methods* **17**:41-44.

924 Dietz, H, Pfeifle, D, Wiedemann, B (1997). The signal molecule for β-lactamase induction in *Enterobacter*
925 *cloacae* is the anhydromuramyl-pentapeptide. *Antimicrob Agents Chemother* **41**:2113-2120.

926 Dik, DA, Fisher, JF, Mobashery, S (2018). Cell-wall recycling of the Gram-negative bacteria and the nexus
927 to antibiotic resistance. *Chem Rev* **118**:5952-5984.

928 Dik, DA, Marous, DR, Fisher, JF, Mobashery, S (2017). Lytic transglycosylases: concinnity in concision of the
929 bacterial cell wall. *Crit Rev Biochem Mol Biol* **52**:503-542.

930 Docquier, JD, Pantanella, F, Giuliani, F, Thaller, MC, Amicosante, G, Galleni, M, Frère, JM, Bush, K, Rossolini,
931 GM (2002). CAU-1, a subclass B3 metallo-β-lactamase of low substrate affinity encoded by an ortholog
932 present in the *Caulobacter crescentus* chromosome. *Antimicrob Agents Chemother* **46**:1823-1830.

933 Edwards, D, Donachie, WD (1993). Construction of a triple deletion of penicillin-binding proteins 4, 5, and
934 6 in *Escherichia coli*. In Bacterial growth and lysis, M. de Pedro, J.-V. Höltje, and W. Löffelhardt, eds.
935 (New York and London: Plenum Press), pp. 369–374.

936 Egan, AJF, Errington, J, Vollmer, W (2020). Regulation of peptidoglycan synthesis and remodelling. *Nat Rev*
937 *Microbiol* **18**:446-460.

938 Eisenbeis, S, Lohmiller, S, Valdebenito, M, Leicht, S, Braun, V (2008). NagA-dependent uptake of *N*-acetyl-
939 glucosamine and *N*-acetyl-chitin oligosaccharides across the outer membrane of *Caulobacter cres-*
940 *centus*. *J Bacteriol* **190**:5230-5238.

941 Ely, B (1991). Genetics of *Caulobacter crescentus*. *Method Enzymol* **204**:372-384.

942 Evinger, M, Agabian, N (1977). Envelope-associated nucleoid from *Caulobacter crescentus* stalked and
943 swarmer cells. *J Bacteriol* **132**:294-301.

944 Fumeaux, C, Bernhardt, TG (2017). Identification of MupP as a new peptidoglycan recycling factor and
945 antibiotic resistance determinant in *Pseudomonas aeruginosa*. *mBio* **8**:e00102-00117.

946 Garner, EC, Bernard, R, Wang, W, Zhuang, X, Rudner, DZ, Mitchison, T (2011). Coupled, circumferential
947 motions of the cell wall synthesis machinery and MreB filaments in *B. subtilis*. *Science* **333**:222-225.

948 Généreux, C, Dehareng, D, Devreese, B, Van Beeumen, J, Frère, JM, Joris, B (2004). Mutational analysis of
949 the catalytic centre of the *Citrobacter freundii* AmpD *N*-acetylmuramyl-L-alanine amidase. *Biochem J*
950 **377**:111-120.

951 Gilmore, MC, Cava, F (2022). Peptidoglycan recycling mediated by an ABC transporter in the plant
952 pathogen *Agrobacterium tumefaciens*. *Nat Commun* **13**:7927.

953 Gilmore, MC, Cava, F (2025). Bacterial peptidoglycan recycling. *Trends Microbiol* **33**:340-353.

954 Gisin, J, Schneider, A, Nagele, B, Borisova, M, Mayer, C (2013). A cell wall recycling shortcut that bypasses
955 peptidoglycan *de novo* biosynthesis. *Nat Chem Biol* **9**:491-493.

956 Glatter, T, Ludwig, C, Ahrne, E, Aebersold, R, Heck, AJ, Schmidt, A (2012). Large-scale quantitative assess-
957 ment of different in-solution protein digestion protocols reveals superior cleavage efficiency of tandem
958 Lys-C/trypsin proteolysis over trypsin digestion. *J Proteome Res* **11**:5145-5156.

959 Glauner, B (1988). Separation and quantification of muropeptides with high-performance liquid
960 chromatography. *Anal Biochem* **172**:451-464.

961 Goedhart, J (2021). SuperPlotsOfData – a web app for the transparent display and quantitative comparison
962 of continuous data from different conditions. *Mol Biol Cell* **32**:470-474.

963 Goedhart, J, Luijsterburg, MS (2020). VolcaNoseR is a web app for creating, exploring, labeling and sharing
964 volcano plots. *Sci Rep* **10**:20560.

965 Goodell, EW, Schwarz, U (1985). Release of cell wall peptides into culture medium by exponentially grow-
966 ing *Escherichia coli*. *J Bacteriol* **162**:391-397.

967 Hernández, SB, Dörr, T, Waldor, MK, Cava, F (2020). Modulation of peptidoglycan synthesis by recycled
968 cell wall tetrapeptides. *Cell Rep* **31**:107578.

969 Höltje, JV (1998). Growth of the stress-bearing and shape-maintaining murein sacculus of *Escherichia coli*.
970 *Microbiol Mol Biol Rev* **62**:181-203.

971 Höltje, JV, Kopp, U, Ursinus, A, Wiedemann, B (1994). The negative regulator of β-lactamase induction
972 AmpD is a *N*-acetyl-anhydromuramyl-L-alanine amidase. *FEMS Microbiol Lett* **122**:159-164.

973 Hottes, AK, Meewan, M, Yang, D, Arana, N, Romero, P, McAdams, HH, Stephens, C (2004). Transcriptional
974 profiling of *Caulobacter crescentus* during growth on complex and minimal media. *J Bacteriol* **186**:1448-
975 1461.

976 Hottmann, I, Borisova, M, Schaffer, C, Mayer, C (2021). Peptidoglycan salvage enables the periodontal
977 pathogen *Tannerella forsythia* to survive within the oral microbial community. *Microb Physiol* **31**:123-
978 134.

979 Izquierdo-Martinez, A, Billini, M, Miguel-Ruano, V, Hernandez-Tamayo, R, Richter, P, Biboy, J, Batuecas,
980 MT, Glatter, T, Vollmer, W, Graumann, PL*, et al.* (2023). DipM controls multiple autolysins and mediates
981 a regulatory feedback loop promoting cell constriction in *Caulobacter crescentus*. *Nat Commun*
982 **14**:4095.

983 Jacobs, C, Frère, JM, Normark, S (1997). Cytosolic intermediates for cell wall biosynthesis and degradation
984 control inducible β-lactam resistance in Gram-negative bacteria. *Cell* **88**:823-832.

985 Jacobs, C, Huang, LJ, Bartowsky, E, Normark, S, Park, JT (1994). Bacterial cell wall recycling provides
986 cytosolic muropeptides as effectors for β-lactamase induction. *EMBO J* **13**:4684-4694.

987 Jaeger, T, Arsic, M, Mayer, C (2005). Scission of the lactyl ether bond of N-acetylmuramic acid by
988 *Escherichia coli* "etherase". *J Biol Chem* **280**:30100-30106.

989 Jones, LJ, Carballido-Lopez, R, Errington, J (2001). Control of cell shape in bacteria: helical, actin-like
990 filaments in *Bacillus subtilis*. *Cell* **104**:913-922.

991 Kocaoglu, O, Carlson, EE (2015). Profiling of beta-lactam selectivity for penicillin-binding proteins in
992 *Escherichia coli strain* DC2. *Antimicrob Agents Chemother* **59**:2785-2790.

993 Kohlrausch, U, Höltje, JV (1991). Analysis of murein and murein precursors during antibiotic-induced lysis
994 of *Escherichia coli*. *J Bacteriol* **173**:3425-3431.

995 Lariviere, PJ, Mahone, CR, Santiago-Collazo, G, Howell, M, Daitch, AK, Zeinert, R, Chien, P, Brown, PJB,
996 Goley, ED (2019). An essential regulator of bacterial division links FtsZ to cell wall synthase activation.
997 *Curr Biol* **29**:1460-1470.

998 Liepinsh, E, Généreux, C, Dehareng, D, Joris, B, Otting, G (2003). NMR structure of *Citrobacter freundii*
999 AmpD, comparison with bacteriophage T7 lysozyme and homology with PGRP domains. *J Mol Biol*
1000 **327**:833-842.

1001 Lima, LM, Silva, B, Barbosa, G, Barreiro, EJ (2020). β-lactam antibiotics: an overview from a medicinal
1002 chemistry perspective. *Eur J Med Chem* **208**:112829.

1003 Lindquist, S, Galleni, M, Lindberg, F, Normark, S (1989). Signalling proteins in enterobacterial AmpC beta-
1004 lactamase regulation. *Mol Microbiol* **3**:1091-1102.

1005 Lommatzsch, J, Templin, MF, Kraft, AR, Vollmer, W, Höltje, JV (1997). Outer membrane localization of
1006 murein hydrolases: MltA, a third lipoprotein lytic transglycosylase in *Escherichia coli*. *J Bacteriol*
1007 **179**:5465-5470.

1008 Marblestone, JG, Edavettal, SC, Lim, Y, Lim, P, Zuo, X, Butt, TR (2006). Comparison of SUMO fusion
1009 technology with traditional gene fusion systems: enhanced expression and solubility with SUMO.
1010 *Protein Sci* **15**:182-189.

1011 Meberg, BM, Sailer, FC, Nelson, DE, Young, KD (2001). Reconstruction of *Escherichia coli mrcA* (PBP 1a)
1012 mutants lacking multiple combinations of penicillin binding proteins. *J Bacteriol* **183**:6148-6149.

1013 Meeske, AJ, Riley, EP, Robins, WP, Uehara, T, Mekalanos, JJ, Kahne, D, Walker, S, Kruse, AC, Bernhardt, TG,
1014 Rudner, DZ (2016). SEDS proteins are a widespread family of bacterial cell wall polymerases. *Nature*
1015 **537**:634-638.

1016 Mengin-Lecreulx, D, van Heijenoort, J, Park, JT (1996). Identification of the *mpl* gene encoding UDP-N-
1017 acetylmuramate: L-alanyl-gamma-D-glutamyl-meso-diaminopimelate ligase in *Escherichia coli* and its
1018 role in recycling of cell wall peptidoglycan. *J Bacteriol* **178**:5347-5352.

1019 Modell, JW, Kambara, TK, Perchuk, BS, Laub, MT (2014). A DNA damage-induced, SOS-independent
1020 checkpoint regulates cell division in *Caulobacter crescentus*. *PLoS Biol* **12**:e1001977.

1021 Modi, M, Chauhan, D, Gilmore, MC, Cava, F, Priyadarshini, R (2025). Deficiency in peptidoglycan recycling
1022 promotes beta-lactam sensitivity in *Caulobacter crescentus*. *mBio* **16**:e0297524.

1023 Mora-Ochomogo, M, Lohans, CT (2021). β-Lactam antibiotic targets and resistance mechanisms: from
1024 covalent inhibitors to substrates. *RSC Med Chem* **12**:1623-1639.

1025 More, N, Martorana, AM, Biboy, J, Otten, C, Winkle, M, Serrano, CKG, Monton Silva, A, Atkinson, L, Yau, H,
1026 Breukink, E*, et al.* (2019). Peptidoglycan remodeling enables *Escherichia coli* to survive severe outer
1027 membrane assembly defect. *mBio* **10**:e02729-02718.

1028 Mukhija, S, Erni, B (1996). Purification by Ni2+ affinity chromatography, and functional reconstitution of
1029 the transporter for N-acetylglucosamine of *Escherichia coli*. *J Biol Chem* **271**:14819-14824.

1030 Navarro, PP, Vettiger, A, Hajdu, R, Ananda, VY, Lopez-Tavares, A, Schmid, EW, Walter, JC, Loose, M, Chao,
1031 LH, Bernhardt, TG (2025). The aPBP-type cell wall synthase PBP1b plays a specialized role in fortifying
1032 the *Escherichia coli* division site against osmotic rupture. *bioRxiv*, DOI:
1033 10.1101/2025.1104.1102.646830.

1034 Nierman, WC, Feldblyum, TV, Laub, MT, Paulsen, IT, Nelson, KE, Eisen, J, Heidelberg, JF, Alley, MRK, Ohta,
1035 N, Maddock, JR*, et al.* (2001). Complete genome sequence of *Caulobacter crescentus*. *Proc Natl Acad*
1036 *Sci U S A* **98**:4136-4141.

1037 O'Callaghan, CH, Morris, A, Kirby, SM, Shingler, AH (1972). Novel method for detection of beta-lactamases
1038 by using a chromogenic cephalosporin substrate. *Antimicrob Agents Chemother* **1**:283-288.

1039 Paintdakhi, A, Parry, B, Campos, M, Irnov, I, Elf, J, Surovtsev, I, Jacobs-Wagner, C (2016). Oufti: an
1040 integrated software package for high-accuracy, high-throughput quantitative microscopy analysis. *Mol*
1041 *Microbiol* **99**:767-777.

1042 Park, JT, Uehara, T (2008). How bacteria consume their own exoskeletons (turnover and recycling of cell
1043 wall peptidoglycan). *Microbiol Mol Biol Rev* **72**:211-227.

1044 Pazos, M, Vollmer, W (2021). Regulation and function of class A penicillin-binding proteins. *Curr Opin*
1045 *Microbiol* **60**:80-87.

1046 Perez-Riverol Y, Bandla C, Kundu DJ, Kamatchinathan S, Bai J, Hewapathirana S, John NS, Prakash A, Walzer
1047 M, Wang S, Vizcaíno JA. (2025) The PRIDE database at 20 years: 2025 update. *Nucleic Acids Res* **53**:
1048 D543-D553.

1049 Plumbridge, J (1996). How to achieve constitutive expression of a gene within an inducible operon: the
1050 example of the *nagC* gene of *Escherichia coli*. *J Bacteriol* **178**:2629-2636.

1051 Plumbridge, J (2009). An alternative route for recycling of N-acetylglucosamine from peptidoglycan
1052 involves the N-acetylglucosamine phosphotransferase system in *Escherichia coli*. *J Bacteriol* **191**:5641-
1053 4647.

1054 Plumbridge, J, Vimr, E (1999). Convergent pathways for utilization of the amino sugars *N*-acetylglucos-
1055 amine, *N*-acetylmannosamine, and *N*-acetylneuraminic acid by *Escherichia coli*. *J Bacteriol* **181**:47-54.

1056 Plumbridge, JA (1991). Repression and induction of the *nag* regulon of *Escherichia coli* K-12: the roles of
1057 *nagC* and *nagA* in maintenance of the uninduced state. *Mol Microbiol* **5**:2053-2062.

1058 Poindexter, JS (1964). Biological properties and classification of the *Caulobacter* group. *Bacteriological*
1059 *Reviews* **28**:231-295.

1060 Ratna, S, Pradhan, L, Vasconcelos, MP, Acharya, A, Carnahan, B, Wang, A, Ghosh, A, Bolt, A, Ellis, J, Hyland,
1061 SN*, et al.* (2025). The *Legionella pneumophila* peptidoglycan recycling kinase, AmgK, is essential for
1062 survival and replication inside host alveolar macrophages. *bioRxiv*, DOI:
1063 10.1101/2025.1103.1121.644609.

1064 Rohs, PDA, Buss, J, Sim, SI, Squyres, GR, Srisuknimit, V, Smith, M, Cho, H, Sjodt, M, Kruse, AC, Garner, EC*,*
1065 *et al.* (2018). A central role for PBP2 in the activation of peptidoglycan polymerization by the bacterial
1066 cell elongation machinery. *PLoS Genet* **14**:e1007726.

1067 Santos, PM, Di Bartolo, I, Blatny, JM, Zennaro, E, Valla, S (2001). New broad-host-range promoter probe
1068 vectors based on the plasmid RK2 replicon. *FEMS Microbiol Lett* **195**:91-96.

1069 Sauvage, E, Kerff, F, Terrak, M, Ayala, JA, Charlier, P (2008). The penicillin-binding proteins: structure and
1070 role in peptidoglycan biosynthesis. *FEMS Microbiol Rev* **32**:234-258.

1071 Schindelin, J, Arganda-Carreras, I, Frise, E, Kaynig, V, Longair, M, Pietzsch, T, Preibisch, S, Rueden, C,
1072 Saalfeld, S, Schmid, B*, et al.* (2012). Fiji: an open-source platform for biological-image analysis. *Nat*
1073 *Methods* **9**:676-682.

1074 Sham, LT, Butler, EK, Lebar, MD, Kahne, D, Bernhardt, TG, Ruiz, N (2014). MurJ is the flippase of lipid-linked
1075 precursors for peptidoglycan biogenesis. *Science* **345**:220-222.

1076 Simpson, BW, Gilmore, MC, McLean, AB, Cava, F, Trent, MS (2023). *Escherichia coli* utilizes multiple
1077 peptidoglycan recycling permeases with distinct strategies of recycling. *Proc Natl Acad Sci U S A*
1078 **120**:e2308940120.

1079 Simpson, BW, Nieckarz, M, Pinedo, V, McLean, AB, Cava, F, Trent, MS (2021). *Acinetobacter baumannii* can
1080 survive with an outer membrane lacking lipooligosaccharide due to structural support from
1081 elongasome peptidoglycan synthesis. *mBio* **12**:e0309921.

1082 Strobel, W, Möll, A, Kiekebusch, D, Klein, KE, Thanbichler, M (2014). Function and localization dynamics of
1083 bifunctional penicillin-binding proteins in *Caulobacter crescentus*. *J Bacteriol* **196**:1627-1639.

1084 Taguchi, A, Welsh, MA, Marmont, LS, Lee, W, Sjodt, M, Kruse, AC, Kahne, D, Bernhardt, TG, Walker, S
1085 (2019). FtsW is a peptidoglycan polymerase that is functional only in complex with its cognate penicillin-
1086 binding protein. *Nat Microbiol* **4**:587-594.

1087 Takacs, CN, Poggio, S, Charbon, G, Pucheault, M, Vollmer, W, Jacobs-Wagner, C (2010). MreB drives *de*
1088 *novo* rod morphogenesis in *Caulobacter crescentus* via remodeling of the cell wall. *J Bacteriol* **192**:1671-
1089 1684.

1090 Templin, MF, Ursinus, A, Höltje, JV (1999). A defect in cell wall recycling triggers autolysis during the
1091 stationary growth phase of *Escherichia coli*. *EMBO J* **18**:4108-4117.

1092 Thanbichler, M, Shapiro, L (2006). MipZ, a spatial regulator coordinating chromosome segregation with
1093 cell division in *Caulobacter*. *Cell* **126**:147-162.

1094 Trindade, BC, Chen, GY (2020). NOD1 and NOD2 in inflammatory and infectious diseases. *Immunol Rev*
1095 **297**:139-161.

1096 Typas, A, Banzhaf, M, Gross, CA, Vollmer, W (2012). From the regulation of peptidoglycan synthesis to
1097 bacterial growth and morphology. *Nat Rev Microbiol* **10**:123-136.

1098 Uehara, T, Park, JT (2007). An anhydro-*N*-acetylmuramyl-L-alanine amidase with broad specificity tethered
1099 to the outer membrane of *Escherichia coli*. *J Bacteriol* **189**:5634-5641.

1100 Uehara, T, Suefuji, K, Jaeger, T, Mayer, C, Park, JT (2006). MurQ etherase is required by *Escherichia coli* in
1101 order to metabolize anhydro-*N*-acetylmuramic acid obtained either from the environment or from its
1102 own cell wall. *J Bacteriol* **188**:1660-1662.

1103 Uehara, T, Suefuji, K, Valbuena, N, Meehan, B, Donegan, M, Park, JT (2005). Recycling of the anhydro-N-
1104 acetylmuramic acid derived from cell wall murein involves a two-step conversion to *N*-acetylglucos-
1105 amine-phosphate. *J Bacteriol* **187**:3643-3649.

1106 UniProt Consortium (2025). UniProt: the Universal Protein Knowledgebase in 2025. *Nucleic Acids Res*
1107 **53**:D609-D617.

1108 Vadlamani, G, Thomas, MD, Patel, TR, Donald, LJ, Reeve, TM, Stetefeld, J, Standing, KG, Vocadlo, DJ, Mark,
1109 BL (2015). The β-lactamase gene regulator AmpR is a tetramer that recognizes and binds the D-Ala-D-
1110 Ala motif of its repressor UDP-*N*-acetylmuramic acid (MurNAc)-pentapeptide. *J Biol Chem* **290**:2630-
1111 2643.

1112 van Heijenoort, J (2011). Peptidoglycan hydrolases of *Escherichia coli*. *Microbiol Mol Biol Rev* **75**:636-663.

1113 van Teeffelen, S, Wang, S, Furchtgott, L, Huang, KC, Wingreen, NS, Shaevitz, JW, Gitai, Z (2011). The bacter-
1114 ial actin MreB rotates, and rotation depends on cell-wall assembly. *Proc Natl Acad Sci U S A* **108**:15822-
1115 15827.

1116 Vollmer, W, Bertsche, U (2008). Murein (peptidoglycan) structure, architecture and biosynthesis in
1117 Escherichia coli. *Biochim Biophys Acta* **1778**:1714-1734.

1118 Vollmer, W, Blanot, D, de Pedro, MA (2008a). Peptidoglycan structure and architecture. *FEMS Microbiol*
1119 *Rev* **32**:149-167.

1120 Vollmer, W, Joris, B, Charlier, P, Foster, S (2008b). Bacterial peptidoglycan (murein) hydrolases. *FEMS*
1121 *Microbiol Rev* **32**:259-286.

1122 West, L, Yang, D, Stephens, C (2002). Use of the *Caulobacter crescentus* genome sequence to develop a
1123 method for systematic genetic mapping. *J Bacteriol* **184**:2155-2166.

1124 Yakhnina, AA, Gitai, Z (2013). Diverse functions for six glycosyltransferases in *Caulobacter crescentus* cell
1125 wall assembly. *J Bacteriol* **195**:4527-4535.

1126 Yang, X, Lyu, Z, Miguel, A, McQuillen, R, Huang, KC, Xiao, J (2017). GTPase activity-coupled treadmilling of
1127 the bacterial tubulin FtsZ organizes septal cell wall synthesis. *Science* **355**:744-747.

1128 Zhao, G, Meier, TI, Kahl, SD, Gee, KR, Blaszczak, LC (1999). BOCILLIN FL, a sensitive and commercially
1129 available reagent for detection of penicillin-binding proteins. *Antimicrob Agents Chemother* **43**:1124-
1130 1128.

1131 Zielinska, A, Billini, M, Möll, A, Kremer, K, Briegel, A, Izquierdo Martinez, A, Jensen, GJ, Thanbichler, M
1132 (2017). LytM factors affect the recruitment of autolysins to the cell division site in *Caulobacter*
1133 *crescentus*. *Mol Microbiol* **106**:419-438.

Acknowledgements

1134 We thank Julia Rausch for excellent technical assistance and Daniela Vollmer for the purification of pep-
1135 tidoglycan. This work was supported by the University of Marburg (core funding to M.T.), the Max Planck
1136 Society (Max Planck Fellowships to M.T.) and the United Kingdom Biotechnology and Biological Sciences
1137 Research Council (grant BB/W013630/1 to W.V.).

Author contributions

1138 P.R. and M.T. conceived the study. P.R. generated plasmids and strains, performed the *in vivo* experiments,
1139 purified the proteins and prepared the samples for metabolomics analysis. A.M. generated plasmids and
1140 strains. J.B. conducted the enzyme assays and muropeptide analysis. N.P. performed the metabolomics
1141 analysis. P.R., J.B., N.P., W.V. and M.T. analyzed the data. V.M. and M.T. secured funding and supervised
1142 the study. P.R. and M.T. wrote the manuscript, with input from all other authors.

Declaration of Interests

The authors declare that they have no competing interests.

Table

1143 **Table 1. List of PG recycling enzymes found in *E. coli* and *P. aeruginosa* and the corresponding homologs of *C.*
1144 *crescentus* identified by reciprocal BLAST analysis.**

Protein	Homolog(s)	Sequence identity (%)	E value	Function
E. coli [1)]	***C. crescentus***			
AmpG	CCNA_00136	40.4	3E-40	Muropeptide permease
NagE	CCNA_00572 CCNA_00458	45.0 45.0	2E-131 3E-131	*N*-acetylglucosamine-specific IIBC component (PTS system)
LdcA	-	-	-	LD-Carboxypeptidase
AmpD	CCNA_02650	33.5	5E-20	1,6-anhydro-*N*-acetylmuramyl-L-alanine amidase
NagZ	CCNA_02085	34.7	6E-44	β-*N*-acetyl-D-glucosaminidase
NagK	CCNA_03849	41.1	2E-66	*N*-actely-D-glucosamine kinase
AnmK	CCNA_01945	34.6	2E-49	anhydro-*N*-acetylmuramic acid kinase
MurQ	-	-	-	*N*-acetylmuramic acid-6-phosphate etherase
NagA	CCNA_00568 CCNA_00452	36.3 39.5	6E-76 1E-84	*N*-acetylglucosamine-6-phosphate deacetylase
GlmM	CCNA_00116	51.5	4E-153	Phosphoglucosamine mutase
GlmU	CCNA_02389	40.4	2E-97	UDP-*N*-acetylglucosamine pyrophosphorylase
P. aeruginosa [2)]	***C. crescentus***			
MupP	CCNA_02390	32.6	3E-27	Phosphoglycolate phosphatase
AmgK	CCNA_03649	30.1	1E-32	*N*-acetylmuramate/*N*-acetylglucosamine kinase
MurU	CCNA_03650	36.6	4E-26	*N*-acetylmuramate-α-1-phosphate uridylyltransferase

[1)] strain *E. coli* K-12 substr. MG1655 (Genbank accession code: U00096.3)
[2)] strain *P. aeruginosa* PAO1 (Genbank accession code: AE004091.2)

Figure legends

1145 **Figure 1. The *C. crescentus* genome encodes a complete PG recycling pathway.** *De novo* PG biosynthesis
1146 starts with the conversion of fructose-6-phosphate, supplied by central carbon metabolism, to glucosam-
1147 ine-6-phosphate. This key metabolite is then transformed by multiple enzymatic steps into the membrane-
1148 attached PG precursor lipid II, which is flipped to the periplasmic face and incorporated into the existing
1149 PG sacculus by glycosyltransferases and transpeptidases. To enable PG remodeling, growth and cell
1150 separation, the PG meshwork is cleaved by a diverse set of enzymes, such as lytic transglycosylases (LTs),
1151 endopeptidases (EPases), amidases and carboxypeptidases (CPases). PG fragments released by these
1152 activities are imported into the cytoplasm by the permease AmpG or two homologs of the phospho-
1153 transferase system (PTS) transporter NagE. In the cytoplasm, the peptide is released by AmiR and the
1154 sugars separated by NagZ. Afterwards, two independent pathways feed the two sugars back into the *de*
1155 *novo* PG biosynthetic pathway. The enzymes are named as established for *E. coli* and *P. aeruginosa*, with
1156 the exception of the *C. crescentus* homolog of AmpD, which was renamed to AmiR due to its different
1157 domain organization. The symbols are defined in the legend on the right.

1158 **Figure 2. The AmiR and NagZ homologs are functional and have a broad substrate specificity. (A)** Over-
1159 view of the PG digestion assay used to assess the hydrolytic activities of AmiR and NagZ. **(B)** HPLC chro-
1160 matograms showing the products generated upon incubation of anhydro-muropeptides from LT-treated
1161 PG sacculi without added proteins (Buffer), with AmiR or with a catalytically inactive AmiR variant (AmiR*).
1162 The identities of anhMur*N*Ac-peptides were determined based on their known retention times (Glauner,
1163 1988). The AmiR reaction product Glc*N*Ac-1,6-anhMur*N*Ac was identified by mass spectrometry (**Figure 2–**
1164 **figure supplement 4A**). **(C)** HPLC chromatograms showing the products generated upon incubation of
1165 anhydro-muropeptides from LT-treated PG sacculi without added proteins (Buffer), with NagZ or with a
1166 catalytically inactive NagZ variant (NagZ*). Disaccharide-containing anhydro-muropeptides were identi-
1167 fied based on their known retention times (Glauner, 1988). The identities of anhMur*N*Ac-peptides were
1168 validated by mass spectrometry analysis of the reaction products obtained after NagZ treatment of
1169 anhydro-muropeptide mixtures (**Figure 2–figure supplement 4B**).

1170 **Figure 2–figure supplement 1. Substrate specificity of AmiR. (A)** Structural models of AmiR and the cata-
1171 lytically inactive AmiR* variant, generated with AlphaFold 3 (Abramson et al., 2024). The magnified region
1172 shows the predicted catalytic site of AmiR and the amino acid substitutions introduced to generate AmiR*.
1173 **(B)** HPLC chromatograms showing the products generated upon incubation of anhydro-muropeptides
1174 from LT-treated PG sacculi for 16 h without added proteins (Buffer) or with the indicated concentrations

1175 of AmiR. **(C)** HPLC chromatograms showing the products generated upon incubation of muropeptides from
1176 muramidase-treated PG sacculi for 16 h without added proteins (Buffer) or with the indicated concentra-
1177 tions of AmiR. Reaction products were identified based on their known retention times (Glauner, 1988).

1178 **Figure 2–figure supplement 2. Lack of AmiR activity towards intact PG sacculi. (A)** Overview of the PG
1179 digestion assay used to assess the hydrolytic activity of AmiR on intact PG sacculi. **(B)** HPLC chromatograms
1180 showing the products generated upon incubation of intact PG sacculi without added proteins (Buffer), with
1181 AmiR and the catalytically inactive AmiR variant (AmiR*) and subsequent cellosyl-mediated cleavage of
1182 the pre-treated sacculi into muropeptides. Muropeptides were identified based on their known retention
1183 times (Glauner, 1988).

1184 **Figure 2–figure supplement 3. Activity of NagZ with muropeptides. (A)** Structural models of NagZ and the
1185 catalytically inactive NagZ* variant, generated with AlphaFold 3 (Abramson et al., 2024). The magnified
1186 region shows the predicted catalytic site of NagZ and the amino acid substitution introduced to generate
1187 NagZ*. **(B)** HPLC chromatograms showing the products generated upon incubation of muropeptides from
1188 muramidase-treated PG sacculi without added proteins (Buffer), with NagZ or with a catalytically inactive
1189 NagZ variant (NagZ*). Disaccharide-containing muropeptides were identified based on their known reten-
1190 tion times (Glauner, 1988). The identities of Mur*N*Ac-peptides were validated by mass spectrometry
1191 analysis of the reaction products obtained after NagZ treatment of anhydro-muropeptide mixtures (**Figure**
1192 **2–figure supplement 4B**).

1193 **Figure 2–figure supplement 4. Mass spectrometric identification of AmiR and NagZ reaction products.**
1194 **(A)** Identification of the Glc*N*Ac–anhMur*N*Ac disaccharide generated by treatment of anhydro-muropep-
1195 tides with AmiR. Sacculi isolated from *E. coli* D456 (Edwards and Donachie, 1993) were treated with the LT
1196 Slt70 *E. coli*. The graph shows the chromatogram obtained after separation of the sugar-containing reac-
1197 tion products by HPLC. The observed m/z ratios of the main product in peak 1 and the calculated molecular
1198 mass of the Glc*N*Ac-1,6-anhMur*N*Ac disaccharide are given in the table on the right. **(B)** Identification of
1199 the anhMur*N*Ac-peptide species generated by treatment of anhydro-muropeptides with NagZ. Sacculi iso-
1200 lated from *E. coli* CS703-1 (Meberg et al., 2001) were treated with the LT MltA from *E. coli*. The graph
1201 shows the chromatogram obtained after separation of the reaction products by HPLC. The table on the
1202 right gives the observed m/z ratios of the main product detected contained in the indicated peaks as well
1203 as the calculated molecular masses of the anhMur*N*Ac-peptides assigned to these peaks.

1204 **Figure 3. Metabolomic analysis reveals aberrant levels of PG recycling intermediates in recycling-defi-**
1205 **cient strains. (A)** Overview of the analysis pipeline used to identify cytoplasmic PG recycling products. **(B)**

1206 Relative levels of the indicated anhMur*N*Ac-peptide species in the cytoplasm of *C. crescentus* wild-type,
1207 Δ*amiR* (PR033) and Δ*amiR* Δ*ampG* (PR221) cells, measured by metabolomics analysis. For each anhydro-
1208 muropeptide, the mass spectrometric peak areas were normalized against the mean obtained for the
1209 Δ*amiR* mutant. The statistical significance of differences between the wild type and the mutant strains
1210 was determined using an unpaired two-sided Welch's t-test. ns indicates p-values > 0.1. **(C)** Relative levels
1211 of the Glc*N*Ac–anhMur*N*Ac disaccharide in *C. crescentus* wild-type, Δ*ampG* (PR207), Δ*amiR* (PR033) and
1212 Δ*nagZ* (PR188) cells, assessed as for panel B. The mass spectrometric peak areas were normalized against
1213 the mean obtained for the Δ*nagZ* mutant. Statistical significance was determined as described for panel
1214 B.

1215 **Figure 4. AmpG, AmiR and NagZ are required for proper cell shape and β-lactam resistance in *C. cres-***
1216 ***centus*. (A)** Phase contrast images of *C. crescentus* wild-type, Δ*ampG* (PR207), Δ*amiR* (PR033) and Δ*nagZ*
1217 (PR188) cells harvested in the exponential and stationary growth phase. Scale bar: 5 µm. **(B)** Superplots
1218 showing the distribution of cell lengths in populations of *C. crescentus* wild-type, Δ*ampG* (PR207), Δ*amiR*
1219 (PR033) and Δ*nagZ* (PR188) cells in the exponential (exp) and stationary (stat) growth phase. Small dots
1220 represent the data of three independent replicates (shown in light blue, teal and dark grey; *n*=100 cells
1221 per replicate). Large dots represent the mean values of the three datasets, with their average indicated by
1222 a red horizontal line. The statistical significance (*p*-value) of differences between conditions was assessed
1223 using an unpaired two-sided Welch's *t*-test. ns indicates *p*-values > 0.1. **(C)** Serial dilution spot assay inves-
1224 tigating the growth of wild-type, Δ*ampG* (PR207), Δ*amiR* (PR033), Δ*nagZ* (PR188) and Δ*blaA* (CS606) cells
1225 on agar plates with different concentrations of ampicillin.

1226 **Figure 4–figure supplement 1. Morphological characterization of catalytically inactive AmiR and NagZ**
1227 **variants. (A)** Phase contrast images of *C. crescentus amiR::amiR** (PR173) and *nagZ:nagZ** (PR196) cells
1228 harvested in the exponential and stationary growth phase. Scale bar: 5 µm. **(B)** Superplots showing the
1229 distribution of cell lengths in populations of wild-type, Δ*amiR* (PR033), *amiR::amiR** (PR173), Δ*nagZ*
1230 (PR188) and *nagZ::nagZ** (PR196) cells in the exponential (exp) and stationary (stat) growth phase. Data
1231 (*n*=100 cells per replicate) are presented as described for **Figure 4B**. The statistical significance (*p*-value)
1232 of differences between conditions was assessed using an unpaired two-sided Welch's *t*-test. ns indicates
1233 *p*-values > 0.1. The data for wild-type, Δ*amiR* and Δ*nagZ* cells are taken from **Figure 3** and shown as a
1234 reference.

1235 **Figure 4–figure supplement 2. Growth of PG recycling-deficient mutants in minimal medium. (A)** Phase
1236 contrast images of *C. crescentus* wild-type, Δ*ampG* (PR207), Δ*amiR* (PR033) and Δ*nagZ* (PR188) cells grown

1237 in minimal (M2G) medium and harvested in the stationary growth phase. **(B)** Superplots showing the
1238 distribution of cell lengths in populations of wild-type, Δ*ampG* (PR207), Δ*amiR* (PR033) and Δ*nagZ* (PR188)
1239 cells grown in rich medium (PYE) and minimal medium (M2G). Data (*n*=100 cells per replicate) are
1240 presented as described for **Figure 4B**. The statistical significance (*p*-value) of differences between condi-
1241 tions was assessed using an unpaired two-sided Welch's *t*-test. ns indicates *p*-values > 0.1. The distribu-
1242 tions of cell lengths in rich medium are taken from **Figure 3** and shown as a reference.

1243 **Figure 4–figure supplement 3. Redundant role of the LT SdpA in the production of anhydro-muropep-**
1244 **tides. (A)** Serial dilution spot assay investigating the growth of *C. crescentus* Δ*sdpA* (AM399) cells on agar
1245 plates containing different concentrations of ampicillin. The cells were spotted on the same plates as those
1246 depicted in **Figure 3**. **(B)** Phase contrast images of *C. crescentus* Δ*sdpA* (AM399) harvested in the expo-
1247 nential or stationary growth phase. **(C)** Superplots showing the distribution of cell lengths in populations
1248 of wild-type and Δ*sdpA* (AM399) cells harvested in the exponential (exp) and stationary (stat) growth
1249 phase. Data (*n*=100 cells per replicate) are presented as described for **Figure 4B**. The statistical significance
1250 (*p*-value) of differences between conditions was assessed using an unpaired two-sided Welch's *t*-test. ns
1251 indicates *p*-values > 0.1. **(D)** Levels of the indicated anhMur*N*Ac-peptide species in the cytoplasm of *C. cres-*
1252 *centus* wild-type, Δ*amiR* (PR033) and Δ*amiR* Δ*sdpA* (PR260) cells, measured by metabolomics analysis
1253 through quantification of the corresponding mass spectrometric peak areas. For each anhydro-muro-
1254 peptide, the mass spectrometric peak areas were normalized against the mean obtained for the Δ*amiR*
1255 mutant. The statistical significance of differences between the wild type and the mutant strains was de-
1256 termined using an unpaired two-sided Welch's t-test. ns indicates p-values > 0.1.

1257 **Figure 5. The Glc*N*Ac recycling pathway is dispensable for proper cell division and β-lactam resistance.**
1258 **(A)** Phase contrast images of *C. crescentus* Δ*nagK* (PR255), Δ*nagA1* (PR256) and Δ*nagA2* (PR257) cells
1259 harvested in the exponential and stationary growth phase. Scale bar: 5 µm. **(B)** Superplots showing the
1260 distribution of cell lengths in populations of *C. crescentus* wild-type, Δ*nagK* (PR255), Δ*nagA1* (PR256) and
1261 Δ*nagA2* (PR257) cells in the exponential (exp) and stationary (stat) growth phase. Data (*n*=100 cells per
1262 replicate) are presented as described for **Figure 4B**. The statistical significance (*p*-value) of differences bet-
1263 ween conditions was assessed using an unpaired two-sided Welch's *t*-test. ns indicates *p*-values > 0.1. **(C)**
1264 Serial dilution spot assays investigating the growth of *C. crescentus* Δ*nagK* (PR255), Δ*nagA1* (PR256) and
1265 Δ*nagA2* (PR257) cells on agar plates containing different concentrations of ampicillin. The cells were
1266 spotted on the same plates as those depicted in **Figure 3**. **(D)** Volcano plot illustrating differential protein
1267 abundance in *C. crescentus* wild-type cells grown in M2G minimal medium with Glc*N*Ac compared to plain
1268 M2G medium. Grey dots represent proteins identified by mass spectrometry. The x-axis indicates the log2

1269 of the average difference in the peptide counts for the two different conditions (*n*=3 independent repli-
1270 cates). The y-axis shows the -log10 of the corresponding *p*-value. Proteins encoded in the two *nag* gene
1271 clusters are highlighted in color and annotated. The colors correspond to those used in panel E. **(E)** Sche-
1272 matic representation of the two *nag* gene clusters. The predicted functions of the gene products are
1273 specified in the legend on the right.

1274 **Figure 6. *C. crescentus* recycles anhMur*N*Ac through a functional MurU pathway. (A)** Phase contrast
1275 images of *C. crescentus* Δ*anmK* (PR252) and Δ*amgK* (PR262) cells, harvested in the exponential and station-
1276 ary growth phase. Scale bar: 5 µm. **(B)** Superplots showing the distribution of cell lengths in populations
1277 of *C. crescentus* wild-type, Δ*anmK* (PR252), and Δ*amgK* (PR262) cells in the exponential (exp) and station-
1278 ary (stat) growth phase. Data (*n*=100 cells per replicate) are presented as described for **Figure 4B**. The
1279 statistical significance (*p*-value) of differences between conditions was assessed using an unpaired two-
1280 sided Welch's *t*-test. ns indicates *p*-values > 0.1. **(C)** Serial dilution spot assay investigating the growth of
1281 *C. crescentus* Δ*anmK* (PR252) and Δ*amgK* (PR262) on plates containing different concentrations of ampi-
1282 cillin. The cells were spotted on the same plates as those depicted in **Figure 3**. **(D)** Levels of Mur*N*Ac in the
1283 cytoplasm of *C. crescentus* wild-type and Δ*amgK* (PR262) cells, measured by metabolomics analysis
1284 through quantification of the corresponding mass spectrometric peak areas. The mass spectrometric peak
1285 areas were normalized against the mean obtained for the Δ*amgK* mutant. The statistical significance of
1286 differences between the two strains was determined using an unpaired two-sided Welch's t-test. **(E)**
1287 Analysis of the growth of *C. crescentus* wild-type, Δ*nagK* (PR255) and Δ*amgK* (PR262) cells on agar contain-
1288 ing a fosfomycin gradient. The fosfomycin concentrations on the MIC test strip are indicate in the legend
1289 on the right.

1290 **Figure 7. Recycling of the disaccharide moiety plays only a minor role in cell division and β-lactam resis-**
1291 **tance. (A)** Phase contrast images of *C. crescentus* Δ*amgK* Δ*nagK* (PR261) cells, harvested in the exponential
1292 and stationary growth phase. Scale bar: 5 µm. **(B)** Superplots showing the distribution of cell lengths in
1293 populations of *C. crescentus* wild-type and Δ*amgK* Δ*nagK* (PR261) cells in the exponential (exp) and station-
1294 ary (stat) growth phase. Data (*n*=100 cells per replicate) are presented as described for **Figure 4B**. The
1295 statistical significance (*p*-value) of differences between conditions was assessed using an unpaired two-
1296 sided Welch's *t*-test. ns indicates *p*-values > 0.1. **(C)** Serial dilution spot assays investigating the growth of
1297 *C. crescentus* Δ*amgK* Δ*nagK* (PR261) cells on agar plates containing different concentrations of ampicillin.
1298 The cells were spotted on the same plates as those depicted in **Figure 3**.

1299 **Figure 8. BlaA function is not regulated at the levels of transcription, protein accumulation or enzymatic**
1300 **activity. (A)** Organization of the putative five-gene operon containing the *blaA* gene. The annotation or
1301 ORF number of the open reading frames and the predicted functions of their gene products are indicated.
1302 **(B)** Activity of the promoter likely driving the expression of the *blaA*-containing operon in different strain
1303 backgrounds. The *C. crescentus* wild-type, Δ*ampG* (PR207), Δ*amiR* (PR033) and Δ*nagZ* (PR188) strains were
1304 transformed with a plasmid carrying a 400 bp fragment of the CCNA_02225 upstream region fused to a β-
1305 galactosidase reporter gene and assayed for reporter activity. Strains transformed with the empty plasmid
1306 served as negative controls (NC). The underlying data are shown as grey dots. The statistical significance
1307 (*p*-value) of differences between strains was calculated using an unpaired two-sided Welch's t-test. ns
1308 indicates p-values > 0.1. **(C)** β-lactamase activity of *C. crescentus* wild-type, Δ*ampG* (PR207), Δ*amiR* (PR033)
1309 and Δ*nagZ* (PR188) cells, as determined by monitoring the hydrolysis of the chromogenic β-lactam
1310 nitrocefin in permeabilized cells over time. **(D)** Volcano plots showing differential protein abundance in
1311 *C. crescentus* Δ*ampG* (PR207), Δ*amiR* (PR033) and Δ*nagZ* (PR188) cells compared to wild-type cells. Grey
1312 dots represent proteins identified by mass spectrometry. The x-axis indicates the log2 of the average
1313 difference in the peptide counts for the two different conditions (*n*=4 independent replicates). The y-axis
1314 shows the -log10 of the corresponding *p*-value. The BlaA protein is highlighted in magenta. **(E)** Serial
1315 dilution spot assays investigating the growth of *C. crescentus* wild-type, Δ*ampG* (PR207), Δ*amiR* (PR033),
1316 Δ*nagZ* (PR188) and Δ*blaA* cells (CS606) on agar plates containing different concentrations of aztreonam.

1317 **Figure 8–figure supplement 1. The two genes forming an operon with *amiR* are dispensible for PG recy-**
1318 **cling or β-lactam resistance. (A)** Genomic context of *amiR*. The gene names and the predicted functions
1319 of the respective gene products are indicated. **(B)** Levels of the indicated anhMur*N*Ac-peptide species in
1320 the cytoplasm of *C. crescentus* wild-type, Δ*amiR* (PR033) and Δ*amiR* Δ*traX* (PR258) cells, measured by
1321 metabolomics analysis through quantification of the corresponding mass spectrometric peak areas. **(C)**
1322 Volcano plot showing differences in protein abundance in *C. crescentus* Δ*regX* (PR154) cells in comparison
1323 to wild-type cells. Grey dots represent proteins identified by mass spectrometry. The x-axis indicates the
1324 log2 of the average difference in the peptide counts for the two different conditions (n=3 independent
1325 replicates). The y-axis shows the -log10 of the corresponding p-value. Proteins with a fold change smaller
1326 than 0.5 or larger than 2 are highlighted in color and numbered. Details on these proteins are given in
1327 **Figure 8–table supplement 1**. **(D)** Phase contrast images of Δ*traX* (PR153) and Δ*regX* (PR154) cells,
1328 harvested in the exponential or stationary growth phase. Scale bar: 5 µm. **(E)** Superplots showing the
1329 distribution of cell lengths in populations of *C. crescentus* wild-type, Δ*traX* (PR153) and Δ*regX* (PR154) cells
1330 in the exponential (exp) and stationary (stat) growth phase. Data (*n*=100 cells per replicate) are presented

1331 as described for **Figure 4B**. The statistical significance (*p*-value) of differences between conditions was
1332 assessed using an unpaired two-sided Welch's *t*-test. ns indicates *p*-values > 0.1. **(F)** Serial dilution spot
1333 assays investigating the growth of *C. crescentus* wild-type, Δ*traX* (PR153), Δ*regX* (PR154) and Δ*blaA* (CS606)
1334 cells on agar plates in the absence or presence of ampicillin.

1335 **Figure 8–figure supplement 2. Changes in protein accumulation upon deletion of CCNA_02225. (A)** Vol-
1336 cano plot showing differential protein abundance in *C. crescentus* ΔCC*NA_02225* (PR218) vs. wild-type
1337 cells. Grey dots represent proteins identified by mass spectrometry. The x-axis indicates the log2 of the
1338 average difference in the peptide counts for the two different conditions (*n*=3 independent replicates).
1339 The y-axis shows the -log10 of the corresponding *p*-value. The 20 proteins with the highest fold change
1340 according to Manhattan distance are highlighted in color and numbered. The functional categorization of
1341 these genes is indicated in the lower left corner of the plot. Proteins encoded in the five-gene operon are
1342 labeled in orange. **(B)** List of the most highly deregulated proteins in the ΔCC*NA_02225* (PR218) mutant.
1343 The table gives the gene name or ORF number, the fold change, the *p*-value and the predicted function for
1344 the proteins numbered in panel A.

1345 **Figure 9. PG recycling defects increase the sensitivity of the septal PG synthetic machinery to ampicillin**
1346 **and reduce PG precursor biosynthesis. (A)** Phase contrast images of *C. crescentus* wild-type and Δ*amiR*
1347 (PR033) cells, incubated for 3 h in the presence of different concentrations of ampicillin. Scale bar: 5 µm.
1348 **(B)** Quantification of the fraction of lysed cells in cultures of *C. crescentus* wild-type and Δ*amiR* (PR033)
1349 cells, incubated for 3 h in the presence of different concentrations of ampicillin. The bars represent the
1350 mean (±SD) of three independent replicates (*n*=100 cells per condition). The underlying data are shown as
1351 grey dots. The statistical significance (*p*-value) of differences between strains was calculated using an un-
1352 paired two-sided Welch's t-test. ns indicates p-values > 0.1. **(C)** Time-lapse microscopy analysis showing
1353 *C. crescentus* wild-type and Δ*amiR* (PR033) cells in a microfluidic flow cell before and after ampicillin treat-
1354 ment. After 3 h of growth in antibiotic-free medium, the cells were shifted to medium containing 20 µg/mL
1355 ampicillin. Images were taken at 5 min intervals for a total duration of 8 h. Shown are representative fra-
1356 mes of the time-lapse series. The full sequences are shown in **Figure 9-Video 1** and **Figure 9-Video 2**. **(D)**
1357 Image of an SDS-gel showing the labeling of PBPs with the fluorescent β-lactam bocillin-FL in the absence
1358 or presence of other β-lactams. Crude membrane fractions of *C. crescentus* Δ*blaA* (CS606) cells were pre-
1359 incubated with the indicated concentrations of ampicillin, 5 µg/mL cefalexin (Cfx) or 100 µg/mL mecillinam
1360 (Mec), treated with bocillin-FL and then subjected to SDS gel electrophoresis to separate the labeled PBPs
1361 prior to fluorescence imaging. **(E)** Levels of UDP-Glc*N*Ac and UDP-Mur*N*Ac in the cytoplasm of *C. crescentus*
1362 wild-type, Δ*ampG* (PR207), Δ*amiR* (PR033) and Δ*nagZ* (PR188) cells, measured by metabolomics analysis

1363 through quantification of the corresponding mass spectrometric peak areas. For each PG precursor, the
1364 mass spectrometric peak areas were normalized against the mean obtained for the wild-type strain. The
1365 statistical significance of differences between the wild type and the mutant strains was determined using
1366 an unpaired two-sided Welch's t-test. ns indicates p-values > 0.1; nd: not detectable.

1367 **Figure 9–video 1. Effect of ampicillin on the growth of *C. crescentus* wild-type cells.** *C. crescentus* wild-
1368 type cells were cultivated in a microfluidic flow cell for 3 h in antibiotic-free medium and then shifted to
1369 medium containing 20 µg/mL ampicillin. Phase contrast images were taken at 5-min intervals. Scale bar: 5
1370 µm.

1371 **Figure 9–video 2. Effect of ampicillin on the growth of *C. crescentus* Δ*amiR* cells.** *C. crescentus* Δ*amiR*
1372 (PR033) cells were cultivated in a microfluidic flow cell for 3 h in antibiotic-free medium and then shifted
1373 to medium containing 20 µg/mL ampicillin. Phase contrast images were taken at 5-min intervals. Scale bar:
1374 5 µm.

1375 **Figure 9–figure supplement 1. Muropeptide composition of PG sacculi from wild-type and Δ*amiR* cells.**
1376 Shown are HPLC chromatograms resolving the muropeptides obtained by muramidase treatment of PG
1377 sacculi isolated from stationary wild-type or Δ*amiR* (PR033) cells. The muropeptides contained in the
1378 different peaks are listed in **Figure 9–table supplement 1**. A summary of the data obtained is given in
1379 **Figure 9–table supplement 2**.

1380 **Figure 9–figure supplement 2. Ampicillin sensitivity of PG recycling-defective mutants in the presence**
1381 **of Glc*N*Ac.** Shown is a serial dilution spot assay investigating the growth of C. crescentus wild-type, Δ*ampG*
1382 (PR207), Δ*amiR* (PR033), Δ*nagZ* (PR188) and Δ*blaA* (CS606) cells on agar plates containing different con-
1383 centrations of ampicillin in the presence of 0.3% Glc*N*Ac.

1384 **Figure 10. The cell filamentation phenotype of Δ*amiR* cells is rescued by hyper-activation of the septal**
1385 **FtsW-PBP3 PG biosynthetic complex. (A)** Phase contrast images of *C. crescentus ftsW::ftsW** (ML2103)
1386 and Δ*amiR ftsW::ftsW** (PR246) cells, harvested in the exponential and stationary growth phase. **(B)**
1387 Superplots showing the distribution of cell lengths in populations of *C. crescentus ftsW::ftsW** (ML2103)
1388 and Δ*amiR ftsW::ftsW** (PR246) cells in the exponential (exp) and stationary (stat) growth phase. Data
1389 (*n*=100 cells per replicate) are presented as described for **Figure 4B**. The statistical significance (*p*-value)
1390 of differences between conditions was assessed using an unpaired two-sided Welch's *t*-test. ns indicates
1391 *p*-values > 0.1. **(C)** Serial dilution spot assay investigating the growth of *C. crescentus ftsW::ftsW**
1392 (ML2103), Δ*amiR* (PR033) and Δ*amiR ftsW::ftsW** (PR246) cells on agar plates containing no or 10 µg/mL
1393 ampicillin.

1394 **Figure 11. Model for the critical role of PG recycling in *C. crescentus* growth and β-lactam. (A)** PBPs medi-
1395 ates the incorporation of new cell wall material into the growing PG sacculus. The PG precursors required
1396 for this process are synthesized in the cytoplasm, using building blocks that are provided by both *de novo*
1397 synthesis and PG recycling. **(B)** If β-lactams enter the periplasm, they compete with PG precursors for
1398 binding to their PBP targets. Most antibiotic molecules are rapidly hydrolyzed by the β-lactamase BlaA.
1399 However, a minor fraction manages to interact with PBPs before they are captured and degraded. The
1400 resulting inactivation of a small proportion of PBPs can be tolerated by cells, as long as they still contain
1401 sufficient active PBPs to maintain cell growth and division. **(C)** Upon disruption of PG recycling, the level of
1402 PG monomers strongly decreases, leaving the substrate binding sites of PBPs unoccupied for longer peri-
1403 ods of time and thus increasing their accessibility to β-lactam molecules. As a result, a larger fraction of
1404 PBPs is inactivated, leading to decreased cell wall integrity and ultimately cell lysis. This effect may be
1405 aggravated by the reduced activity of the remaining, active PBPs due to an insufficient supply of PG pre-
1406 cursors and by the accumulation of anhydro-muropentapeptides in the periplasm, which could interfere
1407 with the activities of PG biosynthetic enzymes, thereby further decreasing the incorporation of new
1408 material into the existing sacculus.

Figures

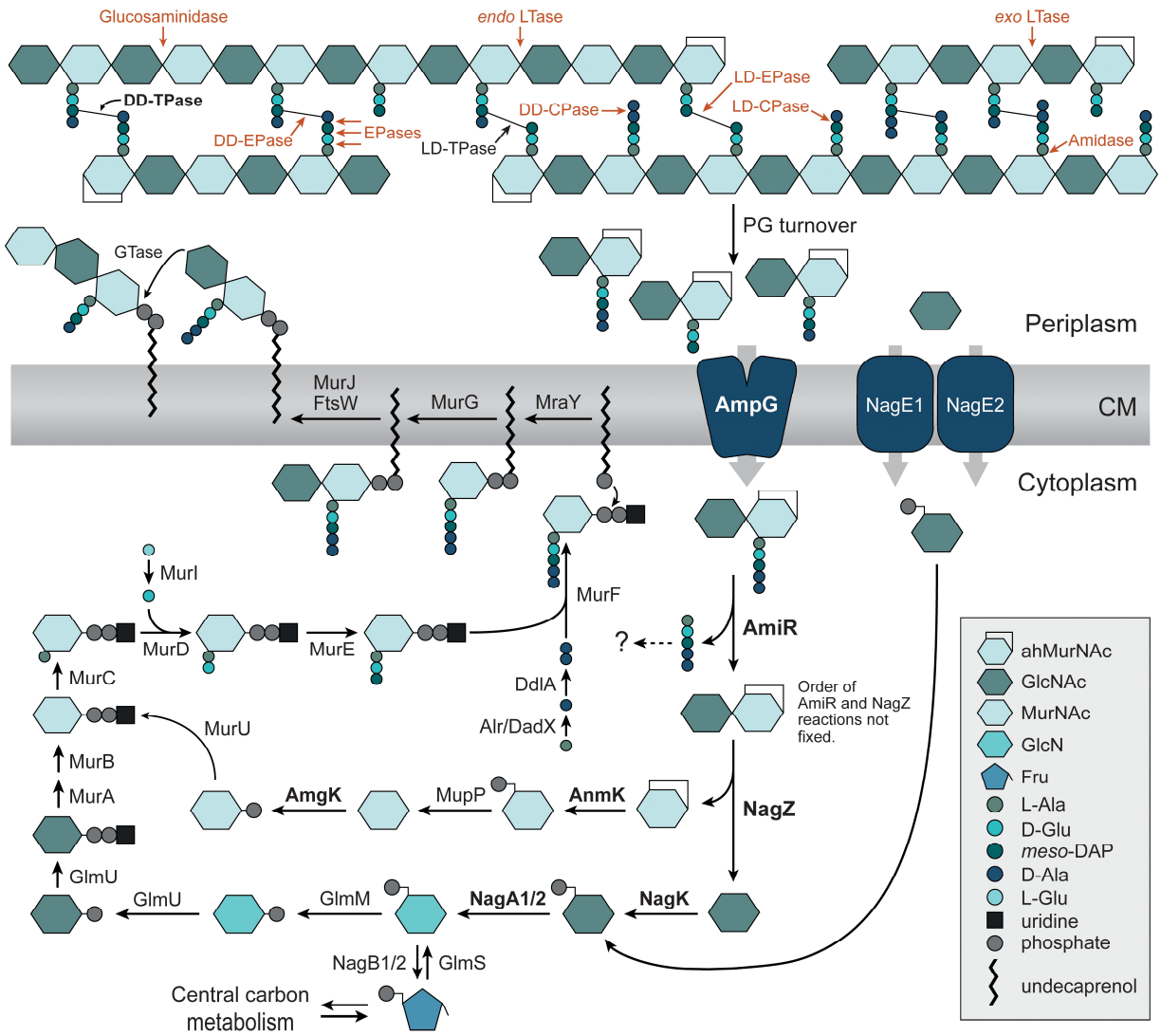

Figure 1. The *C. crescentus* genome encodes a complete PG recycling pathway. *De novo* PG biosynthesis starts with the conversion of fructose-6-phosphate, supplied by central carbon metabolism, to glucosamine-6-phosphate. This key metabolite is then transformed by multiple enzymatic steps into the membrane-attached PG precursor lipid II, which is flipped to the periplasmic face and incorporated into the existing PG sacculus by glycosyltransferases and transpeptidases. To enable PG remodeling, growth and cell separation, the PG meshwork is cleaved by a diverse set of enzymes, such as lytic transglycosylases (LTs), endopeptidases (EPases), amidases and carboxypeptidases (CPases). PG fragments released by these activities are imported into the cytoplasm by the permease AmpG or two homologs of the phosphotransferase system (PTS) transporter NagE. In the cytoplasm, the peptide is released by AmiR and the sugars separated by NagZ. Afterwards, two independent pathways feed the two sugars back into the *de novo* PG biosynthetic pathway. The enzymes are named as established for *E. coli* and *P. aeruginosa*, with the exception of the *C. crescentus* homolog of AmpD, which was renamed to AmiR due to its different domain organization. The symbols are defined in the legend on the right.

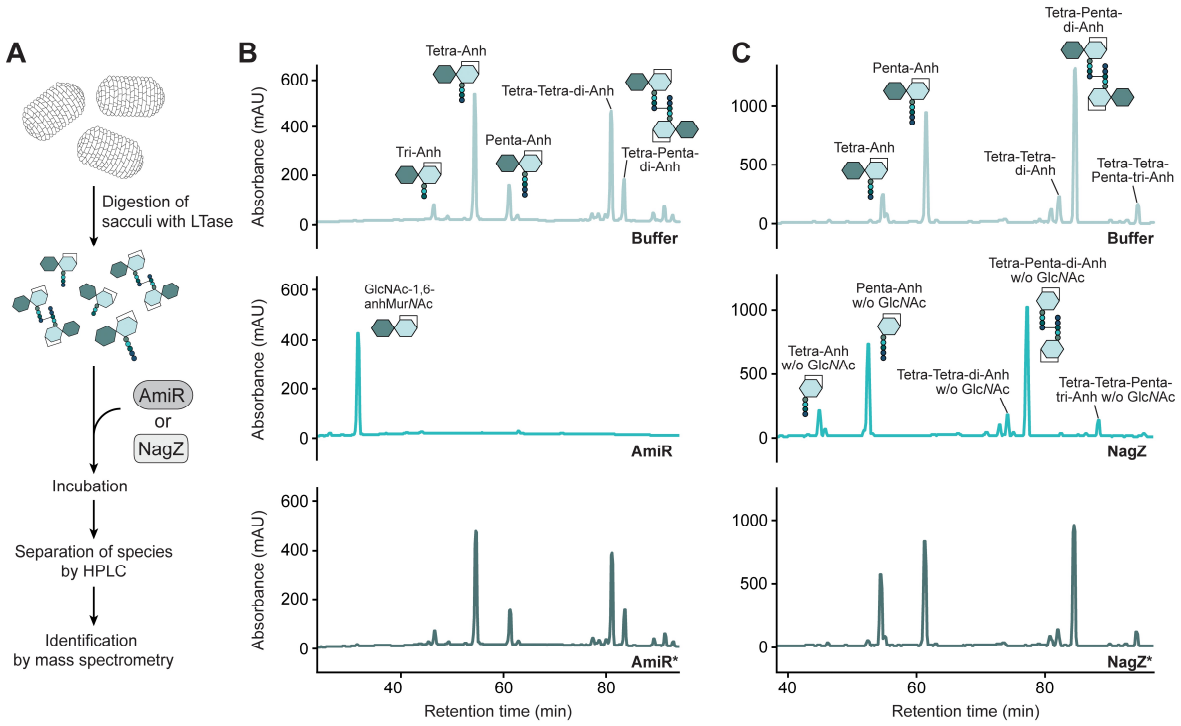

Figure 2. The AmiR and NagZ homologs are functional and have a broad substrate specificity. (A) Overview of the PG digestion assay used to assess the hydrolytic activities of AmiR and NagZ. **(B)** HPLC chromatograms showing the products generated upon incubation of anhydro-muropeptides from LT-treated PG sacculi without added proteins (Buffer), with AmiR or with a catalytically inactive AmiR variant (AmiR*). The identities of anhMur*N*Ac-peptides were determined based on their known retention times (Glauner, 1988). The AmiR reaction product Glc*N*Ac-1,6-anhMur*N*Ac was identified by mass spectrometry (**Figure 2–figure supplement 4A**). **(C)** HPLC chromatograms showing the products generated upon incubation of anhydro-muropeptides from LT-treated PG sacculi without added proteins (Buffer), with NagZ or with a catalytically inactive NagZ variant (NagZ*). Disaccharide-containing anhydro-muropeptides were identified based on their known retention times (Glauner, 1988). The identities of anhMur*N*Ac-peptides were determined by mass spectrometric analysis of the reaction products obtained after NagZ treatment of anhydro-muropeptide mixtures (**Figure 2–figure supplement 4B**).

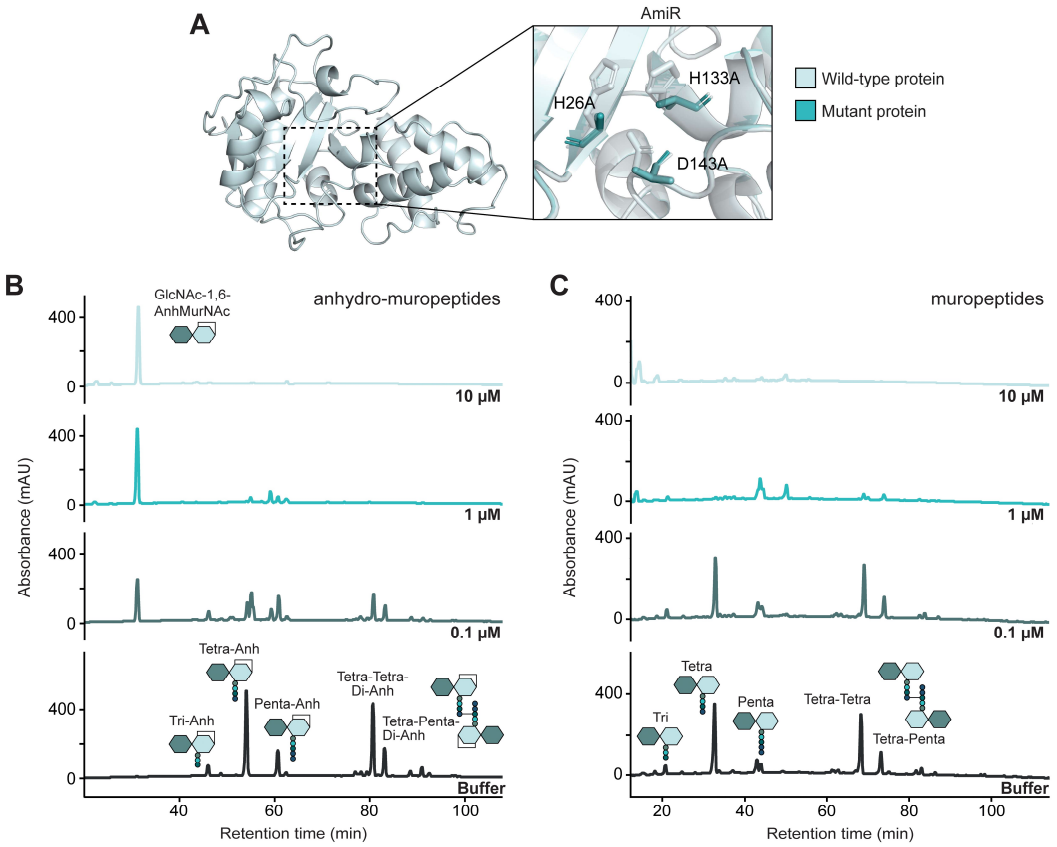

Figure 2–figure supplement 1. Substrate specificity of AmiR. (A) Structural models of AmiR and the catalytically inactive AmiR* variant, generated with AlphaFold 3 (Abramson et al., 2024). The magnified region shows the predicted catalytic site of AmiR and the amino acid substitutions introduced to generate AmiR*. **(B)** HPLC chromatograms showing the products generated upon incubation of anhydro-muropeptides from LT-treated PG sacculi for 16 h without added proteins (Buffer) or with the indicated concentrations of AmiR. **(C)** HPLC chromatograms showing the products generated upon incubation of muropeptides from muramidase-treated PG sacculi for 16 h without added proteins (Buffer) or with the indicated concentrations of AmiR. Reaction products were identified based on their known retention times (Glauner, 1988).

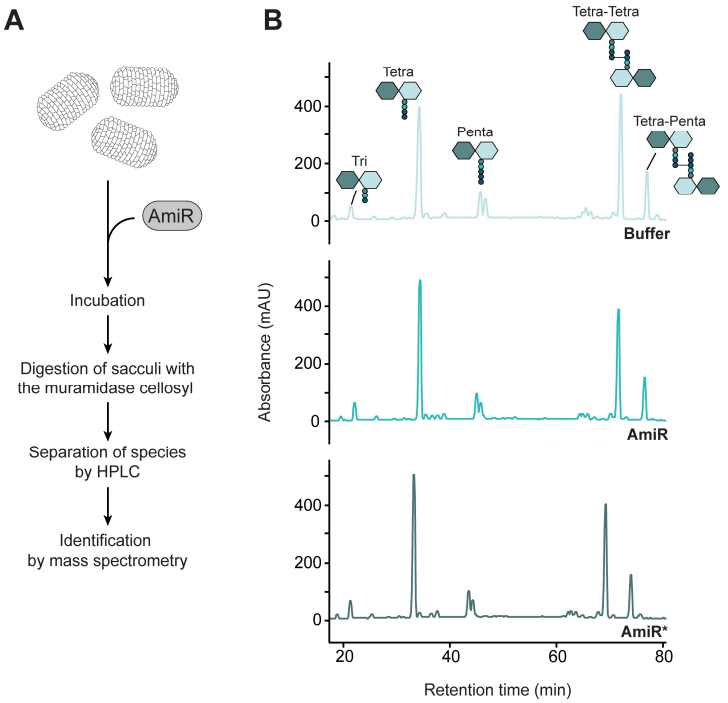

1437 **Figure 2–figure supplement 2. Lack of AmiR activity towards intact PG sacculi. (A)** Overview of the PG digestion assay used to
1438 assess the hydrolytic activity of AmiR on intact PG sacculi. **(B)** HPLC chromatograms showing the products generated upon incu-
1439 bation of intact PG sacculi without added proteins (Buffer), with AmiR and the catalytically inactive AmiR variant (AmiR*) and
1440 subsequent cellosyl-mediated cleavage of the pre-treated sacculi into muropeptides. Muropeptides were identified based on their
1441 known retention times (Glauner, 1988).

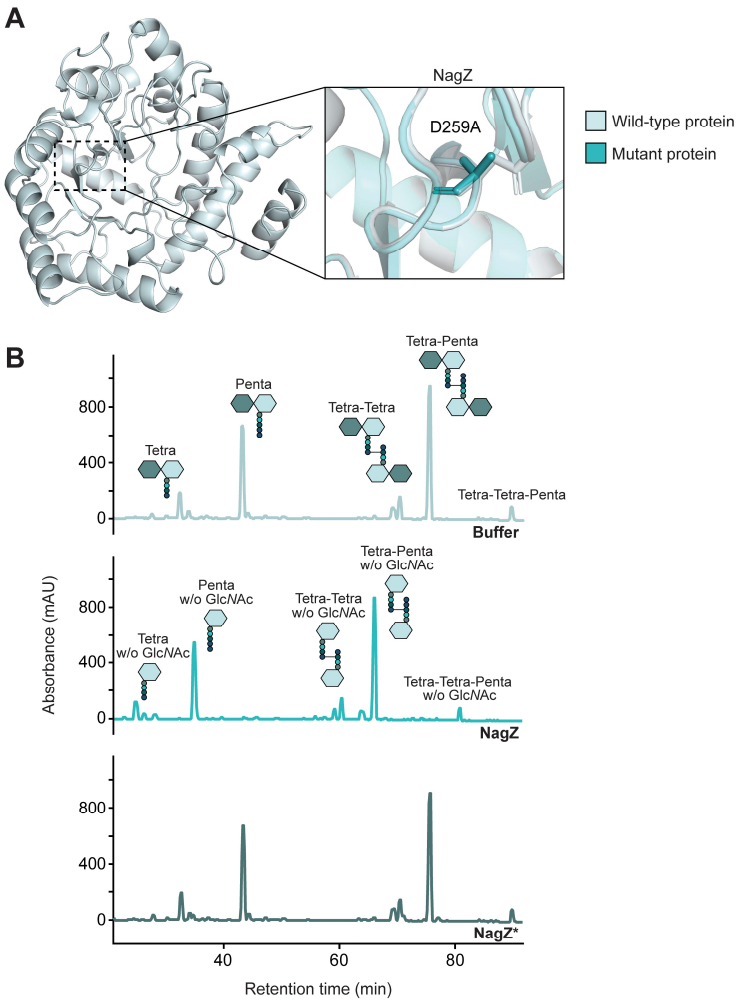

Figure 2–figure supplement 3. Activity of NagZ with muropeptides. (A) Structural models of NagZ and the catalytically inactive NagZ* variant, generated with AlphaFold 3 (Abramson et al., 2024). The magnified region shows the predicted catalytic site of NagZ and the amino acid substitution introduced to generate NagZ*. **(B)** HPLC chromatograms showing the products generated upon incubation of muropeptides from muramidase-treated PG sacculi without added proteins (Buffer), with NagZ or with a catalytically inactive NagZ variant (NagZ*). Disaccharide-containing muropeptides were identified based on their known retention times (Glauner, 1988). The identities of Mur*N*Ac-peptides were validated by mass spectrometry analysis of the reaction products obtained after NagZ treatment of anhydro-muropeptide mixtures (**Figure 2–figure supplement 4B**).

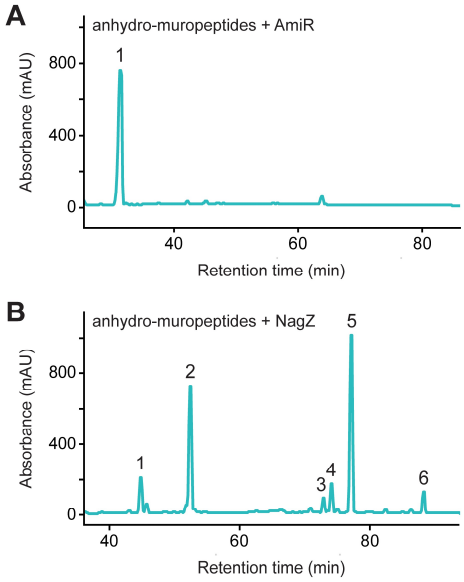

Peak ID	Observed m/z (charge)	Neutral mass (calculated)	Possible ID from MS/MS
1	478.97 (1+)	478.18	Glc*N*Ac-1,6-ahMur*N*Ac

Peak ID	Observed m/z (charge)	Neutral mass (calculated)	Possible ID from MS/MS
1	719.15 (1+)	718.15	Tetra-Anh minus Glc*N*Ac
2	790.18 (1+)	789.18	Penta-Anh minus Glc*N*Ac
3	738.75 (2+)	1475.5	TetraPenta(Gly5)-diAnh minus Glc*N*Ac (x2)
4	710.30 (2+)	1418.6	TetraTetra-diAnh minus Glc*N*Ac (x2)
5	745.92 (2+)	1489.84	TetraPenta-diAnh minus Glc*N*Ac (x2)
6	1095.97 (2+)	2189.94	TetraTetraPenta-triAnh minus Glc*N*Ac (x3)

Figure 2–figure supplement 4. Mass spectrometric identification of AmiR and NagZ reaction products. (A) Identification of the Glc*N*Ac–anhMur*N*Ac disaccharide generated by treatment of anhydro-muropeptides with AmiR. Sacculi isolated from *E. coli* D456 (Edwards and Donachie, 1993) were treated with the LT Slt70 *E. coli*. The graph shows the chromatogram obtained after separation of the sugar-containing reaction products by HPLC. The observed m/z ratios of the main product in peak 1 and the calculated molecular mass of the GlcNAc-1,6-anhMur*N*Ac disaccharide are given in the table on the right. **(B)** Identification of the anhMur*N*Ac-peptide species generated by treatment of anhydro-muropeptides with NagZ. Sacculi isolated from *E. coli* CS703-1 (Meberg et al., 2001) were treated with the LT MltA from *E. coli*. The graph shows the chromatogram obtained after separation of the reaction products by HPLC. The table on the right gives the observed m/z ratios of the main product detected contained in the indicated peaks as well as the calculated molecular masses of the anhMur*N*Ac-peptides assigned to these peaks.

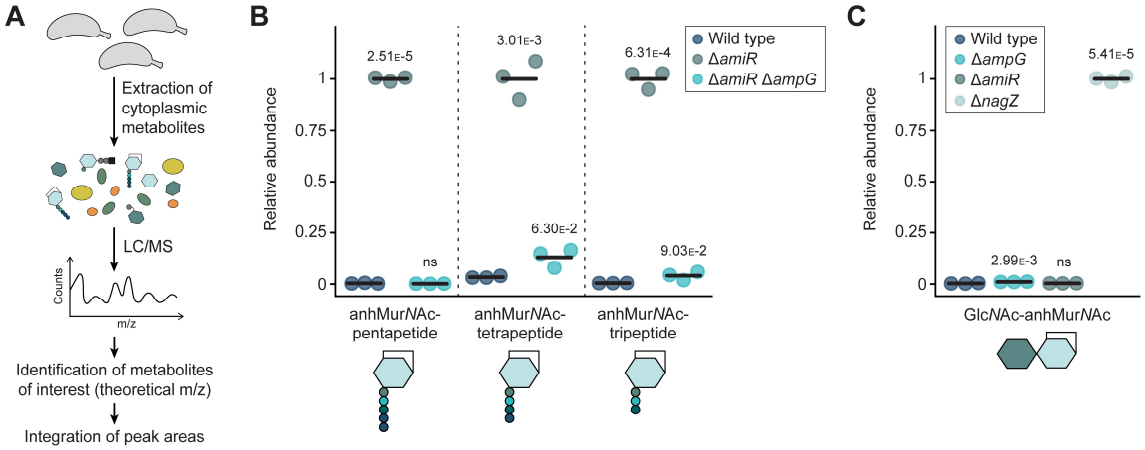

Figure 3. Metabolomic analysis reveals aberrant levels of PG recycling intermediates in recycling-deficient strains. (A) Overview of the analysis pipeline used to identify cytoplasmic PG recycling products. **(B)** Levels of the indicated anhMur*N*Ac-peptide species in the cytoplasm of *C. crescentus* wild-type, Δ*amiR* (PR033) and Δ*amiR* Δ*ampG* (PR221) cells, measured by metabolomics analysis through quantification of the corresponding mass spectrometric peak areas. The statistical significance of differences between the wild type and the mutant strains was determined using an unpaired two-sided Welch's t-test. ns indicates p-values > 0.1. **(C)** Level of the Glc*N*Ac–anhMur*N*Ac disaccharide in *C. crescentus* wild-type, Δ*ampG* (PR207), Δ*amiR* (PR033) and Δ*nagZ* (PR188) cells, assessed as for panel B.

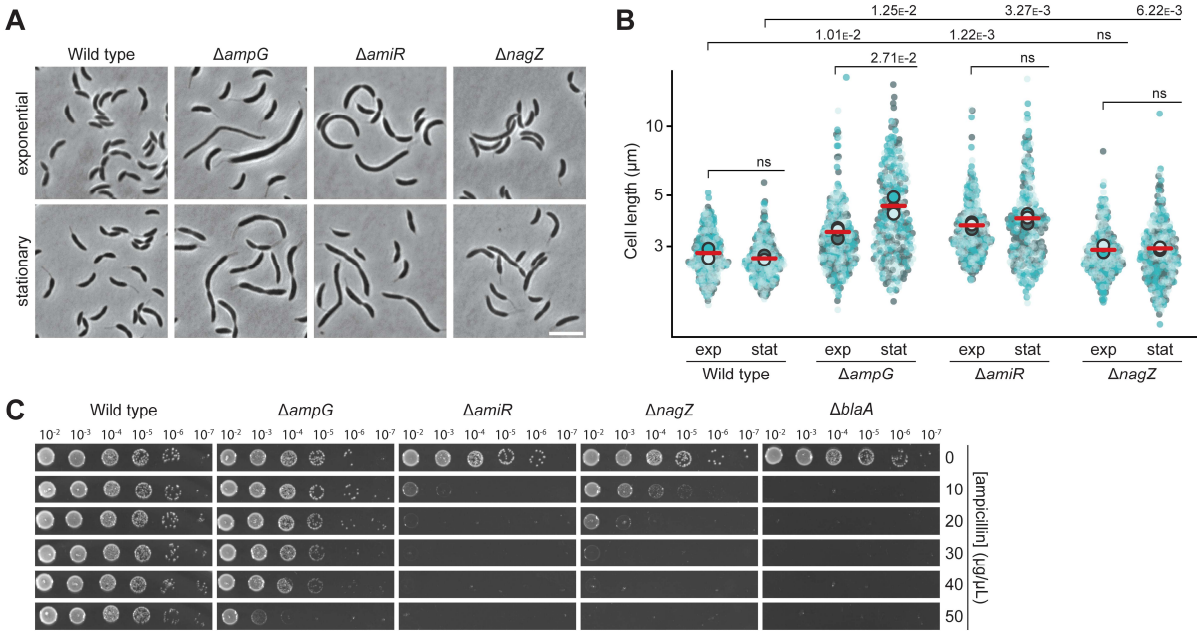

Figure 4. AmpG, AmiR and NagZ are required for proper cell shape and β-lactam resistance in *C. crescentus*. (A) Phase contrast images of *C. crescentus* wild-type, Δ*ampG* (PR207), Δ*amiR* (PR033) and Δ*nagZ* (PR188) cells harvested in the exponential and stationary growth phase. Scale bar: 5 µm. **(B)** Superplots showing the distribution of cell lengths in populations of *C. crescentus* wild-type, Δ*ampG* (PR207), Δ*amiR* (PR033) and Δ*nagZ* (PR188) cells in the exponential (exp) and stationary (stat) growth phase. Small dots represent the data of three independent replicates (shown in light blue, teal and dark grey; *n*=100 cells per replicate). Large dots represent the mean values of the three datasets, with their average indicated by a red horizontal line. The statistical significance (*p*-value) of differences between conditions was assessed using an unpaired two-sided Welch's *t*-test. ns indicates *p*-values > 0.1. **(C)** Serial dilution spot assay investigating the growth of wild-type, Δ*ampG* (PR207), Δ*amiR* (PR033), Δ*nagZ* (PR188) and Δ*blaA* (CS606) cells on agar plates with different concentrations of ampicillin.

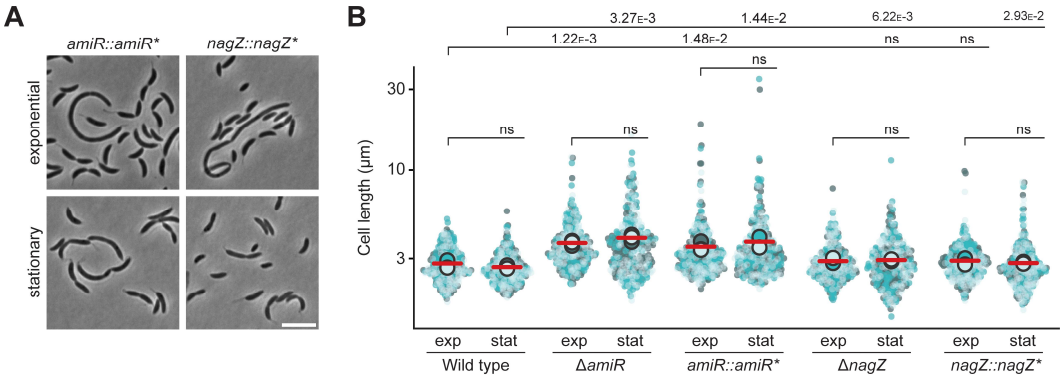

Figure 4–figure supplement 1. Morphological characterization of catalytically inactive AmiR and NagZ variants. (A) Phase contrast images of *C. crescentus amiR::amiR** (PR173) and *nagZ:nagZ** (PR196) cells harvested in the exponential and stationary growth phase. Scale bar: 5 µm. **(B)** Superplots showing the distribution of cell lengths in populations of wild-type, Δ*amiR* (PR033), *amiR::amiR** (PR173), Δ*nagZ* (PR188) and *nagZ::nagZ** (PR196) cells in the exponential (exp) and stationary (stat) growth phase. Data (*n*=100 cells per replicate) are presented as described for **Figure 4B**. The statistical significance (*p*-value) of differences between conditions was assessed using an unpaired two-sided Welch's *t*-test. ns indicates *p*-values > 0.1. The data for wild-type, Δ*amiR* and Δ*nagZ* cells are taken from **Figure 3** and shown as a reference.

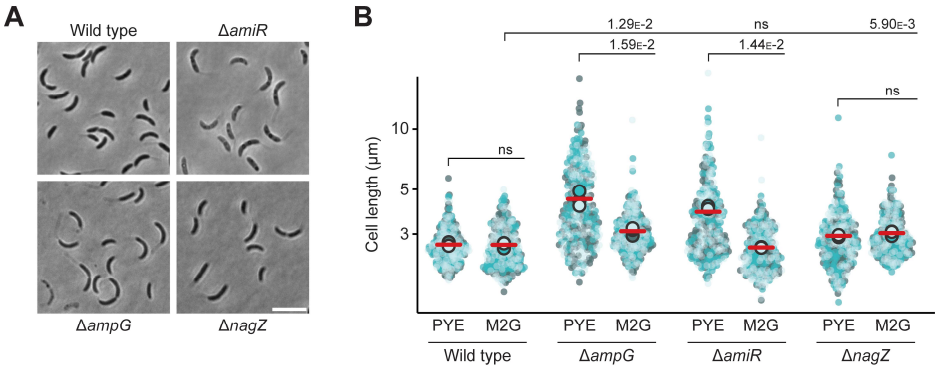

1481 **Figure 4–figure supplement 2. Growth of PG recycling-deficient mutants in minimal medium. (A)** Phase contrast images of *C.*
1482 *crescentus* wild-type, Δ*ampG* (PR207), Δ*amiR* (PR033) and Δ*nagZ* (PR188) cells grown in minimal (M2G) medium and harvested in
1483 the stationary growth phase. **(B)** Superplots showing the distribution of cell lengths in populations of wild-type, Δ*ampG* (PR207),
1484 Δ*amiR* (PR033) and Δ*nagZ* (PR188) cells grown in rich medium (PYE) and minimal medium (M2G). Data (*n*=100 cells per replicate)
1485 are presented as described for **Figure 4B**. The statistical significance (*p*-value) of differences between conditions was assessed
1486 using an unpaired two-sided Welch's *t*-test. ns indicates *p*-values > 0.1. The distributions of cell lengths in rich medium are taken
1487 from **Figure 3** and shown as a reference.

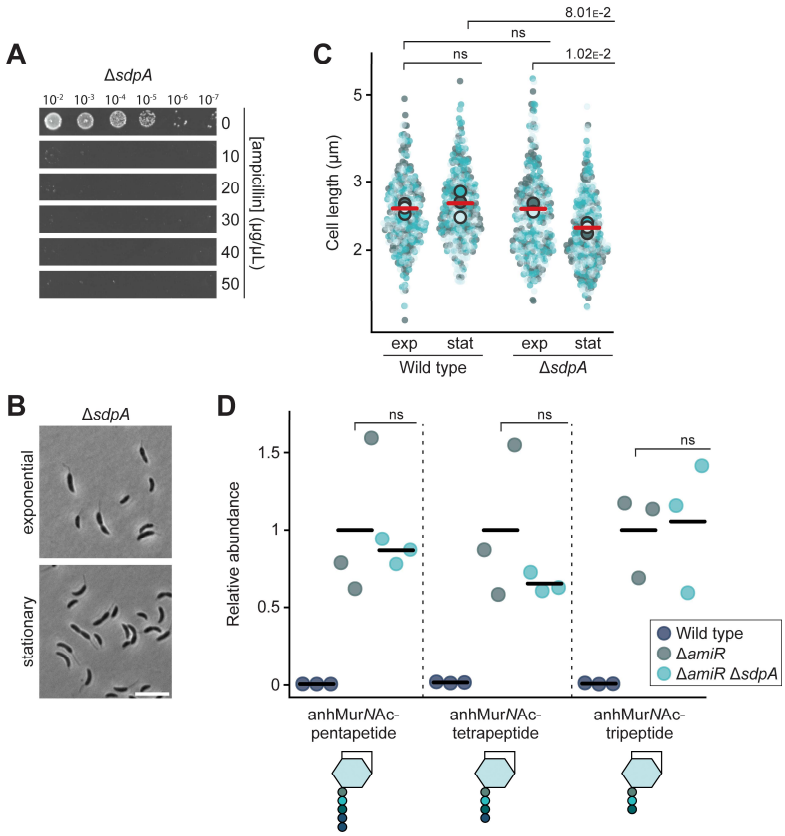

Figure 4–figure supplement 3. Redundant role of the LT SdpA in the production of anhydro-muropeptides. (A) Serial dilution spot assay investigating the growth of *C. crescentus* Δ*sdpA* (AM399) cells on agar plates containing different concentrations of ampicillin. The cells were spotted on the same plates as those depicted in **Figure 3**. **(B)** Phase contrast images of *C. crescentus* Δ*sdpA* (AM399) harvested in the exponential or stationary growth phase. **(C)** Superplots showing the distribution of cell lengths in populations of wild-type and Δ*sdpA* (AM399) cells harvested in the exponential (exp) and stationary (stat) growth phase. Data (*n*=100 cells per replicate) are presented as described for **Figure 4B**. The statistical significance (*p*-value) of differences between conditions was assessed using an unpaired two-sided Welch's *t*-test. ns indicates *p*-values > 0.1. **(D)** Levels of the indicated anhMur*N*Ac-peptide species in the cytoplasm of *C. crescentus* wild-type, Δ*amiR* (PR033) and Δ*amiR* Δ*sdpA* (PR260) cells, measured by metabolomics analysis through quantification of the corresponding mass spectrometric peak areas. The statistical significance of differences between the wild type and the mutant strains was determined using an unpaired two-sided Welch's t-test. ns indicates p-values > 0.1.

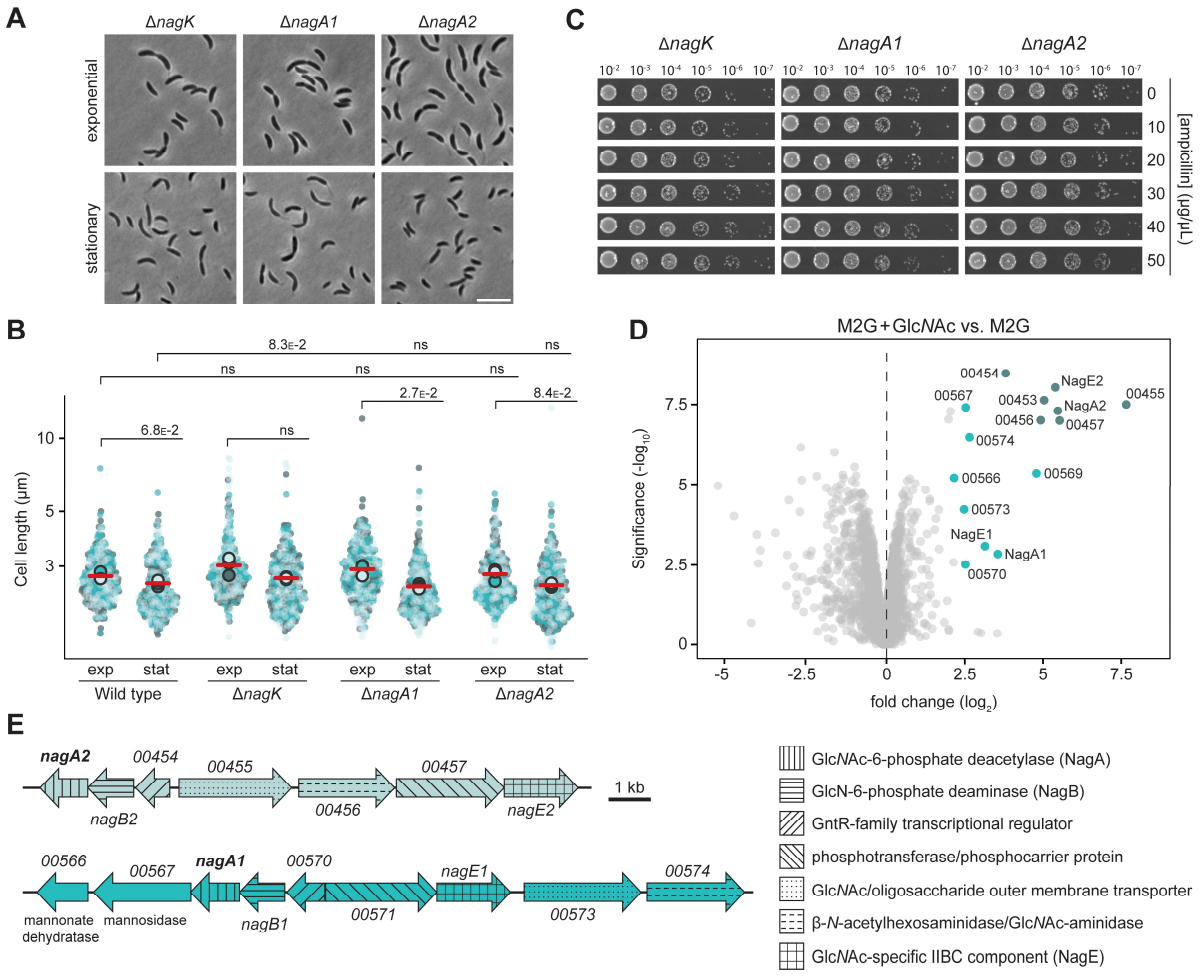

Figure 5. The GlcNAc recycling pathway is dispensable for proper cell division and β-lactam resistance. (A) Phase contrast images of *C. crescentus* Δ*nagK* (PR255), Δ*nagA1* (PR256) and Δ*nagA2* (PR257) cells harvested in the exponential and stationary growth phase. Scale bar: 5 µm. **(B)** Superplots showing the distribution of cell lengths in populations of *C. crescentus* wild-type, Δ*nagK* (PR255), Δ*nagA1* (PR256) and Δ*nagA2* (PR257) cells in the exponential (exp) and stationary (stat) growth phase. Data (*n*=100 cells per replicate) are presented as described for **Figure 4B**. The statistical significance (*p*-value) of differences between conditions was assessed using an unpaired two-sided Welch's *t*-test. ns indicates *p*-values > 0.1. **(C)** Serial dilution spot assays investigating the growth of *C. crescentus* Δ*nagK* (PR255), Δ*nagA1* (PR256) and Δ*nagA2* (PR257) cells on agar plates containing different concentrations of ampicillin. The cells were spotted on the same plates as those depicted in **Figure 3**. **(D)** Volcano plot illustrating differential protein abundance in *C. crescentus* wild-type cells grown in M2G minimal medium with GlcNAc compared to plain M2G medium. Grey dots represent proteins identified by mass spectrometry. The x-axis indicates the log2 of the average difference in the peptide counts for the two different conditions (*n*=3 independent replicates). The y-axis shows the -log10 of the corresponding *p*-value. Proteins encoded in the two *nag* gene clusters are highlighted in color and annotated. The colors correspond to those used in panel E. **(E)** Schematic representation of the two *nag* gene clusters. The predicted functions of the gene products are specified in the legend on the right.

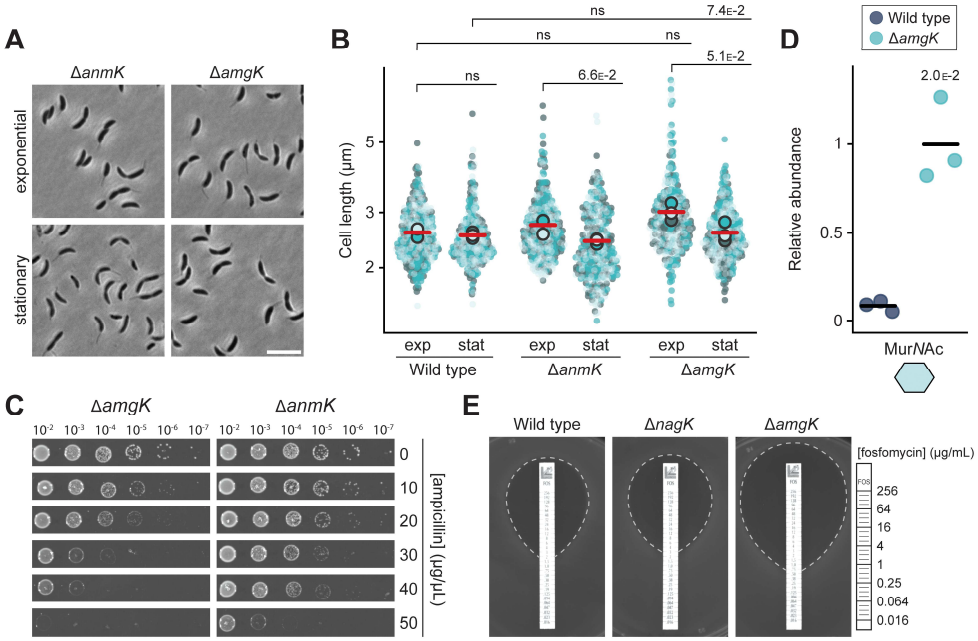

Figure 6. *C. crescentus* recycles anhMur*N*Ac through a functional MurU pathway. (A) Phase contrast images of *C. crescentus* Δ*anmK* (PR252) and Δ*amgK* (PR262) cells, harvested in the exponential and stationary growth phase. Scale bar: 5 µm. **(B)** Superplots showing the distribution of cell lengths in populations of *C. crescentus* wild-type, Δ*anmK* (PR252), and Δ*amgK* (PR262) cells in the exponential (exp) and stationary (stat) growth phase. Data (*n*=100 cells per replicate) are presented as described for **Figure 4B**. The statistical significance (*p*-value) of differences between conditions was assessed using an unpaired two-sided Welch's *t*-test. ns indicates *p*-values > 0.1. **(C)** Serial dilution spot assay investigating the growth of *C. crescentus* Δ*anmK* (PR252) and Δ*amgK* (PR262) on plates containing different concentrations of ampicillin. The cells were spotted on the same plates as those depicted in **Figure 3**. **(D)** Levels of Mur*N*Ac in the cytoplasm of *C. crescentus* wild-type and Δ*amgK* (PR262) cells, measured by metabolomics analysis through quantification of the corresponding mass spectrometric peak areas. The statistical significance of differences between the two strains was determined using an unpaired two-sided Welch's t-test. **(E)** Analysis of the growth of *C. crescentus* wild-type, Δ*nagK* (PR255) and Δ*amgK* (PR262) cells on agar containing a fosfomycin gradient. The fosfomycin concentrations on the MIC test strip are indicate in the legend on the right.

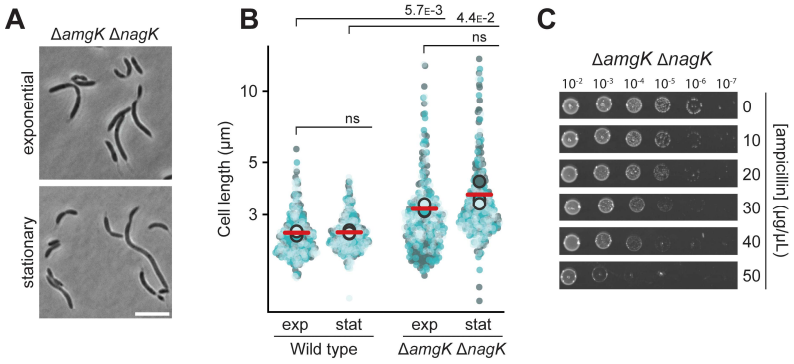

Figure 7. Recycling of the disaccharide moiety plays only a minor role in cell division and β-lactam resistance. (A) Phase contrast images of *C. crescentus* Δ*amgK* Δ*nagK* (PR261) cells, harvested in the exponential and stationary growth phase. Scale bar: 5 µm. **(B)** Superplots showing the distribution of cell lengths in populations of *C. crescentus* wild-type and Δ*amgK* Δ*nagK* (PR261) cells in the exponential (exp) and stationary (stat) growth phase. Data (*n*=100 cells per replicate) are presented as described for **Figure 4B**. The statistical significance (*p*-value) of differences between conditions was assessed using an unpaired two-sided Welch's *t*-test. ns indicates *p*-values > 0.1. **(C)** Serial dilution spot assays investigating the growth of *C. crescentus* Δ*amgK* Δ*nagK* (PR261) cells on agar plates containing different concentrations of ampicillin. The cells were spotted on the same plates as those depicted in **Figure 3**.

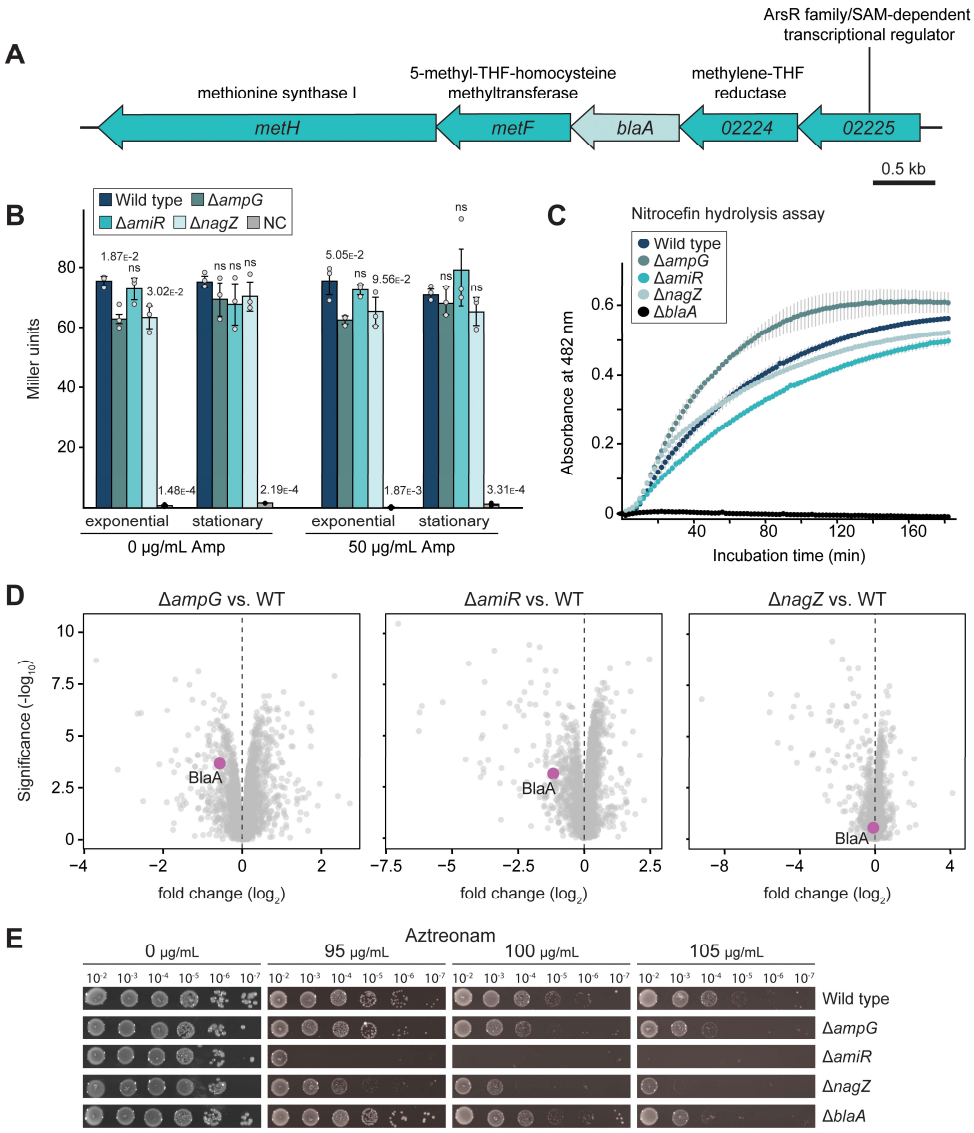

Figure 8. BlaA function is not regulated at the levels of transcription, protein accumulation or enzymatic activity. (A) Organization of the putative five-gene operon containing the *blaA* gene. The annotation or ORF number of the open reading frames and the predicted functions of their gene products are indicated. **(B)** Activity of the promoter likely driving the expression of the *blaA*-containing operon in different strain backgrounds. The *C. crescentus* wild-type, Δ*ampG* (PR207), Δ*amiR* (PR033) and Δ*nagZ* (PR188) strains were transformed with a plasmid carrying a 400 bp fragment of the CCNA_02225 upstream region fused to a β-galactosidase reporter gene and assayed for reporter activity. Strains transformed with the empty plasmid served as negative controls (NC). The underlying data are shown as grey dots. The statistical significance (*p*-value) of differences between strains was calculated using an unpaired two-sided Welch's t-test. ns indicates p-values > 0.1. **(C)** β-lactamase activity of *C. crescentus* wild-type, Δ*ampG* (PR207), Δ*amiR* (PR033) and Δ*nagZ* (PR188) cells, as determined by monitoring the hydrolysis of the chromogenic β-lactam nitrocefin in permeabilized cells over time. **(D)** Volcano plots showing differential protein abundance in *C. crescentus* Δ*ampG* (PR207), Δ*amiR* (PR033) and Δ*nagZ* (PR188) cells compared to wild-type cells. Grey dots represent proteins identified by mass spectrometry. The x-axis indicates the log2 of the average difference in the peptide counts for the two different conditions (*n*=4 independent replicates). The y-axis shows the -log10 of the corresponding *p*-value. The BlaA protein is highlighted in magenta. **(E)** Serial dilution spot assays investigating the growth of *C. crescentus* wild-type, Δ*ampG* (PR207), Δ*amiR* (PR033), Δ*nagZ* (PR188) and Δ*blaA* cells (CS606) on agar plates containing different concentrations of aztreonam.

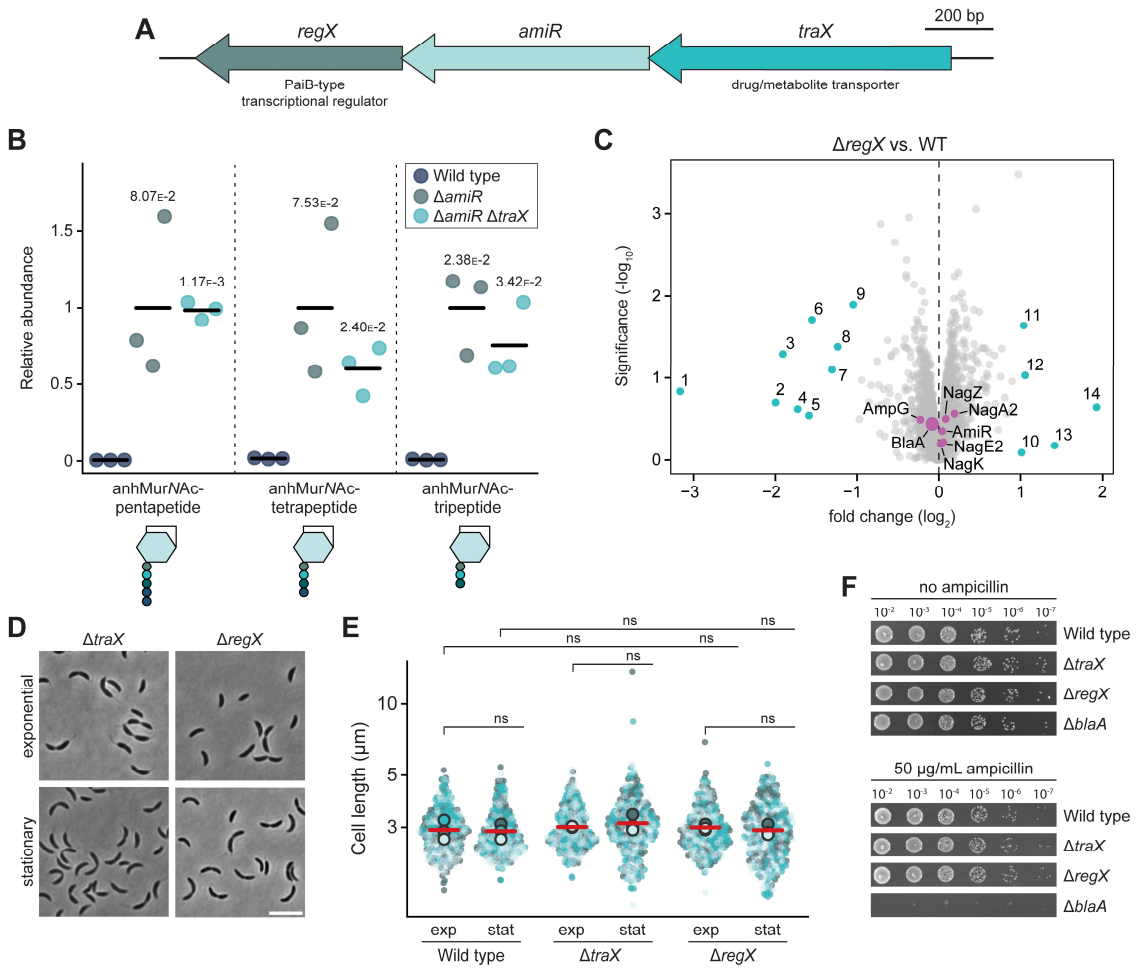

Figure 8–figure supplement 1. The two genes forming an operon with *amiR* are dispensible for PG recycling or β-lactam resistance. (A) Genomic context of *amiR*. The gene names and the predicted functions of the respective gene products are indicated. **(B)** Levels of the indicated anhMur*N*Ac-peptide species in the cytoplasm of *C. crescentus* wild-type, Δ*amiR* (PR033) and Δ*amiR* Δ*traX* (PR258) cells, measured by metabolomics analysis through quantification of the corresponding mass spectrometric peak areas. **(C)** Volcano plot showing differences in protein abundance in *C. crescentus* Δ*regX* (PR154) cells in comparison to wild-type cells. Grey dots represent proteins identified by mass spectrometry. The x-axis indicates the log2 of the average difference in the peptide counts for the two different conditions (n=3 independent replicates). The y-axis shows the -log10 of the corresponding p-value. Proteins with a fold change smaller than 0.5 or larger than 2 are highlighted in color and numbered. Details on these proteins are given in **Figure 8–table supplement 1**. **(D)** Phase contrast images of Δ*traX* (PR153) and Δ*regX* (PR154) cells, harvested in the exponential or stationary growth phase. Scale bar: 5 µm. **(E)** Superplots showing the distribution of cell lengths in populations of *C. crescentus* wild-type, Δ*traX* (PR153) and Δ*regX* (PR154) cells in the exponential (exp) and stationary (stat) growth phase. Data (*n*=100 cells per replicate) are presented as described for **Figure 4B**. The statistical significance (*p*-value) of differences between conditions was assessed using an unpaired two-sided Welch's *t*-test. ns indicates *p*-values > 0.1. **(F)** Serial dilution spot assays investigating the growth of *C. crescentus* wild-type, Δ*traX* (PR153), Δ*regX* (PR154) and Δ*blaA* (CS606) cells on agar plates in the absence or presence of ampicillin.

Figure 8–table supplement 1. Proteins found to be differentially accumulated in Δ*regX* cells compared to wild-type cells. The table lists the ORF numbers and predicted functions of the numbered proteins in **Figure 8–figure supplement 1C**.

Protein number	ORF number	Predicted function
1	*CCNA_00845*	Antitoxin protein RelB-1
2	*CCNA_02277*	TonB-dependent outer membrane channel HutA
3	*CCNA_00081*	uncharacterized protein
4	*CCNA_03558*	ATP synthase epsilon chain AtpC
5	*CCNA_02275*	ABC transporter, periplasmic component
6	*CCNA_00437*	Methyl-accepting chemotaxis protein
7	*CCNA_03263*	TonB-dependent receptor
8	*CCNA_01707*	Gluconate 2-dehydrogenase subunit 3-family protein
9	*CCNA_03446*	Feruloyl-CoA synthetase
10	*CCNA_01186*	uncharacterized protein
11	*CCNA_00987*	Stress response protein CsbD
12	*CCNA_00928*	GntR family transcriptional regulator
13	*CCNA_00374*	ATP synthase protein I
14	*CCNA_01205*	ABC transporter ATP-binding protein

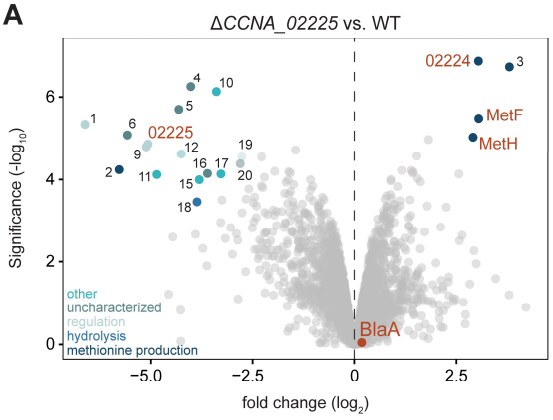

B

	Name	Fold change (log2)	Significance ($-\log_{10}$)	Protein
1	*fixK*	-6.6139	5.3295	Hypoxia transcriptional regulator FixK
2	*hemN*	-5.7751	4.2390	Coproporphyrinogen-III oxidase
3	*metE*	3.8010	6.7442	5-methyltetrahydropteroyltriglutamate-homocysteine methyltransferase
4	CCNA_01464	-4.0213	6.2515	Uncharacterized protein
5	CCNA_03363	-4.3145	5.7053	Conserved hypothetical membrane protein
6	CCNA_02604	-5.5765	5.0750	Host cell attachment protein
7	CCNA_02225	-5.0726	4.8569	ArsR family/SAM-dependent transcriptional regulator
8	CCNA_02224	3.0385	6.8826	Methylenetetrahydrofolate reductase
9	*ftrB*	-5.1131	4.7917	CRP-family transcription regulator FtrB
10	CCNA_01592	-3.3914	6.1318	SN-glycerol-3-phosphate transport ATP-binding protein
11	CCNA_01144	-4.8556	4.1205	Cytochrome c oxidase polypeptide II
12	CCNA_01704	-4.2552	4.6199	Cytochrome c
13	CCNA_02222	3.0447	5.4711	5-methyltetrahydrofolate-homocysteine methyltransferase homocysteine-binding subunit
14	CCNA_02221	2.9066	5.0214	Methionine synthase
15	*fixH*	-3.8114	3.9951	Cation pump-linked membrane protein fixH
16	CCNA_00391	-3.6098	4.1459	Secreted protein
17	CCNA_01745	-3.2790	4.1348	thioredoxin-dependent peroxiredoxin
18	CCNA_02313	-3.8669	3.4553	Alpha/beta hydrolase family protein
19	CCNA_00220	-2.7669	4.5496	Thiol-disulfide isomerase and thioredoxin
20	CCNA_01716	-2.8058	4.3821	MotA/TolQ/ExbB proton channel family protein

Figure 8–figure supplement 2. Changes in protein accumulation upon deletion of CCNA_02225. (A) Volcano plot showing differential protein abundance in *C. crescentus* ΔCC*NA_02225* (PR218) vs. wild-type cells. Grey dots represent proteins identified by mass spectrometry. The x-axis indicates the log2 of the average difference in the peptide counts for the two different conditions (*n*=3 independent replicates). The y-axis shows the -log10 of the corresponding *p*-value. The 20 proteins with the highest fold change according to Manhattan distance are highlighted in color and numbered. The functional categorization of these genes is indicated in the lower left corner of the plot. Proteins encoded in the five-gene operon are labeled in orange. **(B)** List of the most highly deregulated proteins in the ΔCC*NA_02225* (PR218) mutant. The table gives the gene name or ORF number, the fold change, the *p*-value and the predicted function for the proteins numbered in panel A.

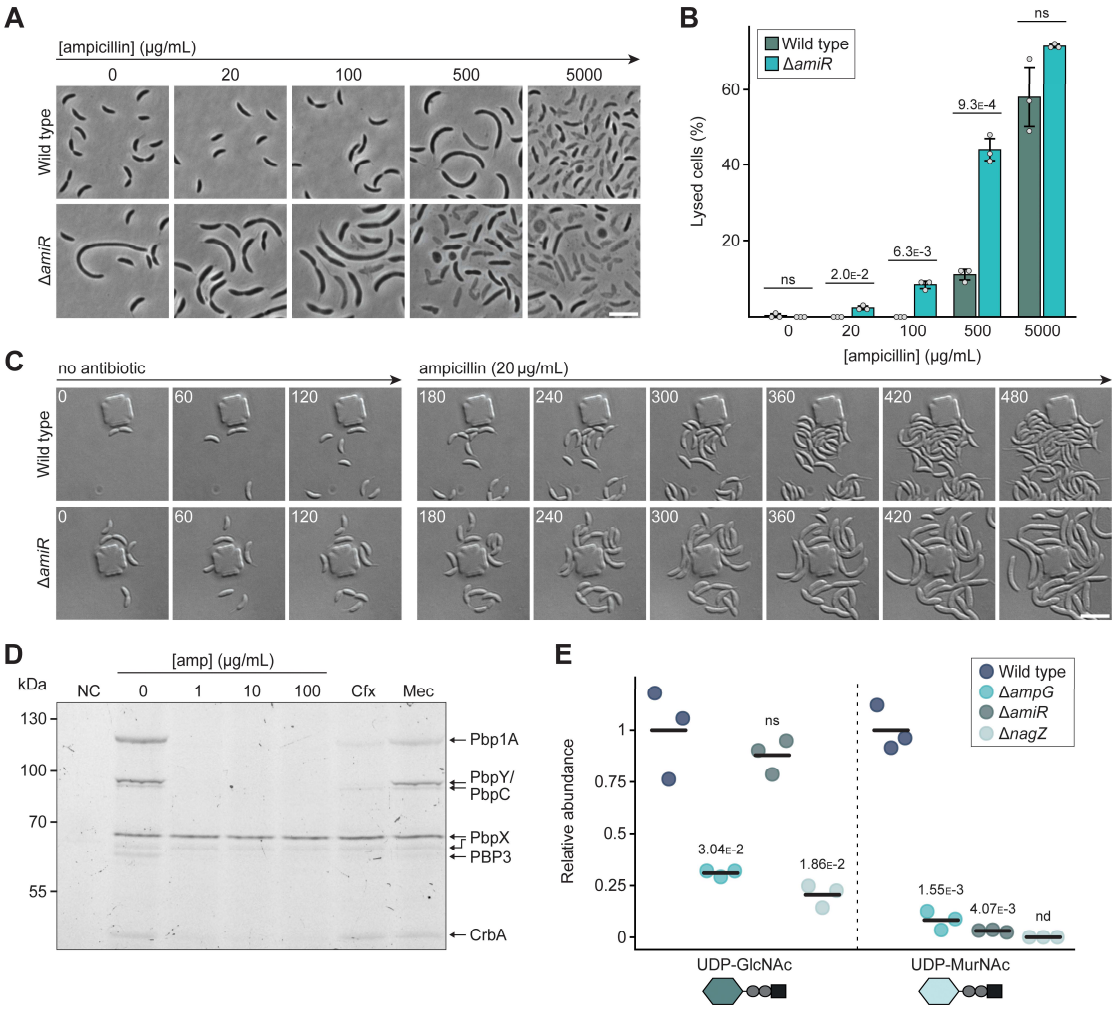

Figure 9. PG recycling defects increase the sensitivity of the septal PG synthetic machinery to ampicillin and reduce PG precursor biosynthesis. (A) Phase contrast images of *C. crescentus* wild-type and Δ*amiR* (PR033) cells, incubated for 3 h in the presence of different concentrations of ampicillin. Scale bar: 5 µm. **(B)** Quantification of the fraction of lysed cells in cultures of *C. crescentus* wild-type and Δ*amiR* (PR033) cells, incubated for 3 h in the presence of different concentrations of ampicillin. The bars represent the mean (±SD) of three independent replicates (*n*=100 cells per condition). The underlying data are shown as grey dots. The statistical significance (*p*-value) of differences between strains was calculated using an unpaired two-sided Welch's t-test. ns indicates p-values > 0.1. **(C)** Time-lapse microscopy analysis showing *C. crescentus* wild-type and Δ*amiR* (PR033) cells in a microfluidic flow cell before and after ampicillin treatment. After 3 h of growth in antibiotic-free medium, the cells were shifted to medium containing 20 µg/mL ampicillin. Images were taken at 5 min intervals for a total duration of 8 h. Shown are representative frames of the time-lapse series. The full sequences are shown in **Figure 9-Video 1** and **Figure 9-Video 2**. **(D)** Image of an SDS-gel showing the labeling of PBPs with the fluorescent β-lactam bocillin-FL in the absence or presence of other β-lactams. Crude membrane fractions of *C. crescentus* Δ*blaA* (CS606) cells were pre-incubated with the indicated concentrations of ampicillin, 5 µg/mL cefalexin (Cfx) or 100 µg/mL mecillinam (Mec), treated with bocillin-FL and then subjected to SDS gel electrophoresis to separate the labeled PBPs prior to fluorescence imaging. **(E)** Levels of UDP-Glc*N*Ac and UDP-Mur*N*Ac in the cytoplasm of *C. crescentus* wild-type, Δ*ampG* (PR207), Δ*amiR* (PR033) and Δ*nagZ* (PR188) cells, measured by metabolomics analysis through quantification of the corresponding mass spectrometric peak areas. The statistical significance of differences between the wild type and the mutant strains was determined using an unpaired two-sided Welch's t-test. ns indicates p-values > 0.1; nd: not detectable.

1589 **Figure 9–video 1. Effect of ampicillin on the growth of *C. crescentus* wild-type cells.** *C. crescentus* wild-type cells were cultivated
1590 in a microfluidic flow cell for 3 h in antibiotic-free medium and then shifted to medium containing 20 µg/mL ampicillin. Phase
1591 contrast images were taken at 5-min intervals. Scale bar: 5 µm.

1592 **Figure 9–video 2. Effect of ampicillin on the growth of *C. crescentus* Δ*amiR* cells.** *C. crescentus* Δ*amiR* (PR033) cells were
1593 cultivated in a microfluidic flow cell for 3 h in antibiotic-free medium and then shifted to medium containing 20 µg/mL ampicillin.
1594 Phase contrast images were taken at 5-min intervals. Scale bar: 5 µm.

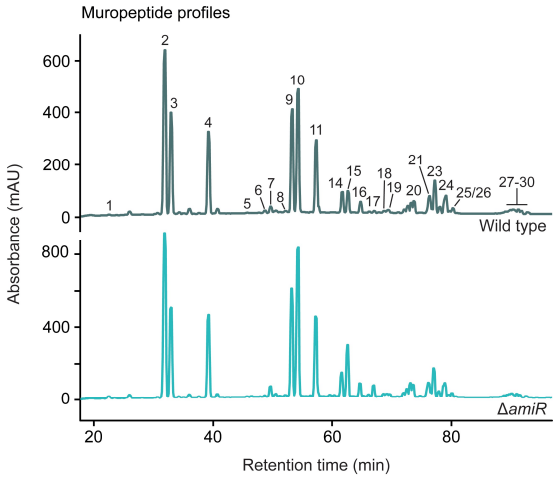

1595 **Figure 9–figure supplement 1. Muropeptide composition of PG sacculi from wild-type and Δ*amiR* cells.** Shown are HPLC
1596 chromatograms resolving the muropeptides obtained by muramidase treatment of PG sacculi isolated from stationary wild-type
1597 or Δ*amiR* (PR033) cells. The muropeptides contained in the different peaks are listed in **Figure 9–table supplement 1**. A summary
1598 of the data obtained is given in **Figure 9–table supplement 2**.

Figure 9–table supplement 1. Muropeptide composition of peptidoglycan isolated from stationary *C. crescentus* wild-type and Δ*amiR* cells. The table gives the relative abundance of the indicated muropeptide species, calculated from the areas of the corresponding peaks in the HPLC chromatograms from **Figure 9–figure supplement 1**. Two independent replicates were analyzed per strain.

Peak no.	Muropeptide	Peak area (%)			
		Wild type		Δ*amiR*	
1	Tri	0.0	0.0	0.3	0.0
2	Tetra	20.2	20.1	19.2	19.3
3	Penta(Gly5)	11.7	11.6	9.7	10.9
	unknown-possibly Di	0.6	0.7	0.4	0.7
4	Penta	9.2	9.2	8.6	9.7
5	TriTri(Dap)	0.0	0.0	0.0	0.0
6	TetraTri (Dap))	0.2	0.2	1.0	0.2
7	Tri-Anh (+small amount of TetraTri (D,L))	0.7	0.7	0.3	0.7
8	TetraTetra(Dap)	0.0	0.2	0.2	0.2
9	TetraPenta(Gly5)	10.8	11.0	10.5	11.2
10	TetraTetra	13.5	13.4	16.2	13.3
11	TetraPenta	7.6	8.2	8.1	8.9
12	TetraTetraTri or TetraTetraTri(Dap)	0.0	0.0	0.0	0.0
13	TetraAnh	0.5	0.0	0.2	0.0
14	TetraTetraPenta(Gly5)	2.2	2.2	2.3	2.6
15	TetraTetraTetra	2.2	2.2	4.7	2.4
16	TetraTetraPenta	1.1	1.2	1.2	1.3
17	TetraTetraTetraTetra	0.2	0.2	1.0	0.3
18	TetraTetraTetraPenta	0.3	0.3	0.3	0.3
19	Penta-Anh	0.5	0.5	0.4	0.5
20	TetraTetra-Anh	2.4	2.2	2.4	2.3
21	TetraPenta-Anh	2.4	2.4	2.1	2.3
22	TetraTetraTriAnh or TetraTetraTri(Dap)Anh	0.4	0.4	0.4	0.4
23	TetraTetraTetra-Anh	3.4	3.3	2.7	3.0
24	TetraTetraPenta-Anh	2.9	2.8	2.1	2.6
25	TetraTetraTetraPenta-Anh I	0.3	0.3	0.3	0.3
26	TetraTetraTetraPenta-Anh II	0.6	0.6	0.4	0.6
27	TetraTetraTetra-diAnh	1.0	1.0	0.6	0.9
28	TetraTetraTetraPenta-diAnh	0.5	0.5	0.4	0.5
29	TetraTetra-diAnh	0.4	0.4	0.3	0.3
30	TetraTetraPenta-diAnh	0.3	0.3	0.0	0.2

Figure 9–table supplement 2. Overview of the muropeptide species identified in peptidoglycan from stationary *C. crescentus* wild-type and Δ*amiR* cells. The table summarizes the relative abundance of different muropeptide species, calculated from the values listed in **Figure 9–table supplement 1**. Two independent replicates were analyzed per strain.

Muropeptide species	Peak area (%)			
	Wild type		Δ*amiR*	
All known	95.8	95.9	96.1	96.0
Monomers (total)	44.5	43.9	40.2	43.0
Dimers (total)	38.9	39.6	42.4	40.2
Trimers (total)	14.0	13.9	14.5	14.1
Tetramers (total)	1.9	2.0	2.5	2.0
Tripeptides (total)	0.9	1.0	1.3	1.0
Tetrapeptides (total)	62.6	62.2	65.7	61.8
Pentapeptides (total)	35.8	36.2	32.6	36.5
Chain ends (anhydros)	8.3	7.6	6.1	7.4
Average chain length	12.0	13.1	16.2	13.4
3-3 crosslinks	0.3	0.4	0.8	0.3
Degree of cross-linkage	30.2	30.5	32.7	31.0
% peptides in cross-links	55.5	56.1	59.8	57.0

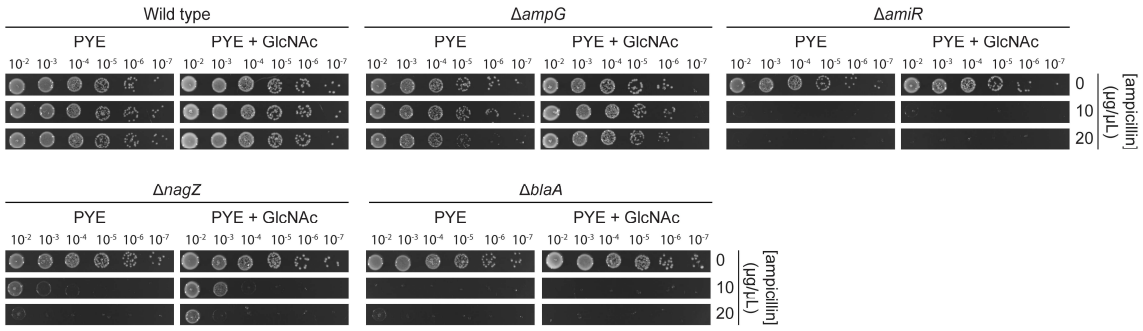

Figure 9–figure supplement 2. Ampicillin sensitivity of PG recycling-defective mutants in the presence of Glc*N*Ac. Shown is a serial dilution spot assay investigating the growth of C. crescentus wild-type, Δ*ampG* (PR207), Δ*amiR* (PR033), Δ*nagZ* (PR188) and Δ*blaA* (CS606) cells on agar plates containing different concentrations of ampicillin in the presence of 0.3% Glc*N*Ac.

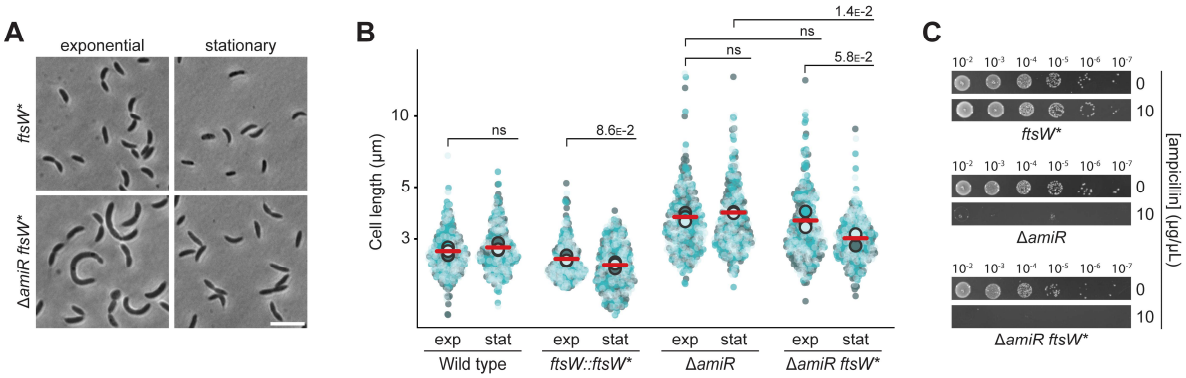

Figure 10. The cell filamentation phenotype of Δ*amiR* cells is rescued by hyper-activation of the septal FtsW-PBP3 PG biosynthetic complex. (A) Phase contrast images of *C. crescentus ftsW::ftsW** (ML2103) and Δ*amiR ftsW::ftsW** (PR246) cells, harvested in the exponential and stationary growth phase. **(B)** Superplots showing the distribution of cell lengths in populations of *C. crescentus ftsW::ftsW** (ML2103) and Δ*amiR ftsW::ftsW** (PR246) cells in the exponential (exp) and stationary (stat) growth phase. Data (*n*=100 cells per replicate) are presented as described for **Figure 4B**. The statistical significance (*p*-value) of differences between conditions was assessed using an unpaired two-sided Welch's *t*-test. ns indicates *p*-values > 0.1. **(C)** Serial dilution spot assay investigating the growth of *C. crescentus ftsW::ftsW** (ML2103), Δ*amiR* (PR033) and Δ*amiR ftsW::ftsW** (PR246) cells on agar plates containing no or 10 µg/mL ampicillin.

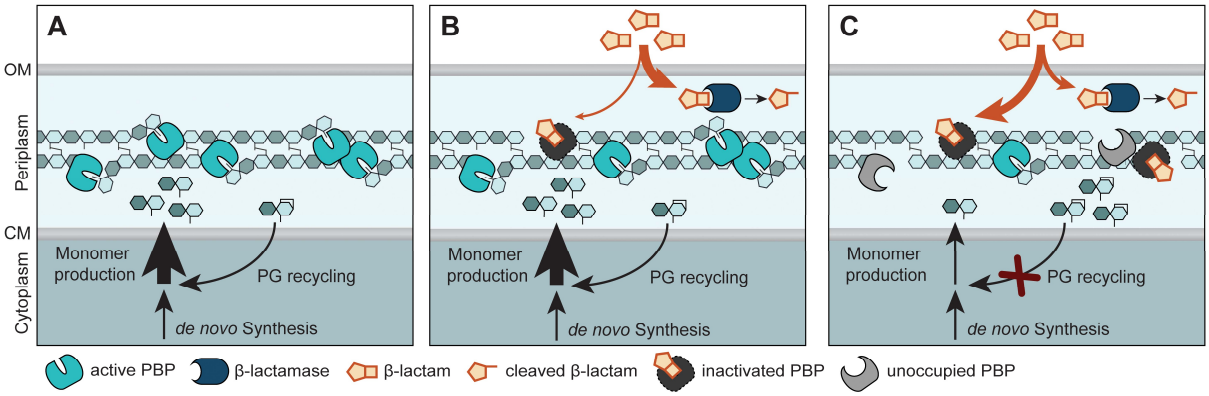

Figure 11. Model for the critical role of PG recycling in *C. crescentus* growth and β-lactam. (A) PBPs mediates the incorporation of new cell wall material into the growing PG sacculus. The PG precursors required for this process are synthesized in the cytoplasm, using building blocks that are provided by both *de novo* synthesis and PG recycling. **(B)** If β-lactams enter the periplasm, they compete with PG precursors for binding to their PBP targets. Most antibiotic molecules are rapidly hydrolyzed by the β-lactamase BlaA. However, a minor fraction manages to interact with PBPs before they are captured and degraded. The resulting inactivation of a small proportion of PBPs can be tolerated by cells, as long as they still contain sufficient active PBPs to maintain cell growth and division. **(C)** Upon disruption of PG recycling, the level of PG monomers strongly decreases, leaving the substrate binding sites of PBPs unoccupied for longer periods of time and thus increasing their accessibility to β-lactam molecules. As a result, a larger fraction of PBPs is inactivated, leading to decreased cell wall integrity and ultimately cell lysis. This effect may be aggravated by the reduced activity of the remaining, active PBPs due to an insufficient supply of PG precursors and by the accumulation of anhydro-muropentapeptides in the periplasm, which could interfere with the activities of PG biosynthetic enzymes, thereby further decreasing the incorporation of new material into the existing sacculus.